ADVANCING HYDROLOGIC AND HYDRAULIC UNDERSTANDING AND APPLICATION THROUGH INUNDATION MAPPING AND ESTIMATION OF LOSSES

By

JIAQI ZHANG

DISSERTATION

Presented to the Faculty of the Graduate School of

The University of Texas at Arlington

in Partial Fulfillment of the Requirements

for the Degree of

DOCTOR OF PHILOSOPHY

THE UNIVERSITY OF TEXAS AT ARLINGTON

August 2020

DEDICATION

This dissertation is dedicated to my parents

for their love and support in every circumstance

and to my husband Shang

who shares life with me

ACKNOWLEDGEMENTS

First and foremost, I would like to thank my advisor Dr Nick Z. Fang for his tremendous support during my Ph.D. journey. He's always willing to discuss ideas and share knowledge with me in hydrology and hydraulics. Not only in scientific aspect, I also learnt a lot of practical engineering experiences from him.

I would like to thank my committee members, Professor Dong-Jun Seo, Yu Zhang, and Zong-Liang Yang. Taking classes with Dr Seo paves a solid foundation for my Ph.D. study. Every time I asked questions, Dr Seo always explains well and gives me insightful comments, which benefit my research along the way. Constructive suggestions form Dr Zhang and Dr Yang help me clear confusions and guide me to the right direction.

I would like to thank all the people I met in the 2016 Summer Institute held at the National Water Center. Working with students and professors from various universities and background was a great experience, which helped me to think from different perspectives and improved my critical thinking. Especially I want to thank Dr David Maidment and Dr Sagy Cohen, who had been advising and guiding our research in the Summer Institute; Dinuke Munasinghe and Yu-Fen Huang, who had been my team members; Ryan McGehee and Lingcheng Li, who had been working closely with us as friends and collaborators; Peirong Lin, Adnan Rajib, and Xing Zheng, as the course and research coordinators.

I would also like to thank my friends who are encouraging and supportive during these years. Without them, my Ph.D. journey won't be complete. In addition, I want to thank my family for their love and supports in every situation. For my husband Shang, thank you for always being with me and growing with me along the way.

ABSTRACT

ADVANCING HYDROLOGIC AND HYDRAULIC UNDERSTANDING AND APPLICATION THROUGH INUNDATION MAPPING AND ESTIMATION OF LOSSES

Jiaqi Zhang, Ph.D.

The University of Texas at Arlington, 2020

Flooding is the most frequent weather hazard that can cause serious fatalities and property damages worldwide. Climate change with extreme weather has further increased the impact from flooding and brought unprecedented challenges to engineering infrastructure and design. Scientists and engineers have used models to investigate and forecast the hydrologic and hydraulic responses to environmental changes in meteorological forcing and land use. With recent advances in sensing and computing technologies, models have been reaching higher levels of spatiotemporal granularity and scale. However, gaps exist between the scientific exploration and engineering practices. This doctoral study has been conducted to bridge such gaps via investigating 1) inundation mapping approaches and 2) infiltration loss models in various modeling frameworks. The obtained insights are firstly beneficial to modelers/engineers who can strategically choose the optimal modeling scheme based on the needs and resources. For scientists studying hydrology and hydrology-atmosphere feedbacks, understanding how different factors synergize or counteract with each other to affect hydrologic processes is rewarding. For the community and emergency responders, increasingly detailed and realistic representations of physical processes marks a shift in the paradigm of operational flood forecast from a past that heavily relies on human judgment/adjustment towards a computationally expensive but more robust future.

Table of Contents

Acknowledgement.....iv

Abstract.....v

Chapter 1: Introduction.....1

Chapter 2: Comparative Analysis of Inundation Mapping Approaches for the 2016 Flood in the Brazos River, Texas.....4

Chapter 3: Understanding the Re-infiltration Process to Simulating Streamflow in North Central Texas using the WRF-Hydro Modeling System.....35

Chapter 4: Investigation of Loss Estimation to Facilitate Design Flood Practices in North Central Texas.....75

Chapter 5: Conclusion and Future Research.....107

Chapter 1: Introduction

RESEARCH GOALS

The overarching goals of this Ph.D. work are 1) *to improve our understanding of strength and weakness in achieving the optimal accuracy and efficiency for operational inundation mapping* and 2) *to improve water resource management via better representing infiltration loss using realistic and abstract infiltration schemes in hydrologic models.* There are still gaps between design practices and most updated data/science in hydrology and hydraulics, which is reflected by the vast variety of models. With recent advances in remote sensing, high-performance computing, and in-situ measurements, hydrologic/hydraulic models have rapidly evolved from simplistic, lumped models to physics-based distributed models. My Ph.D. study primarily focuses on bridging the gap between science and engineering via investigating capability of various models in achieving realism and efficiency to better facilitate water resource management. To this end, the whole dissertation aims to answer the following first-order research questions.

1. How do terrain- and dynamic-based inundation models perform with respect to comparison with remotely sensed observation as well as the feasibility in near real-time, large scale inundation mapping?

2. What is the role of re-infiltration in the whole hydrologic process and its significance in flood forecasting in response to various hydrometeorological, geographical, and parameter settings?

3. How can we advance the parameterization of empirical infiltration loss models using all available in-situ and remotely sensed observation, in order to enhance the design practices?

DISSERTATION STRUCTURE

This dissertation consists of five chapters. Chapter 1 introduces the research goals, questions and structure of this dissertation. Subsequent chapters contain three manuscripts focusing on the following topics: comparison of different inundation mapping approaches (Chapter 2); representation of infiltration loss in a distributed process-based model (Chapter 3); and infiltration loss estimation in a lumped hydrologic model (Chapter 4). Chapter 5 presents conclusions and future research.

Terrain-based and hydraulic-based inundation models are compared in Chapter 2. This study utilized the Height Above the Nearest Drainage (HAND) as terrain-based model and the International River Interface Cooperative (iRIC) as hydraulic-based model to estimate the inundation area for a large flooding event occurring in May of 2016 in the Brazos River. The inundation extents simulated from these two modeling approaches are then compared against the observed inundation extent derived from a Landsat-8 Satellite image. The results highlighted the pros and cons for each modeling approach. Chapter 2 also helps to identify potential improvements for HAND-based simulation.

Chapter 3 investigates the representation of infiltration loss in a distributed process-based modeling system, WRF-Hydro. An important component that WRF-Hydro introduced, re-infiltration process, is evaluated under different hydrometeorological and geographical conditions with model parameter settings. A series of idealized numerical experiments and two real storm events are simulated using 18 watersheds in North Central Texas as a testbed. The results show that the runoff coefficient and the re-infiltration ratio are positively correlated in the study area from both hypothetical and real events, indicating re-infiltration effects can become more pronounced as flood potential increases. Findings in Chapter 3 also demonstrate the necessity in

representing the re-infiltration process in flood forecasting. Models that do not incorporate this process may be over-calibrated to compensate errors originated from the missing process.

Chapter 4 presents the loss estimation in a lumped hydrologic model: HEC-HMS. The specific loss method utilized is the Initial Abstraction and Constant Loss (IACL) method, which has been widely applied in the engineering practices due to its simplicity and relative accuracy. A data-driven approach is applied to quantify the total loss and its initial abstraction (IA) and constant loss (CL) components. Compared to the traditional calibration approach to estimate IACL, data-driven approach brings a lot more IA and CL samples, which can help to identify the statistical behavior of IA and CL values in a probability sense. The statistics of IACL from this study establish a solid foundation for future Monte-Carlo rainfall-runoff simulations, which can provide a better estimation in derived flood frequency curves.

Chapters 2, 3, and 4 are three manuscripts published or intended for publication in peer-reviewed journals. Their full references are as follows:

Zhang, J., Munasinghe, D., Huang, Y.F., Fang, Z., Cohen, S., and Tsang, Y.P (2018). "Comparative Analysis of Inundation Mapping Approaches for the 2016 Flood in the Brazos River, Texas", AWRA Journal of the American Water Resources Association (JAWRA) 1–14. https://doi.org/10.1111/1752-1688.12623

Zhang. J., Lin, P., Gao, S., and Fang, Z. (2020). "Understanding the Re-infiltration Process to Simulating Streamflow in North Central Texas using the WRF-Hydro Modeling System". Journal of Hydrology, 124902. https://doi.org/10.1016/j.jhydrol.2020.124902

Zhang. J., Gao, S., and Fang, Z. (2020). "Investigation of Loss Estimation to Facilitate Design Flood Practices in North Central Texas". (In Preparation).

Chapter 2: Comparative Analysis of Inundation Mapping Approaches for the 2016 Flood in the Brazos River, Texas [1]

Zhang, J., Munasinghe, D., Huang, Y.F., Fang, Z., Cohen, S., and Tsang, Y.P (2018). "Comparative Analysis of Inundation Mapping Approaches for the 2016 Flood in the Brazos River, Texas", AWRA Journal of the American Water Resources Association (JAWRA) 1–14. DOI: https://doi.org/10.1111/1752-1688.12623

[1] Used with Permission from Wiley, the publisher of Journal of the American Water Resources Association, 2020

ABSTRACT

Accurate and timely flood inundation maps serve as crucial information for hydrologists, first-responders and decision makers of natural disaster management agencies. In this study, two modeling approaches are applied to estimate the inundation area for a large flooding event occurring in May of 2016 in the Brazos River: (1) Height Above the Nearest Drainage combined with National Hydrograph Dataset Plus (NHDPlus-HAND) and (2) International River Interface Cooperative ─ Flow and Sediment Transport with Morphological Evolution of Channels (iRIC-FaSTMECH). The inundation extents simulated from these two modeling approaches are then compared against the observed inundation extents derived from a Landsat-8 Satellite image. The simulated results from NHDPlus-HAND and iRIC- FaSTMECH show 56% and 70% of overlaps with the observed flood extents, respectively. A modified version of the NHDPlus-HAND model, considering networked catchment behaviors, is also tested with an improved fitness of 67%. This study suggests that the NHDPlus-HAND has the potential for real-time continental inundation forecast due to its low computational cost and ease to couple with the NWM. Better performance of NHDPlus-HAND can be achieved by considering the inter-catchment flows during extreme riverine flood events. Overall, this study presents a comprehensive examination made of remote sensing compared with HAND-based inundation mapping in a region of complex topography.

KEY TERMS

Flooding; Inundation; NHDPlus-HAND; iRIC; Simulation; Observation; Remote Sensing

INTRODUCTION

Flooding is one of the leading causes of natural disaster related deaths worldwide (Federal Emergency Management Agency, 1992; Conrad *et al.*, 1998; Merwade *et al.*, 2008; Cook and Merwade, 2009). According to a study on flood damage in the United States, flood damage increases over time due to rapidly growing population and urban development (Pielke *et al.*, 2002). Accurate and timely inundation maps not only provide first-hand information for rescuing and emergency operations during floods, but also potentially improve flood risk management and better estimate flood insurance rates (Merwade *et al.*, 2008; Cook and Merwade, 2009; Fang *et al.*, 2011). In the United States, most major river systems have flood risk maps delineated by the Federal Emergency Management Agency (FEMA) through the National Flood Insurance Program (NFIP). Although FEMA has produced approximately 100,000 flood risk maps based on 100-year return period flows (NFIP, 2002), inundation maps for real events are unavailable or limited by uncertainties in data sources or modeling (Christian *et al.*, 2013).

Flood inundation modeling approaches are essentially to convert flows from either hydrologic models or observation gages into inundation extent/depth based upon topographic information. In general, inundation models can be classified as terrain-based and dynamic-based approaches. Terrain-based approaches refer to the methods employing topography and simplifying the fluid mechanics process to predict inundation extents. Intersecting topography surface with a planar water surface is normally defined as the simplest terrain-based approach to generate inundated area (Priestnall *et al.*, 2000). Some terrain-based models are also known as storage cell models by treating the floodplain as many storage cells and solving uniform flow formulas like Manning's and weir-type equations for floodplain routing (Cunge *et al.*,1976; Estrela, 1994; Romanowicz *et al.*, 1996, Bates and De Roo, 2000). Another type of terrain-based approach

calculates the elevation difference between each grid cell and its nearest flowpath grid based on topographic information (Nobre *et al*., 2011). In summary, the terrain-based approaches aim to reduce computational cost while generating satisfactory inundation results.

Dynamic-based approaches include hydraulic/hydrodynamic models which are generally categorized as one-, two- and three-dimensional models. One-dimensional hydraulic models consider fluid continuity and momentum, which solve one-dimensional St. Venant equations. One example of such hydraulic models is the Hydrologic Engineering Center's River Analysis System (HEC-RAS) developed by the U.S. Army Corps of Engineers (USACE). The general steps of inundation mapping using one-dimensional hydraulic models involve: (1) obtaining discharge information from gage observation or a calibrated hydrologic model; (2) developing perpendicular cross sections along the flow path based on Digital Elevation Model (DEM) or survey information with hydraulic parameters (e.g. surface roughness); (3) calculating the water surface elevations based on the discharge and cross-sectional information from the previous steps; (4) comparing the water surface elevations with DEMs, and the area where water surface is higher than terrain elevation is defined as inundated (IACWD 1982; Maidment and Djokic, 2000; Noman *et al.*, 2001; FEMA 2003; Merwade *et al.*, 2008). Two-dimensional hydraulic models use finite-element mesh as a calculation unit and have capability to simulate the lateral unsteady flow dynamics including backflow condition (Crowder and Diplas, 2000; Merwade *et al*., 2008). Three-dimensional hydraulic models can fully represent the comprehensive form of the Navier-Stokes equations (White, 1974; Lane *et al*, 1999). Since three-dimensional approaches might be unnecessarily complex and computationally expensive (Bates and De Roo, 2000; Horritt and Bates, 2001; Hunter *et al*., 2007), one- and two-dimensional models are the primarily used in floodplain prediction to

date (Hunter *et al*., 2007). **Table 1** shows the comparison between dynamic-based and terrain-based inundation mapping approaches.

Table 1. Comparison of dynamic-based and terrain-based inundation approaches

Model Type		Reference	Routing	Data requirement	Run time	Calibration	Validation
Dynamic-based	1D	Fread (1984); Fread (1993)	Full solution of the 1D St. Venant equations	Discharge, DEM, Cross-sections, Channel parameters, Land use/type	Fast	Necessary	Yes
	2D	Bates *et al*. (1992)	Full solution of the 2D St. Venant equations with turbulence closure	Discharge, DEM, Land use/type	Moderate	Contingent	Yes
	3D	White (1974); Lane *et al*. (1999)	Full solution of the Navier-Stokes equations	3D DEM, 3D bathymetry, 3D velocity, Land use/type	Slow	Contingent	Yes
Terrain-based	Planar water surface	Priestnall *et al*.(2000)	None	DEM, water surface elevation	Fast	Limited	Yes
	Storage cell	Cunge *et al*. (1976); Estrela (1994); Romanowicz *et al*. (1996); Bates and De Roo (2000);	Uniform flow formula (Manning equation or weir-type equations); Kinematic wave and Manning equation	DEM, discharge, Initial channel flow depth, Land use/type	Fast	Limited	Yes
	HAND	Nobre *et al*. (2011)	Uniform flow formula (Manning equation)	DEM, discharge/water surface elevation, Land use/type	Fast	Limited	Yes

Height Above the Nearest Drainage combined with National Hydrograph Dataset Plus (NHDPlus-HAND) is a terrain-based flood indundation model. The Height Above the Nearest Drainage (HAND) concept was first introduced by Rennó *et al.* (2008). The HAND model normalizes topography based on relative heights found along the nearest drainage network (Nobre *et al*., 2011). The HAND raster is generated by subtracting the elevation of each grid cell from the elevation of its nearest stream grid cell. Nobre *et al.* (2016) has validated the HAND method using a flood event in Southern Brazil with a finding that HAND can be used to predict inundation extents. Since HAND rasters are computed based on topography and flowpath information, accurate Digital Elevation Model (DEM) and flowline are essential components in establishing a

HAND model. The National Hydrograph Dataset Plus (NHDPlus) is an integrated geo-spatial, hydrologic dataset built by the U.S. Environmental Protection Agency (USEPA) Office of Water and the US Geological Survey (USGS). The NHDPlus Version 2 dataset provides a reliable stream network consisting of approximately 2.7 million reaches in the continental United States (http://www.horizon-systems.com/nhdplus/). Liu *et al*. (2016) calculated HAND rasters for the contiguous United States using a 10-m resolution DEM combined with NHDPlus streamlines (termed NHDPlus-HAND). For delineating inundation maps, HAND needs discharge and rating curve information from hydrologic/hydraulic models. Brought into operations in August of 2016, the National Water Model (NWM) is a high-resolution hydrologic model simulating discharge for 2.7 million NHDPlus (Version 2) stream reaches over the continental United States (NOAA, 2016). The NWM is developed based on the Weather Research and Forecasting Model Hydrological (WRF-Hydro) framework, which utilizes meteorological forcing from the operational High Resolution Rapid Refresh (HRRR) model and precipitation forcing from the Multi-Radar/Multi-Sensor System (MRMS). To obtain discharge information, the NWM utilizes a vector-based channel routing module based on the NHDPlus reaches, which was firstly demonstrated using the Routing Application of the Parallel Computation of Discharge (RAPID) in 2015 (Maidment, 2017; Lin *et al.*, 2017), and then evolved into the Muskingum-Cunge routing method in 2016 (NOAA, 2016). This study uses a set of the pre-operational NWM discharge data that ingests the streamflow data assimilation capability at ~7000 gauge stations (NOAA, 2016) on top of the Muskingum-Cunge routing. The NHDPlus-HAND is chosen as the terrain-based model for the study due to its ease of application to be coupled with the existing hydrologic model (NWM).

A dynamic-based model, International River Interface Cooperative - Flow and Sediment Transport with Morphological Evolution of Channels (iRIC-FaSTMECH) is a two-dimensional

hydrodynamic model employing a channel-fitted coordinate system (cylindrical coordinate system), where the curvature follows the stream direction (FaSTMECH Model Note. Accessed March 1, 2017, http://i-ric.org/en/downloads). It provides information of velocity and water surface elevation for a given discharge and roughness by hydrostatic-distribution pressure and a quasi-steady approximation (Nelson and McDonald, 1996), which allows the discharges to vary in time, and simplifies unsteady terms in the equations of motion. The iRIC system includes different models with less restrictive assumptions and more applicability but requires more extensive calibration data (Nelson *et al*., 2016, www.i-ric.org). The iRIC model framework is upgraded from the Multidimensional-Surface Water System Modeling System (MD-SWMS) (McDonald *et al*., 2001, 2005), which employs a finite difference approach on a curvilinear grid to solve the depth and Reynolds-averaged Navier-Stokes equations (Nelson *et al.*, 2003). Not only can the iRIC-FaSTMECH provide the maximum inundation area at peak stage but also be used for simulating water level, flow velocity distribution for the floodplain, etc. (Ku and Kim, 2014; Son *et al*., 2014; Kail *et al*., 2015). Kenney and Freeman (2011) suggested that iRIC-FaSTMECH give a fair spatial understanding of water-surface elevation, velocities, and sheer stress associated with high flows. Son *et al.* (2014) showed that iRIC-FaSTMECH well simulated water-surface levels in South Korea. Due to its simulation efficiency and utility in predicting water-surface elevation during the flood event, iRIC-FaSTMECH is selected as the dynamic-based model in this study.

Lack of reliable observed spatial extents of flood inundation limits the validation and utility of both approaches in flood inundation mapping. Fortunately, the advent of satellite-based remote sensing technology has become a key tool for flood monitoring (e.g. Dartmouth Flood Observatory: http://floodobservatory.colorado.edu). Such applications of satellite imagery for river inundation

(e.g. the U.S. Flood Inundation Map Repository: http://sdml.ua.edu/usfimr) serve as observations on flooding areal extents within the region of interest (Khan *et al.*, 2011).

In this regard, the authors are motivated to investigate the performances of various inundation simulations based on observation derived using remote sensing techniques. A better understanding of mechanisms of terrain- and dynamic-based inundation approaches can then be achieved. Furthermore, deeper insights are gained to improve the timeliness and accuracy of real-time flood inundation mapping. This study is conducted to achieve the following objectives:

1. To validate the NHDPlus-HAND's simulation using streamflow information from the NWM along with the observation derived from the satellite imagery.

2. To evaluate the terrain-based (NHDPlus-HAND) and dynamic-based (iRIC-FaSTMECH) models with respect to modeling accuracy, modeling efficiency (running time), and feasibility in real-time mode.

3. To provide suggestions for future model development and explore potential efficient ways to improve NHDPlus-HAND towards accurate large-scale inundation mapping.

STUDY AREA

Based on a request for presidential disaster declaration by Abbott (2016), 12 counties in Texas with a population of 3.9 million were impacted by a flood event occurring in the Brazos River in May of 2016. There were over 11,000 people evacuated from their impacted homes along the Brazos River (Abbott, 2016). Due to the severity of the flood, the May of 2016 event is particularly selected for this study to seek useful information for future decision making under severe weather conditions.

The study area (**Figure 1**) is a section of the Brazos River spanning 27 km of main-stem distance upstream of the USGS gage near Hempstead (ID: 8111500). The inundation of the May 2016 event over the study area was captured in a relatively cloud-free Landsat 8 image. As shown in Figure 2B, the majority of the area appears to be flooded in comparison with the pre-flood condition (**Figure 2A**). The USGS gage (ID: 8111500) recorded a total rainfall of 255.8 mm within 25 hours, as well as the peak stage of 16.78 m (above the datum) at 3 p.m. on May 27th, 2016, Central Daylight Time (CDT). The Landsat 8 imagery (**Figure 2B**) was captured at 12 p.m. on May 28th (CDT), 21 hours after the peak stage occurred. However, at the moment when satellite imagery was taken, it shows that the stage elevation decreased from the peak stage elevation only by 2.5% (**Figure 3**), implying the slow recession of the river after the peak stage occurred. Because of such a small difference, the flood extents captured by satellite imagery is assumed to represent the peak inundation in this study.

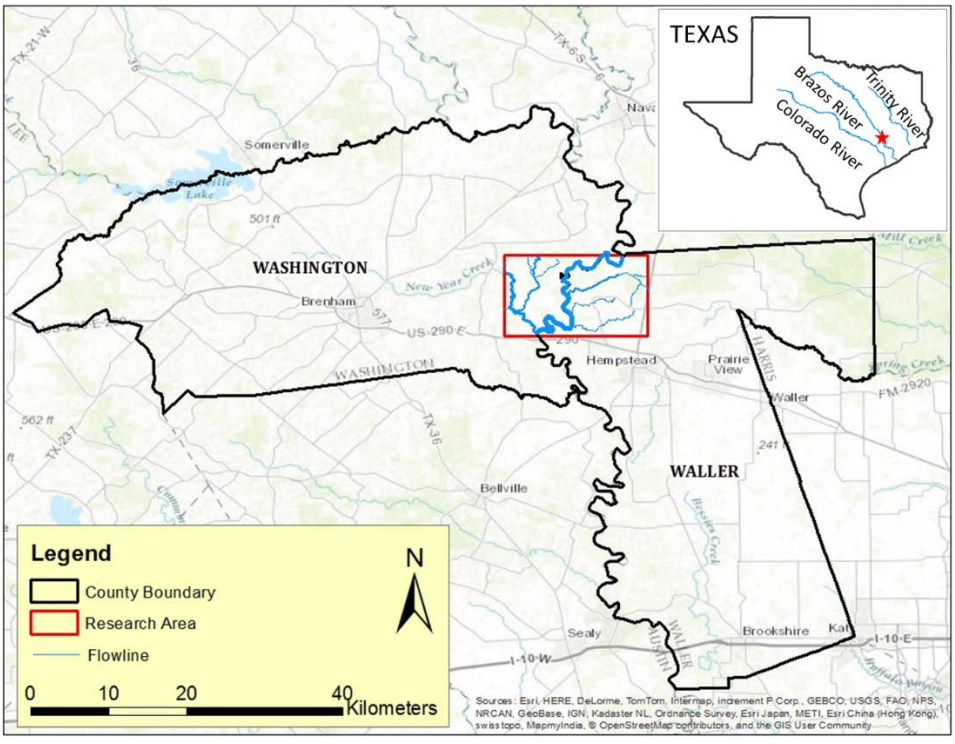

Figure 1. The study area and stream reaches in the Brazos River, Texas.

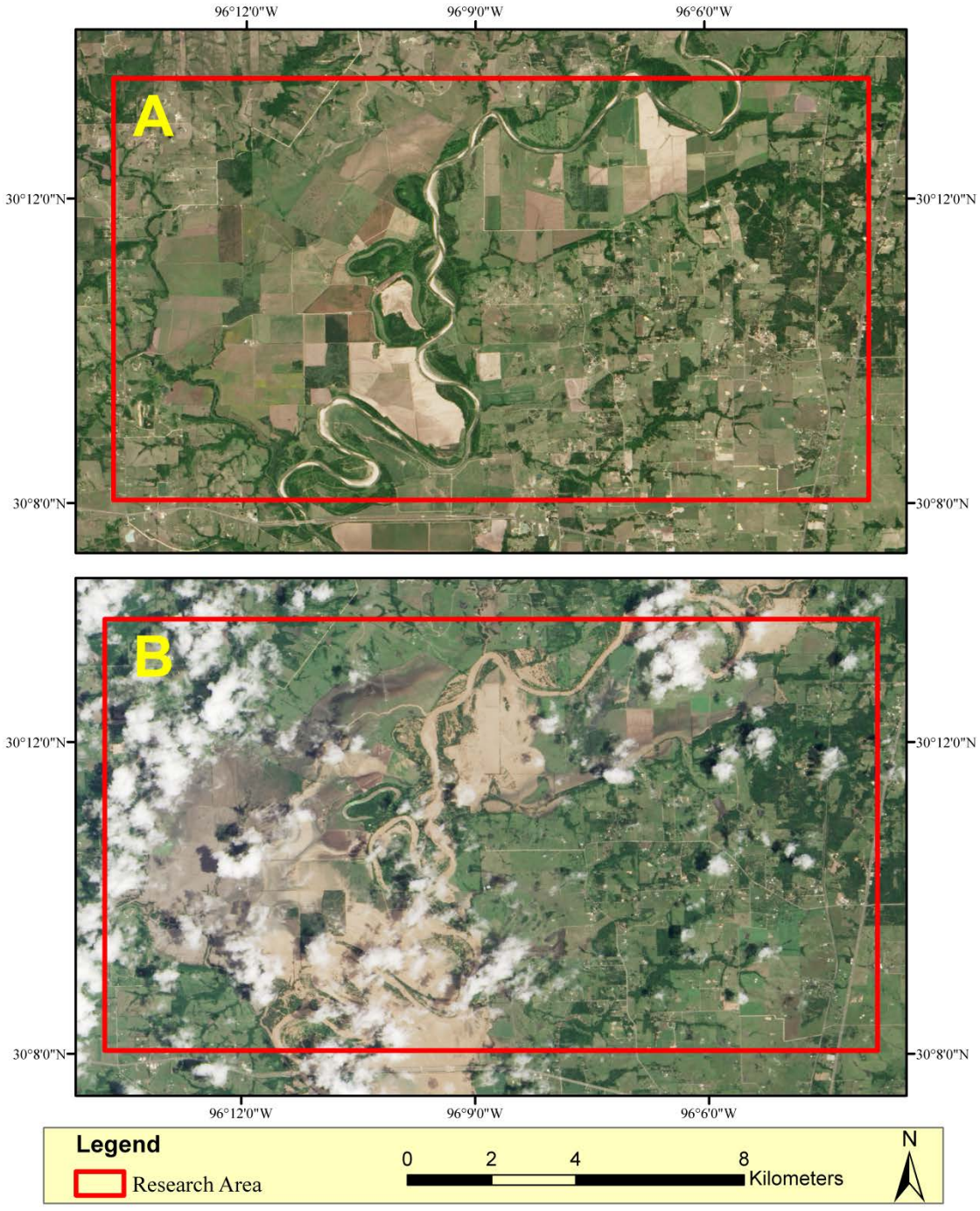

Figure 2. Satellite imageries showing A. pre-flood (12 p.m. on March 25th, 2016(CDT)) and B. post-flood condition (12 p.m. on May 28th, 2016(CDT)) in the study area.

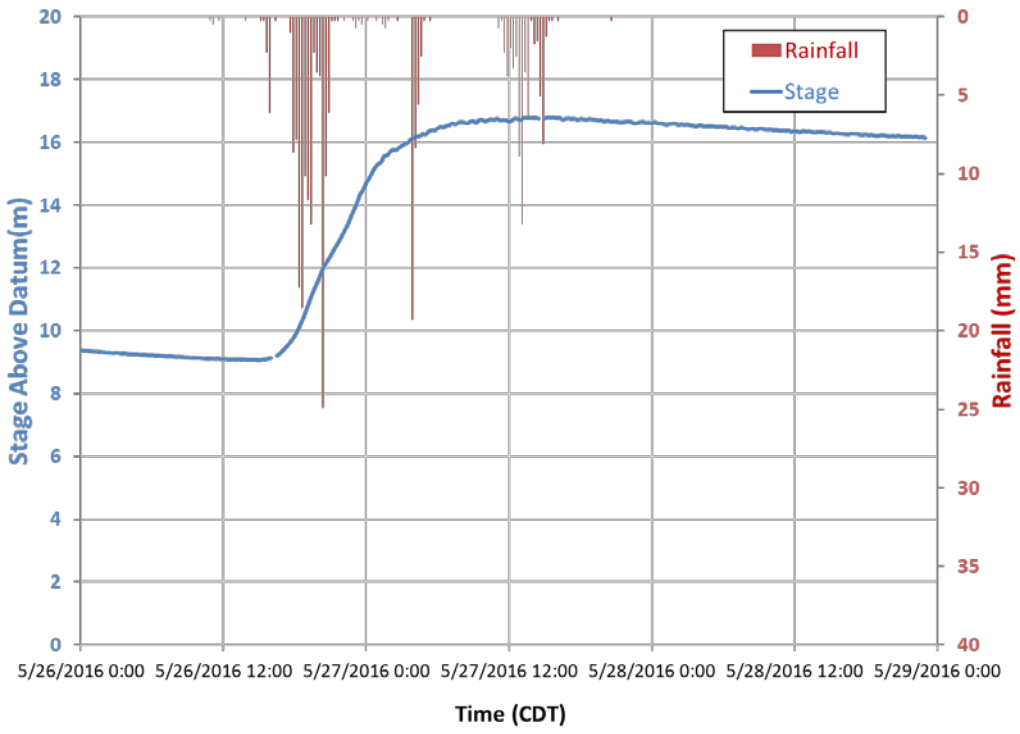

Figure 3. Stage hydrograph and rainfall hyetograph shows the target timing of model simulation and the timing of satellite observation.

METHODOLOGY

To better understand and evaluate two inundation modeling methods and their corresponding performances, the authors conduct a series of comparisons of simulated inundation from both approaches, i.e. terrain-based (NHDPlus-HAND and the modified HAND) and dynamic-based (iRIC-FaSTMECH), with observed inundation from the satellite imagery for the study area during the May 2016 event. For simplicity, NHDPlus-HAND and iRIC-FaSTMECH are referred to as HAND and iRIC respectively in the following sections. The methodology consists of three major parts: HAND, iRIC, and remote sensing. The HAND model uses hydrologic model's outcome as the input discharge to delineate flood inundation. As a supplementary approach, a modified version of HAND is also tested for inundation mapping. The iRIC is a two-

dimensional hydraulic model, to simulate flood inundation maps. Satellite imagery is used as observation for further comparisons with simulations in the third part. **Figure 4** illustrates the data and workflow of the methodology with more details in the following sections.

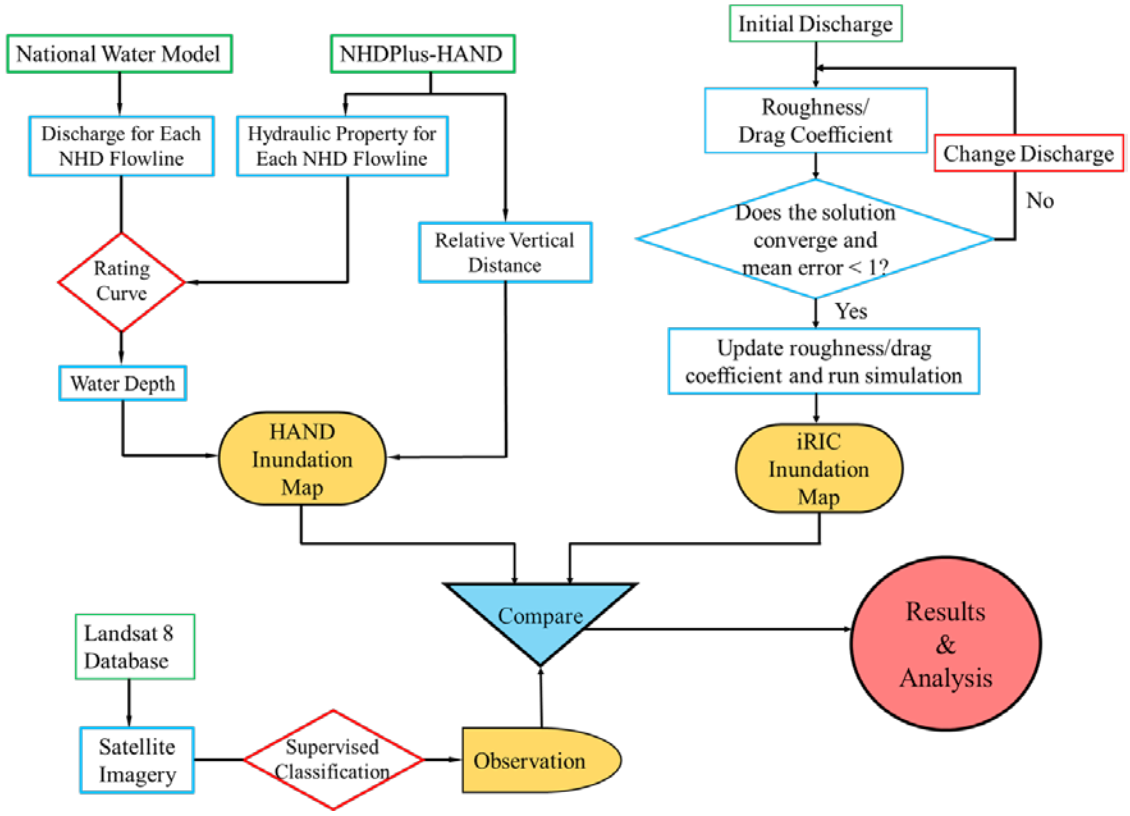

Figure 4. Schematic diagram of this study.

NHDPlus-HAND

NHDPlus-HAND generates inundation maps through the procedure as shown in Figure 4. First, the NWM output provides hourly discharge information for each NHDPlus flowline (identified by a unique ID number - ComID). In general, the discharge from the NWM undergoes nudging-based data assimilation wherever/whenever gage-observed values become available, which leads to a close match between the NWM discharge and observed discharge as shown in **Figure 5**. Then these NWM flow information is converted into stage height using rating curves (stage-discharge relationship). The rating curve for each reach is generated from channel properties

in the HAND model based on Manning's equation. These interpreted stage height information allows us to determine inundation extents from the HAND raster. In each catchment, HAND cells with lower elevation than the interpreted stage height information can be classified as 'wet' cells. For example if the calculated stage for a given catchment (ComID) is 5 m, all HAND cells with a value between 0 and 5 will be classified as 'wet' cells. A simple GIS-based Raster Calculator equation is applied to identify the 'wet' cells. The whole methodology of creating inundation map using HAND is automated with a Python script utilizing a number of ArcGIS tools for a better efficiency.

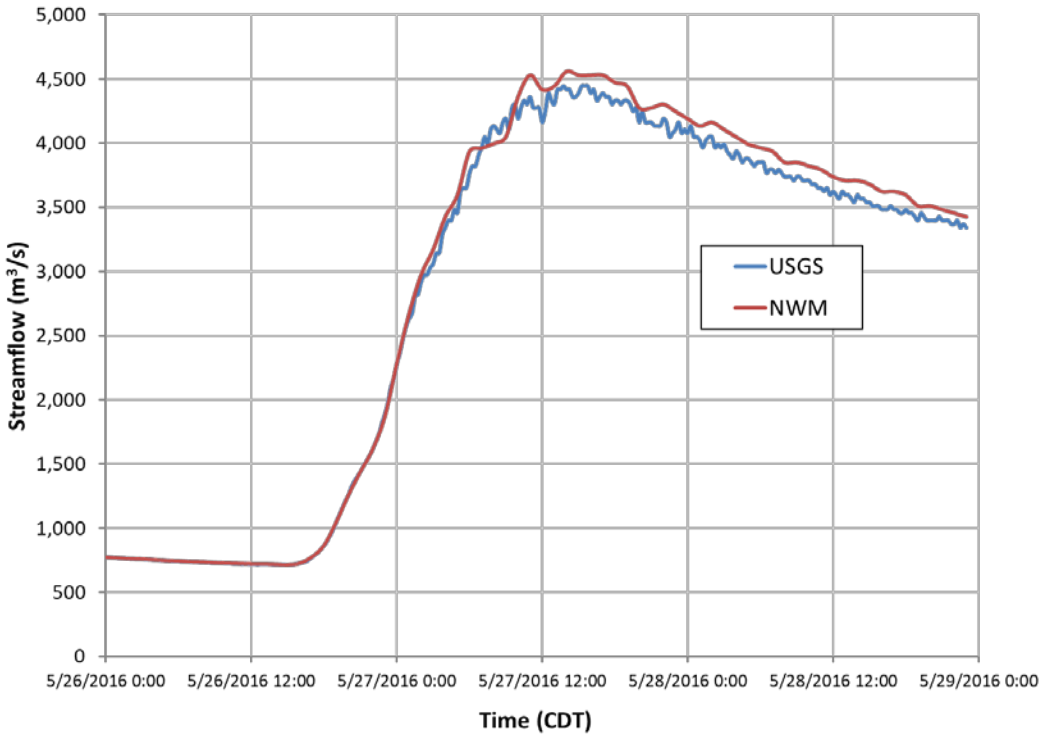

Figure 5. U.S. Geological Survey gage observed hydrograph and the National Water Model hydrograph with nudging-based data assimilation.

Modified HAND

The NHDPlus-HAND method typically enables users to determine inundated area based on individual NHDPlus catchment with corresponding water depth. However, with the assumption of applying uniform water depth for each catchment, NHDPlus-HAND cannot consider inter-catchment flow mechanisms, i.e. the flow transfer between adjacent catchments. To tackle this deficiency, McGehee *et al*. (2016) developed the modified HAND method by taking stream orders into account when determining the nearest drainage. In essence, the modified HAND method provides an approach to re-define channel network, i.e. deleting streams with low stream orders. McGehee *et al*. (2016) stated that such a modification, if applied locally where the original HAND overlooks catchment interaction, can potentially improve the accuracy of inundation mapping (as demonstrated later). Therefore, the modified HAND method is used to improve the HAND simulation in this study and compare with other inundation mapping results.

iRIC-FaSTMECH

The terrain used to develop iRIC-FaSTMECH model is 10-meter resolution DEM obtained from USGS database (https://earthexplorer.usgs.gov), and the NHDPlus-HAND is developed using DEM of the same resolution (10 meters). **Table 2** shows the final model settings for generating inundation by iRIC, and specific procedures are illustrated in Figure 4. The researchers first assign a water surface elevation as the initial upstream condition and the peak discharge (4,445.7 m^3/s) with stage information (49.7 m) from USGS gage (8111500) as the downstream boundary condition, respectively. After numerous iterations, the iRIC model is able to compute a converged solution as upstream discharge (4,300 m^3/s). During the iterations, drag coefficient is updated as it is a function of Manning's coefficient and water depth which varies with upstream discharge. Three Manning's coefficients (0.03, 0.05 and 0.035) are used to corresponding land

cover types (main channel, brushy and cultivated) (Chow 1959). Finally, inundation maps are delineated using the optimal drag coefficient and discharge after 1,500 iterations. Suggested by Nelson (2016), re-wetting option is turned during the modeling process on since it can improve inundation estimations in large and shallow areas by re-evaluating the wet/dry status of each node during the simulation.

Table 2. iRIC model settings

Setting Menu	Description
Initial Condition	Initial Water Surface Elevation: 1D step-backwater
Boundary Condition	Downstream Peak Discharge: 4445.7 m^3/s
	Downstream Peak Stage: 49.7 m
Iteration	1500
Upstream Discharge	4300 m^3/s
Upstream Stage	Constant (time-invariant)
Drag Coefficient	Variable
Re-wetting	On

Satellite-based Flood Inundation Mapping

Landsat Satellite missions have been applied in delineating floodplain boundaries over a few regions under different conditions in climate, morphology and land use since 1972 (Rango *et al.*, 1975; Hollyday, 1976; Sollers *et al.*,1978; Smith, 1997; Ho *et al.*, 2010). Amongst the many different techniques of identifying water pixels using a suite of the Landsat Satellites, Supervised Classification has been proven as a robust method to classify features of interest (Frazer and Page, 2000; Shalaby and Tateishi, 2007). The Supervised Classification technique allows users to select sample pixels (end members) in an image as representatives of a specific spectral signature (e.g. water). Image processing software is then used to classify all the image pixels based on the maximum likelihood that these pixels' spectral signature is similar to that of a specific end member.

The remote sensing imagery used in this study is obtained from the Landsat 8-Operational Land Imager (OLI) multispectral database (http://earthexplorer.usgs.gov). The pre-flood (March 25, 2016) and post-flood (May 28, 2016) images are classified via Erdas Imagine® 2015 Image processing software (Hexagon Geospatial, Norcross, GA, USA) for pre-processing and subsequent data manipulation. The resultant Geometrically and Radiometrically rectified imagery is subject to Supervised Classification of flooded pixels based on the maximum likelihood classifier. Typically, the presence of clouds is a common problem in remote sensing imagery, which hinders the identification of flooded water pixels beneath the clouds, leading to under-representation of flood water extents in the study domain. In an attempt to alleviate this problem, the DEM of the flooded region is used to identify the height of the pixels beneath the clouded areas. Each pixel with a lower height than that of the lowest height of an apparent flooded pixel in the neighborhood of the cloud is considered as 'wet'. Spatial filling techniques are then applied to convert these pixels into water pixels. Accuracy assessments are finally performed on the classified imagery subsequent to being post-processed through a 3×3 high pass kernel (Zhang *et al.*, 2016). A high pass kernel has the effect of highlighting boundaries between features (e.g., where water body meets the vegetated land), thus water features can be easily classified by sharpening edges between water and non-water pixels.

Advanced Fitness index (AFI)

In order to evaluate the correspondence between the simulated and observed inundation, the advanced fitness index (AFI) method is applied in this study. The AFI accounts for the match in terms of both inundated and non-inundated area, as shown in **Equation 1**:

$$\text{Advanced Fitness (\%)} = \frac{IA_{obs} \cap IA_{model} + NIA_{obs} \cap NIA_{model}}{A_{total}} \times 100 \quad (1)$$

where IA_{obs} /NIA_{obs} is inundated/non-inundated area of the observation; IA_{model}/NIA_{model} is inundated/non-inundated area of the model simulation, and A_{total} is the total area of the study region.

The simulated and observed inundation results cannot be compared directly because of their different resolution and patchy nature of the classified water body in a satellite image. To tackle this technical difficulty, the simulated inundation is further resampled to 30 m x 30 m grids and aligned to be consistent with the observed inundation. To evaluate the mapping performances based on corresponding AFI values, the raster calculator function in ArcGIS is used to quantify the inundated/non-inundated area with number of pixels. The following section demonstrates the results from aforementioned methods with an evaluation on their performances.

RESULTS AND DISCUSSION

Inundation maps for the 2016 May flood event in the Brazos River using terrain-based, physical modeling methods and remote sensing classification technique are shown in **Figures 6A**, **6B**, **6C** and **6D**. In general, inundation areas derived from the iRIC and modified HAND methods have more overlaps with the observed inundation than the original HAND simulation. Also, the HAND simulation clearly misses a few areas considered inundated by all other two methods. As the advanced fitness indices (AFI) indicated, the HAND model has a 56% match with the observation, while iRIC and the modified HAND have higher AFI values of 70% and 67%, respectively. The modified HAND appears to delineate larger inundated area than iRIC, but still generates inferior AFI. As a supplementary approach to HAND, the modified HAND method is found to improve the AFI value by 11% with capturing a few missed areas. Interestingly, the inundation classified from satellite imagery has the least area of only 41.3 km^2, compared to the other three modeling approaches (55.9 km^2 for iRIC, 41.7 km^2 for HAND and 70.8 km^2 for

modified HAND). Although as shown in **Figure 6D**, the inundated area appears to have some discontinuous features or gaps, leading to the reduced inundation area, the authors consider the inundation from satellite imagery as the 'true' flooded area during the study.

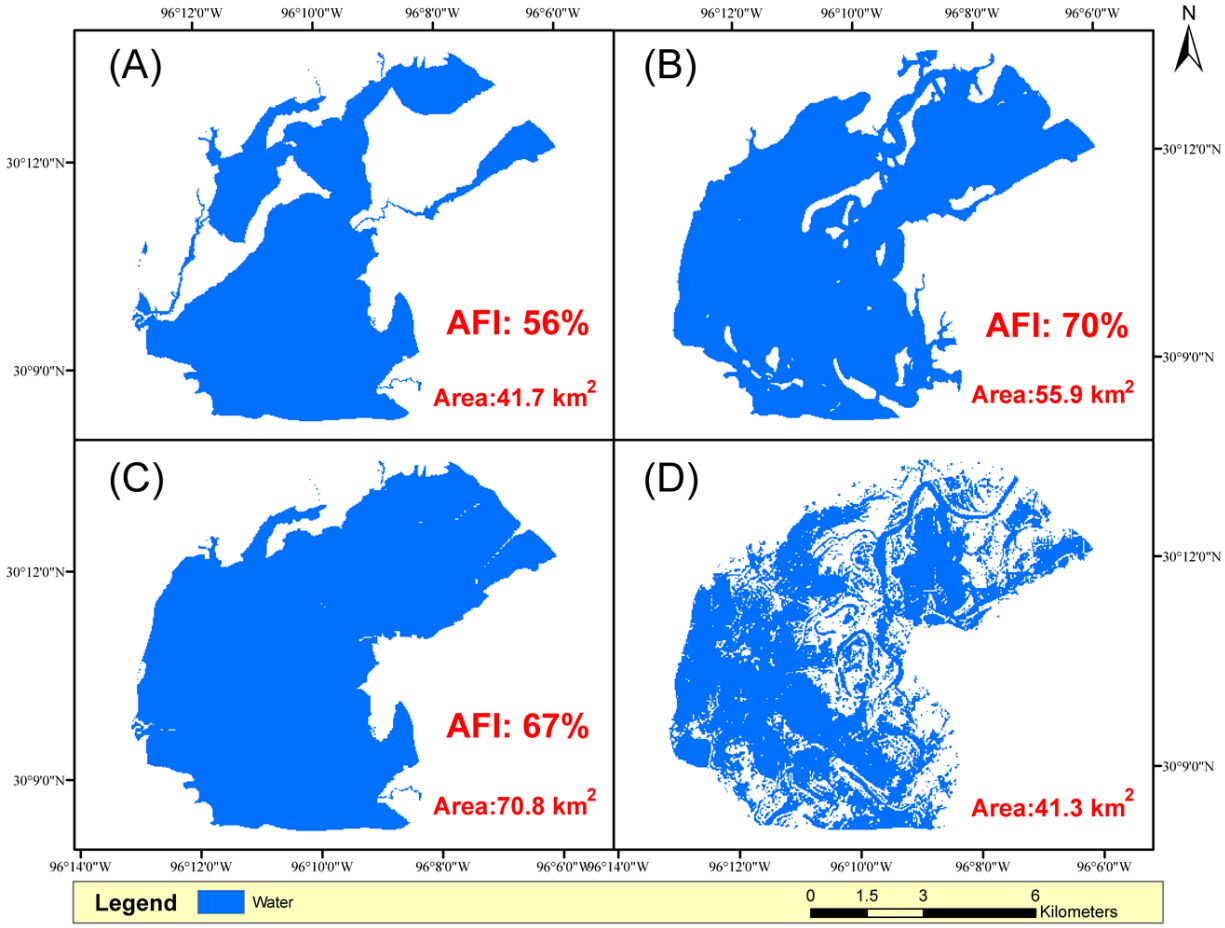

Figure 6. Results of inundation maps and fitness indices from simulation of (A) HAND, (B) iRIC, (C) Modified HAND, and (D) Satellite Observation.

Further investigation is performed to discover why HAND misses certain areas that are captured by the other two methods. Compared to HAND (**Figures 7A** and **7B**), an in-depth illustration for the improvement of the modified HAND simulation is shown in **Figures 7C** and **7D**. The left two panels (**7A** and **7C**) respectively show inundated areas of the HAND and modified HAND simulations on top of the topography. The two highlighted NHDPlus catchments 1 and 2

are chosen to exemplify the difference between the HAND and modified HAND methods. It is found that discrepancy between the results of two methods mainly takes place in catchment 2. Catchment 1 is located along the Brazos River main stem with a higher stream order than that of catchment 2 which drains into the main stream as tributary. The cross-sectional views of selected cutting line across catchment 1 and 2 with corresponding simulated water surface elevation (blue lines in the right panels) are shown in **Figures 7B** and **7D**, respectively. The disconnected water surface shown in **Figure 7B** indicates that the catchment-based calculation by HAND overlooks the inter-catchment flow. However, the water surface would be more realistically simulated as shown in **Figure 7D** if the modified HAND is strategically applied to the problematic areas. Therefore, the results show that the modified HAND can essentially replace the water depth of the low-stream-order catchment (catchment 2 herein) with that of the adjacent catchment with high stream order (catchment 1), instead of determining the inundation of the catchments based on their individual water depth solely.

Overall, iRIC is found to generate the best match with the observation in this case study. Bates and De Roo (2000) also reported in their study that two-dimensional models would perform better than terrain-based models when their resolution was similar. If the problematic catchments in HAND simulation are excluded from the comparison, the HAND and iRIC models would generate comparable AFI values (65% and 68% respectively). Such results indicate that aside from HAND's deficiency to model inter-catchment inundation, it has equivalent capability as iRIC in terms of matching the observation. This study suggests that simplification on the intricacy of flow dynamics employed by terrain-based models has relatively minor influence on peak inundation prediction. This finding confirms that using a simple terrain-based model could adequately simulate the flood inundation area as discovered by Bates and De Roo (2000).

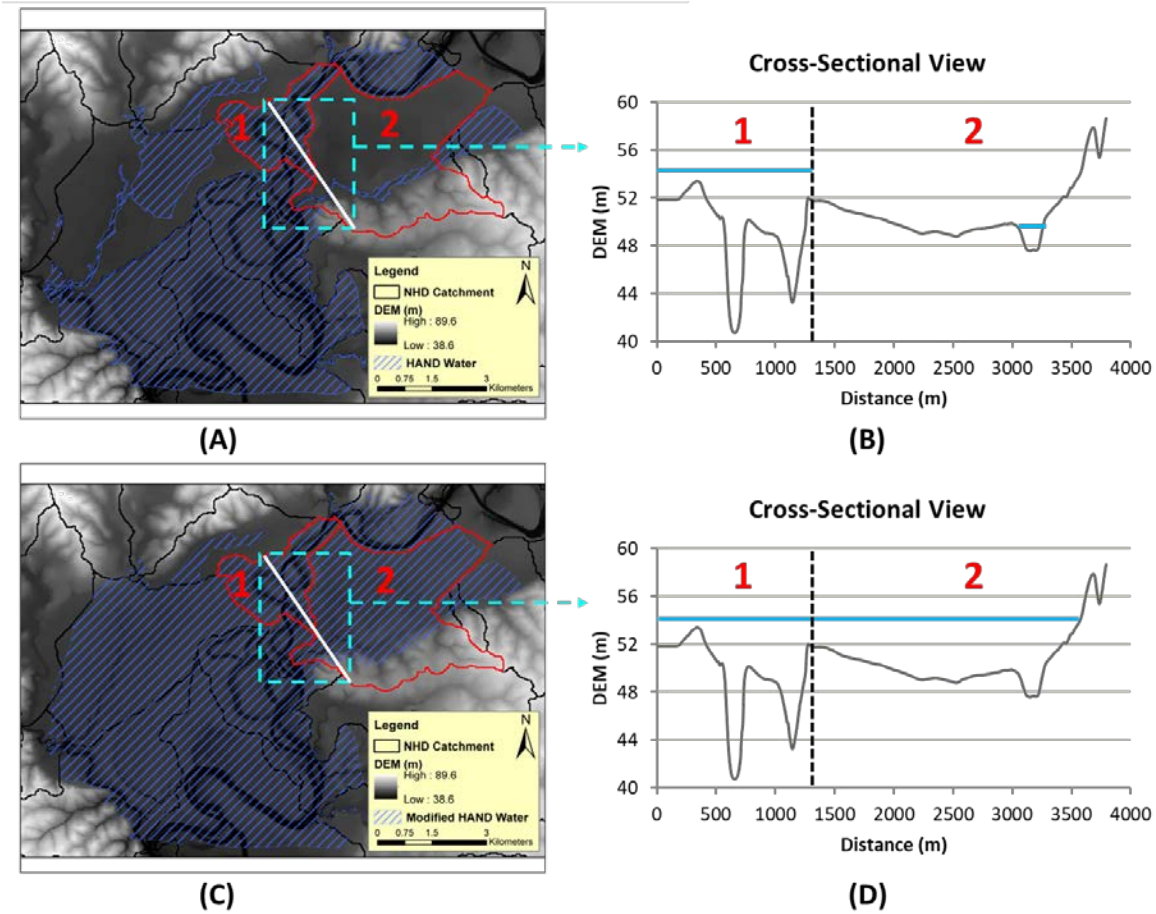

Figure 7. (A) Inundation map derived from HAND on top of DEM, (B) Cross-sectional view of the selected area and water surface simulated in HAND, (C) Inundation map derived from the modified HAND on top of DEM, (D) Cross-sectional view of the selected area and water surface simulated in modified HAND.

Although the dynamic-based model represented by iRIC in this study provides more accurate estimates under high flow conditions, the model needs intensive calibrations using various historical data to achieve a reliable performance (Nobre *et al*., 2016). Promisingly, terrain-based model, as represented by HAND in this study, demonstrates a unique inundation mapping capability for a river section without much historical data. Given the fact that solving the St.Venant

equations for hydraulic/hydrodynamic models through iterating process is very computationally expensive, their utility is limited in real-time flood prediction (Fang *et al.*, 2008). In our case, the iRIC model needs approximately 90 minutes (5,400 seconds) to run 1,500 iterations, while the HAND model only takes about 2 minutes (120 seconds) for 37 NHDPlus river reaches to generate the inundation. For a large-scale hydrologic forecasting system like the NWM, the HAND inundation mapping approach clearly shows benefits in coupling with the model as demonstrated in this study, potentially addressing the real-time continental-scale inundation mapping problem in an efficient way.

However, the HAND calculation does not explicitly reflect interactions between the main stem and its tributaries. This issue likely becomes more pronounced for larger riverine floods. In addition to the modified HAND, one remedy to this problem is to incorporate a mass balance process into the modeling framework as suggested by Bates and De Roo (2000). The authors think that while not observed in this study, the accuracy of the HAND model would be inferior to a traditional hydraulic model if the flooded area has complex urban hydraulic components like culverts, pipes and bridges. Therefore, extra caution should be taken when choosing proper inundation models for flood risk prediction due to the uncertainties in data requirement, computation demand, accuracy, types of land cover, etc.

CONCLUSIONS AND FUTURE WORK

This paper demonstrates a unique analysis of using terrain-based (NHDPlus-HAND and the modified HAND) and physical (iRIC-FaSTMECH) models to simulate the maximum inundation extents during the May 2016 flood event in the Brazos River, TX. A supervised classification method is used to classify water from Landsat 8 satellite imagery and generate an observed inundation map. To better understand and evaluate the performances of three methods,

the goodness of overlapping between the simulated and observed is quantified via the advanced fitness index (AFI). The main conclusions from this study are summarized as follows:

1. NHDPlus-HAND, the modified HAND and iRIC generated a fair (> 50% of AFI) fit with the satellite imagery. iRIC performed a slight better (~ 70% in AFI) than other two methods (NHDPlus-HAND and the modified HAND) during this extreme flood event.

2. Although the NHD catchment-based calculation does not allow NHDPlus-HAND to explicitly account for inter-catchment flows between the main stem and its tributaries, the modified HAND method provides a remedy to this issue when strategically applied to the areas overlooked by NHDPlus-HAND.

3. For extreme events, simplification on the intricacy of flow dynamics has relatively minor influence on predictions, which can positively justify the utility of NHDPlus-HAND for large-scale inundation mapping.

4. Even though the current version of NHDPlus-HAND may not be a superior choice for handling accurate inundation mapping for urban areas, its low computational cost and ease to couple with the National Water Model (NWM) provide great potential to support real-time continental inundation forecast in the future.

The authors think that there is room for future investigation in uncertainty analysis of observations using multiple sources of raw imagery along with various classification techniques. Potential sources of raw imagery will be used including synthetic aperture radar (SAR), unmanned aerial vehicle (UAV) and so on; while classification methods like Delta-cue change detection on pre/during flooding scenarios, normalized difference water index and image fusion techniques will

be also used to generate inundation extents. The results of the future research will be reported in a forthcoming paper.

Overall, this study presents a comprehensive examination made of remote sensing compared with HAND-based inundation mapping in a region of complex topography. Findings from this paper can also help identify potential improvements for HAND-based simulation. In light of frequent floods, the information provided from this study is valuable for the scientific/engineering communities, floodplain managers, emergency personnel and governmental entities that were impacted by the storm and/or had a vested interest in the region.

ACKNOWLEDGMENT

This research was conducted during the 2016 NOAA National Water Center (NWC) Summer Institute administered by the Consortium of Universities for the Advancement of Hydrologic Science, Inc. (CUAHSI). The authors would like to thank Peirong Lin and Adnan Rajib for their coordination and all the advisory faculty, theme leaders and coordinators involved in the 2016 Summer Institute. The authors would especially like to thank, Dr. David Maidment, Dr. Sarah Praskievicz and Dr. Richard McDonald for their generous support and thoughtful comments during the period of our project work.

Fang and Zhang would like to thank the Tarrant Reginal Water District (TRWD) and the National Science Foundation (NSF) under Grant No. CyberSEES-1442735 for their support. Tsang and Huang would like to thank Dr. Yi-Leng Chen for his assistance to the workshop travel and application. Cohen and Munasinghe would like to thank the University Corporation for Atmospheric Research (UCAR) and the NWC for their support via the COMET Program

Cooperative Project Grant under Cooperative Agreement No. Z16-23487 with the National Oceanic and Atmospheric Administration (NOAA).

LITERATURE CITED

Abbott, G., 2016. Request for Presidential Disaster Declaration — Major Disaster. http://gov.texas.gov/files/press-office/FederalDisasterRequest_06092016.pdf

Bates, P.D., M.G. Anderson, L. Baird, D.E. Walling, and D. Simm, 1992. Modelling Floodplain Flow with A Two-Dimensional Finite Element Scheme. *Earth Surface Processes and Landforms* 17: 575–588. DOI: 10.1002/esp.3290170604

Bates, P.D. and A.P.J. De Roo, 2000. A Simple Raster-based Model for Flood Inundation Simulation. *Journal of Hydrology* 236(1): 54-77. DOI: 10.1016/S0022-1694(00)00278-X

Chow, V.T., 1959. Open Channel Hydraulics. McGraw-Hill Book Company, Inc; New York, ISBN-13: 978-0070107762

Christian, J., L. Duenas-Osorio, A. Teague, Z. Fang, and P. Bedient, 2013. Uncertainty in Floodplain Delineation: Expression of Flood Hazard and Risk in A Gulf Coast Watershed. *Hydrological Processes* 27(19): 2774-2784. DOI: 10.1002/hyp.9360

Cook, Aaron and Venkatesh Merwade, 2009. Effect of Topographic Data, Geometric Configuration and Modeling Approach on Flood Inundation Mapping. *Journal of Hydrology* 377(1): 131-142. DOI: 10.1016/S0022-1694(00)00177-3

Crowder, D.W. and P. Diplas, 2000. Using Two-dimensional Hydrodynamic Models at Scales of Ecological Importance. *Journal of Hydrology* 230(3): 172-191. DOI: 10.1016/S0022-1694(00)00177-3

Conrad, D., M. Stout, and B. McNitt, 1998. Higher Ground: A Report on Voluntary Property Buyouts in the Nation's Floodplains. *National Wildlife Federation*, Vienna, Va.

Cunge, J.A., F.M. Holly, and A. Verwey, 1976. Practical Aspects of Computational River Hydraulics. Pitman, London, ISBN-13: 978-0273084426

Estrela, T., 1994. Use of A GIS in the Modelling of Flows on Flood-plains. In: *Proceedings of the 2nd International Conference on River Flood Hydraulics*, White, W.R. and J. Watts (Editors). Wiley, Chichester, UK, Vol. 177, p. 190.

Fang, Z., P.B. Bedient, J. Benavides, and A.L. Zimmer, 2008. Enhanced Radar-Based Flood Alert System and Floodplain Map Library. *Journal of Hydrologic Engineering* 13(10): 926-938. DOI: 10.1061/(ASCE)1084-0699(2008)13:10(926)

Fang, Z., P.B. Bedient, and B. Buzcu-Guven, 2011. Long-Term Performance of A Flood Alert System and Upgrade to FAS3: A Houston, Texas, Case Study. *Journal of Hydrologic Engineering* 16(10): 818-828. DOI: 10.1061/(ASCE)HE.1943-5584.0000374

Federal Emergency Management Agency (FEMA), 1992. Floodplain Management in the United States: An Assessment Report. *Federal Interagency Floodplain Management Task Force*, prepared by L. R. Johnston Associates.

Federal Emergency Management Agency (FEMA), 2003. Guidelines and Specifications for Flood Hazard Mapping Partners, Appendix C: Guidance for Riverine Flooding Analysis and Mapping. http:// www.fema.gov/pdf/fhm/frm_gsac.pdf.

Frazier, P.S. and K. J. Page, 2000. Water Body Detection and Delineation with Landsat TM Data. *Photogrammetric Engineering and Remote Sensing* 66(12): 1461-1468. DOI: 10.1109/Argo-Geoinformatics.2013.6621909

Fread, D.L., 1984. In: *Hydrological Forecasting*, Anderson, M.G. and T.P. Burt (Editors). Wiley, Chichester, Chapter 14.

Fread, D.L., 1993. In: *Handbook of Applied Hydrology*, Maidment, D.R. (Editor). McGraw-Hill, New York, Chapter 10.

Ho, L.T.K., M. Umitsu, and Y. Yamaguchi, 2010. Flood Hazard Mapping by Satellite Images and SRTM DEM in the Vu Gia–Thu Bon Alluvial Plain, Central Vietnam. *International Archives of the Photogrammetry, Remote Sensing and Spatial Information Science* 38(Part 8): 275-280.

Hollyday, E.F.,1976. Improving Estimates of Streamflow Characteristics by Using Landsat-1 Imagery. *U. S. Geological Survey, Journal of Research* 4: 517-531.

Horritt, M.S. and P.D. Bates, 2001. Predicting Floodplain Inundation: Raster-based Modelling versus the Finite-Element Approach. *Hydrological Processes* 15(5): 825-842. DOI: 10.1002/hyp.188

Hunter, N.M., P.D. Bates, M.S. Horritt, and M.D. Wilson, 2007. Simple Spatially-distributed Models for Predicting Flood Inundation: A Review. *Geomorphology* 90(3): 208-225. DOI: 10.1016/j.geomorph.2006.10.021

Interagency Advisory Committee on Waster Data (IACWD), 1982. Guidelines for Determining Flood Flow Frequency. *Bulletin 17B of the Hydrology Subcommittee*. Office of Water Data Coordination, U.S. Geological Survey, Reston, VA.

Kail, J., B. Guse, J. Radinger, M. Schröder, J. Kiesel, et al., 2015. A Modelling Framework to Assess the Effect of Pressures on River Abiotic Habitat Conditions and Biota. *PloS one* 10(6): e0130228. DOI: 10.1371/journal.pone.0130228

Kenney, T.A., and M.L. Freeman, 2011. Two-dimensional Streamflow Simulations of the Jordan River, Midvale and West Jordan, Utah. US Geological Survey Scientific Investigations Report 2011-5043. https://pubs.er.usgs.gov/publication/sir20115043

Khan, S.I., Y. Hong, J. Wang, K.K. Yilmaz, J.J. Gourley, R.F. Adler, et al., 2011. Satellite Remote Sensing and Hydrologic Modeling for Flood Inundation Mapping in Lake Victoria Basin: Implications for Hydrologic Prediction in Ungauged Basins. *IEEE Transactions on Geoscience and Remote Sensing* 49(1): 85-95. DOI: 10.1109/TGRS.2010.2057513

Ku, Y.H. and Y.D. Kim, 2014. Comparison of Two-dimensional Model for Inundation Analysis in Flood Plain Area. *Journal of Wetlands Research* 16(1): 93-102. DOI: 10.17663/JWR.2014.16.1.093

Lane, S.N., K.F. Bradbrook, K.S. Richards, P.A. Biron, and A.G. Roy, 1999. The Application of Computational Fluid Dynamics to Natural River Channels: Three-Dimensional versus Two-dimensional Approaches. *Geomorphology* 29(1): 1-20. DOI: 10.1016/S0169-555X(99)00003-3

Lin, P., M.A.Rajib, Z.L.Yang, M. Somos-Valenzuela, V. Merwade, D.R.Maidment, et al., 2017. Spatiotemporal Evaluation of Simulated Evapotranspiration and Streamflow over Texas using the WRF-Hydro-RAPID Modeling Framework. *Journal of the American Water Resources Association (JAWRA)* 1-15. DOI: 10.1111/1752-1688.12585

Liu Y.Y., D.R. Maidment, D.G. Tarboton, et al., 2016. A Cybergis Approach to Generating High-resolution Height Above Nearest Drainage (HAND) Raster for National Flood Mapping. CyberGIS Center Technical Report: CYBERGIS-TR-2016-005-i

Maidment, D.R., 2017. Conceptual Framework for the National Flood Interoperability Experiment. *Journal of the American Water Resources Association* 53(2): 245-257. DOI: 10.1111/1752-1688.12474

Maidment, D.R., and D. Djokic, 2000. Hydrologic and Hydraulic Modeling Support: With Geographic Information Systems. Environmental Systems Research Institute, Inc. (ESRI); Redlands, CA. ISBN-13: 978-1879102804

McDonald, R.R., J.P. Bennett, and J.M. Nelson, 2001. The USGS Multi-dimensional Surface Water Modeling System. In *Proceedings, 7th US Interagency Sedimentation Conference,* Reno, Nev., p. I-161-I-167.

McDonald, R.R., J.M. Nelson, P.J. Kinzel, and J. Conaway, 2005. Modeling Surface-water Flow and Sediment Mobility with the Multi-Dimensional Surface Water Modeling System (MD_SWMS). U.S. Geological Survey Fact Sheet 2005-3078. https://pubs.er.usgs.gov/publication/fs20053078

McGehee, R., L. Li, and E. Poston, 2016. The Modified HAND Method. In: *National Water Center Innovators Program Summer Institute Report*, Maidment, D.R., A. Rajib, P. Lin, and E.P. Clark (Editors). Consortium of Universities for the Advancement of Hydrologic Science, Inc. Technical Report No. 13, 122 p. DOI: 10.4211/technical.20161019

Merwade, V., F. Olivera, M. Arabi, and S. Edleman, 2008. Uncertainty in Flood Inundation Mapping: Current Issues and Future Directions. *Journal of Hydrologic Engineering* 13(7): 608-620. DOI: 10.1061/(ASCE)1084-0699(2008)13:7(608)

National Oceanic and Atmospheric Administration (NOAA), 2016. National Water Model: Improving NOAA's Water Prediction Services. http://water.noaa.gov/documents/wrn-national-water-model.pdf

Nelson, J.M., and R.R. McDonald, 1996. Mechanics and Modeling of Flow and Bed Evolution in Lateral Separation Eddies. *USGS Director's Approved report submitted to the USGS Grand Canyon Monitoring and Research Center*. http://www. gcmrc. gov/library/reports/GCES/Physical/hydrology/Nelson1996.pdf

Nelson, J.M., J.P. Bennett, and S.M. Wiele, 2003. Flow and Sediment-transport Modeling. *Tools in Fluvial Geomorphology* 18: 539-576.

Nelson, J.M., Y. Shimizu, T. Abe, K. Asahi, M. Gamou, et al., 2016. The International River Interface Cooperative: Public Domain Flow and Morphodynamics Software for Education and Applications. *Advances in Water Resources* 93: 62-74.

National Flood Insurance Program (NFIP), 2002. National Flood Insurance Program Description. Federal Emergency Management Agency. http://www.fema.gov/library/viewRecord.do?id=1480.

Nobre, A.D., L.A. Cuartas, M. Hodnett, C.D. Rennó, G. Rodrigues, A. Silveira, et al., 2011. Height Above the Nearest Drainage – A Hydrologically Relevant New Terrain Model. *Journal of Hydrology* 404.1: 13-29. DOI: 10.1016/j.jhydrol.2011.03.051

Nobre, A.D., L.A. Cuartas, M.R. Momo, D.L. Severo, A.Pinheiro, and C.A. Nobre, 2016. HAND Contour: A New Proxy Predictor of Inundation Extent. *Hydrological Processes* 30(2): 320-333. DOI: 10.1002/hyp.10581

Noman, N. S., E. J. Nelson, and A. K. Zundel, 2001. Review of Automated Floodplain Delineation from Digital Terrain Models. *Journal of Water Resource Planning and Management* 127(6): 394–402.

Pielke, R.A., M.W. Downton, and J.B. Miller, 2002. Flood Damage in the United States, 1926-2000: A Reanalysis of National Weather Service Estimates. Boulder, CO: University Corporation for Atmospheric Research.

Priestnall, G., J. Jaafar, and A. Duncan, 2000. Extracting Urban Features from Lidar Digital Surface Models. *Computers, Environment and Urban Systems* 24(2): 65-78. DOI: 10.1016/S0198-9715(99)00047-2

Rango, A., J. Foster, and V.V. Salomonson, 1975. Extraction and Utilization of Space Acquired Physiographic Data for Water Resources Development. *Journal of the American Water Resources Association* 11(6): 1245-1256. DOI: 10.1111/j.1752-1688.1975.tb01846.x

Romanowicz, R., K.J. Beven, J. Tawn, 1996. Bayesian Calibration of Flood Inundation Models. In: *Floodplain Processes*, Anderson, M.G., D.E. Walling, and P.D. Bates (Editors). Wiley, Chichester, pp. 333-360.

Rennó, C.D., A.D. Nobre, L.A. Cuartas, J.V. Soares, M.G. Hodnett, J. Tomasella, et al., 2008. HAND, A New Terrain Descriptor using SRTM-DEM: Mapping Terra-firme Rainforest Environments in Amazonia. *Remote Sensing of Environment* 112(9): 3469-3481. DOI: 10.1016/j.rse.2008.03.018

Shalaby, A. and R. Tateishi, 2007. Remote Sensing and GIS for Mapping and Monitoring Land Cover and Land-use Changes in the Northwestern Coastal Zone of Egypt. *Applied Geography* 27(1): 28-41. DOI: 10.1016/j.apgeog.2006.09.004

Smith, L. C., 1997. Satellite Remote Sensing of River Inundation Area, Stage, and Discharge: A Review. *Hydrological processes* 11(10): 1427-1439. DOI: 10.1002/(SICI)1099-1085(199708)11:10<1427::AID-HYP473>3.0.CO;2-S

Sollers, S. C., A. Rango, and D.L. Henninger, 1978. Selecting Reconnaissance Strategies for Floodplain Surveys. *Journal of the American Water Resources Association* 14(2): 359-373. DOI: 10.1111/j.1752-1688.1978.tb02173.x

Son, G., H. You, and D. Kim, 2014. Feasibility Calculation of FaSTMECH for 2D Velocity Distribution Simulation in Meandering Channel. *Journal of the Korean Society of Civil Engineers* 34(6): 1753-1764. DOI: 10.12652/Ksce.2014.34.6.1753

White F., 1974. Viscous Fluid Flow. McGraw-Hill, New York, ISBN-13: 978-1259002120

Zhang, J., D. Munasinghe, and Y.F. Huang, 2016. Comparison of Flood Inundation Mapping Techniques between Different Modeling Approaches and Satellite Imagery. In: *National Water Center Innovators Program Summer Institute Report*, Maidment, D.R., A. Rajib, P. Lin, and E.P. Clark (Editors). Consortium of Universities for the Advancement of Hydrologic Science, Inc. Technical Report No. 13, 122 p. DOI: 10.4211/technical.20161019

Chapter 3: Understanding the Re-infiltration Process to Simulating Streamflow in North Central Texas using the WRF-Hydro Modeling System [2]

Zhang. J., Lin, P., Gao, S., and Fang, Z. (2020). "Understanding the Re-infiltration Process to Simulating Streamflow in North Central Texas using the WRF-Hydro Modeling System". Journal of Hydrology, 124902. DOI: https://doi.org/10.1016/j.jhydrol.2020.124902

[2] Used with Permission from Wiley, the publisher of Journal of Hydrology, 2020

ABSTRACT

WRF-Hydro (Weather Research and Forecasting model-Hydrological modeling system), as the core engine of the United States National Water Model (NWM), has now been used in many hydrometeorological applications throughout the world. One important feature that WRF-Hydro introduced is to allow infiltration excess ("ponded water") for subsequent lateral re-distribution and soil re-infiltration, which is a major enhancement in terms of physical realism. However, due to a lack of direct observations, how well WRF-Hydro models re-infiltration is largely unknown. To gain an in-depth understanding of re-infiltration process under different hydrometeorological/geographical conditions with model parameter settings, we start conducting a series of idealized numerical experiments using 18 watersheds in North Central Texas as a testbed. Next, the model is automatically calibrated to best quantify re-infiltration amounts during two major storms (2010 Tropical Storm Hermine and 2015 May Event), which is accomplished by coupling the dynamically dimensioned search (DDS) algorithm with WRF-Hydro to achieve optimal calibration efficiency. The results show that re-infiltration has quite substantial impacts on streamflow simulation in WRF-Hydro, especially for areas with flat terrains and soils with high clay content. Among all examined factors, precipitation, saturated hydraulic conductivity (K_{sat}) and runoff partition parameter (REFKDT) are found to impose relatively higher impacts on both re-infiltration ratio and runoff coefficient. It is also found that the runoff coefficient and the re-infiltration ratio are positively correlated based on results from both hypothetical and real events, indicating re-infiltration effects can become more pronounced as flood potential increases. These findings collectively show the significance of representing the re-infiltration process in flood forecasting. Models that do not incorporate this process may be over-calibrated to compensate errors originated from the missing process.

KEY TERMS

WRF-Hydro; Run-on, Re-infiltration; Calibration; Saturated hydraulic conductivity, REFKDT; Runoff coefficient

HIGHLIGHTS

- Re-infiltration process simulated by WRF-Hydro is comprehensively assessed under various hydrometeorological/geographical conditions with different model parameters;
- A tailored calibration scheme that is coupled to WRF-Hydro for best quantifying the re-infiltration amount during two real events efficiently improves simulation results;
- Re-infiltration is more important for areas with flat terrain and soil with high clay content, and is positively correlated with runoff coefficient

1 INTRODUCTION

Flooding is the most frequent weather hazard that can cause serious fatalities and property damages (Morrs, 2010; Deb et al., 2018). Extreme weather and the impacts of climate change are expected to increase the frequency and severity of flood events globally (IPCC, 2014). To provide early warnings and improve the emergency response for floods, the National Water Model (NWM), a continental-scale high-resolution hydrologic forecasting system for the United States, has been brought into operations in August of 2016 (NOAA, 2016). This hydrologic forecasting system simulates discharge for 2.7 million NHDPlus (National Hydrography Dataset Plus) stream reaches and extends the watershed hydrology to continental hydrology (Maidment, 2017; Lin et al., 2017). The NWM is developed from the community-based WRF-Hydro model (Gochis et al., 2013), an architectural framework which couples the Noah land surface model (LSM) with multi-parameterization (Noah-MP; Niu et al., 2011) with atmospheric models and hydrological routing schemes. Since its operational use in the NWM, WRF-Hydro has been tested and applied in different regions throughout the world for a range of applications in predicting runoff/streamflow (Gochis et al., 2015; Senatore et al., 2015), floods (Yucel et al., 2015; Lin et al., 2018), and land-atmosphere feedbacks (Arnault et al., 2015).

While the enclosed Noah and Noah-MP components simulate the one-dimensional (1-D) soil–vegetation–atmosphere interactions between surface and atmosphere (Gochis and Chen 2003), WRF-Hydro further extends the calculation of the surface overland flow, saturated subsurface flow, channel routing, and baseflow processes on a 2-D gridded planar surface (Gochis et al., 2013). Prior to being transformed to overland flow, surface runoff in WRF-Hydro is described as infiltration excess while subsurface runoff is the vertical drainage accumulated at the bottom of the soil column. Other hydrological components, which are not the focus of this study,

include throughfall, direct soil evaporation, transpiration, re-evaporation of precipitation intercepted by the canopy, vertical soil water movement and a simple lake/reservoir routing scheme (Ek et al., 2003). In this study, we are particularly interested in one major enhancement that WRF-Hydro introduces, which is to allow the infiltration excess to remain as "ponded water" for subsequent lateral re-distribution in combined with precipitation in the following model time step (Yucel et al., 2015). When ponded water starts to move downslope as overland flow, an important process previously known as the "run-on" effect (Smith and Hebbert, 1979) will occur. The "run-on" process can be defined as the surface water running from the upstream areas on downslope areas where moisture deficit has not yet been satisfied (Corradini et al., 1998; Nahar, et al., 2004). In addition to the direct infiltration caused by rainfall-runoff process in the vertical direction, this "run-on" process can also be viewed as re-infiltration due to the runoff re-distribution (Güntner and Bronstert, 2004). Hereafter, we use the word "re-infiltration" to refer to this process for simplicity.

Previous studies using field/numerical experiments have observed that re-infiltration can cause a decrease in unit area runoff as watershed size increases (Yair and Kossovsky, 2002; Yair and Raz-Yassif, 2004; Gomi et al., 2008; Heras et al., 2010). Woolhiser et al. (1996) conducted numerical experiments and found that re-infiltration has a major impact on runoff peaks, volumes and time to peak as saturated hydraulic conductivity (K_{sat}) increases downslope. Nahar et al. (2004) examined the role of infiltration on field-scale infiltration and one-dimensional overland flow using analytical models and Monte-Carlo simulations. They found that field-scale mean of infiltration would increase in the presence of run-on, which in turn affects the hydrograph. Corradini et al. (1998, 2002) suggests the re-infiltration process cannot be disregarded especially

when the spatial randomness of soil properties is taken into account in hydrologic modeling as it produces a significant decrease in overland flow.

As an influencing factor to the re-infiltration process, K_{sat} has been the focal point in numerous previous studies investigating its heterogeneous effect on this process (e.g. Smith and Hebbert, 1979; Saghafian et al., 1995; Woolhiser et al., 1996; Nahar et al., 2004). Saghafian et al. (1995) solved the diffusive wave equations and Green-Ampt infiltration equation to examine the impacts of K_{sat} spatial variability, where they concluded strong sensitivity of runoff volume and peak to this parameter. Corradini et al. (1998, 2002) evaluated run-on effects under conditions of horizontal heterogeneity of K_{sat} using a model with kinematic wave approximation and conceptual infiltration approach, where they found the level of spatial correlation in K_{sat} is less important when the overland flow volume was appreciable. Nahar et al. (2004) found re-infiltration is less important when the ratio of rainfall intensity to K_{sat} is large.

Besides K_{sat} and precipitation, other hydrometeorological and geographic conditions such as soil moisture saturation degree, terrain slope as influencing factors to re-infiltration have been largely understudied. The reason behind the lack of research attentions is partly because this runoff re-distribution and subsequent re-infiltration is often ignored in traditional rainfall-runoff modeling (Nahar et al., 2004). Indeed, many flood modeling frameworks are based on conceptual models or simple water balance equations (e.g., Burnash et al.,1973; Bergström, 1992; Ponce and Shetty, 1995). Ignoring such processes is often justified as long as good model performance can be still achieved by finding appropriate model parameters. Contrary to these conceptual/simple models, most modern process-based distributed hydrologic models like DHSVM (Wigmosta et al., 1994), Tethys-Chloris (Fatichi et al., 2012), Ech2O (Maneta and Silverman, 2013), etc., can represent the re-infiltration process.

WRF-Hydro explicitly models the run-on process, which should yield more confidence in spatiotemporal representations of real-world physical processes. Therefore, we are motivated to more comprehensively investigate the role of re-infiltration with regard to streamflow simulation by leveraging WRF-Hydro as the ideal modeling platform.

In this paper, the authors seek to systematically answer the following questions: (1) How do different hydrometeorological conditions such as the intensity of precipitation, soil moisture levels affect re-infiltration? (2) How do different geographic conditions such as digital elevation model (DEM)/terrain slope, roughness, soil type influence re-infiltration? (3) How do model parameters impact the re-infiltration process? (4) What is the role of re-infiltration in real storm events and how important is it?

The paper is organized as follows: Section 2 describes the methodology of different scenarios experiments, including the study area, model configurations, simulations, and calibrations; Section 3 summarizes the results and conducts discussions; Section 4 provides the conclusions and insights gained from this study.

2 METHODOLOGY

2.1 STUDY AREA AND MODEL CONFIGURATIONS

The Upper Trinity River Basin (UTRB) is located in the North Central Texas with 16,602 km^2. Undeveloped portion of the land constitutes a large percentage of UTRB (**Figure 1A**), which makes infiltration loss a vital component in the regional hydrologic cycle. Moreover, sitting in a region of temperate mean climatological conditions (USACE, 2013), UTRB experiences occasional extremes of temperature and precipitation with relatively short duration. The complexity of infiltration process and climate variability imposes challenges to water resources engineering practices like flow frequency analysis and flood forecasting. **Figure 1B** shows the

configuration of domain with Digital Elevation Model (DEM) and the locations of USGS stream gauges with corresponding contribution areas.

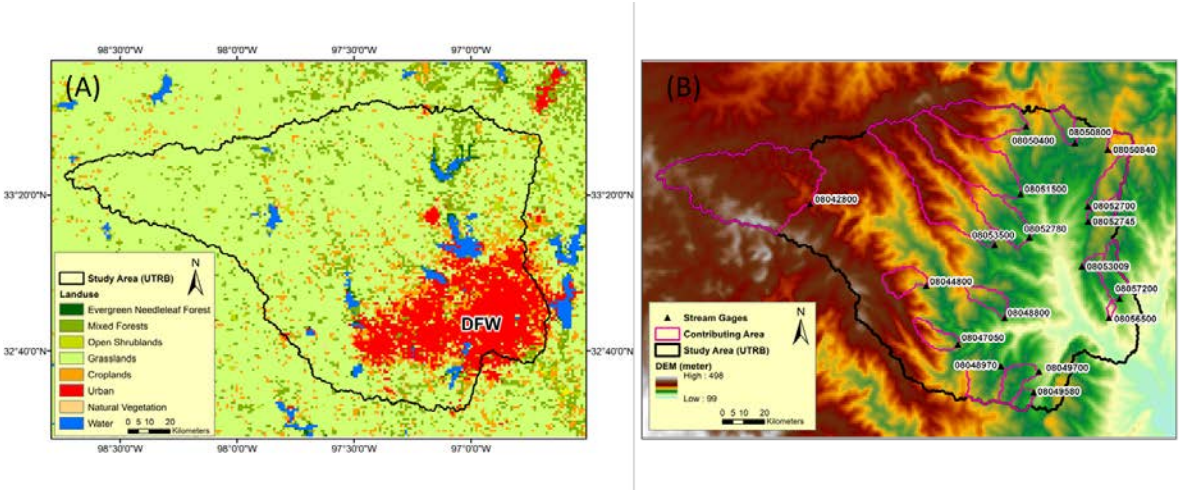

Figure 1: Study area and modeling domain. (A) Land use type. (B) Digital Elevation Model (DEM) and stream gauges with corresponding contributing area.

The complete description of the WRF-Hydro system version 5.0 can be found in Gochis et al. (2018). While the Noah-MP LSM provides several physical parameterizations, the same surface runoff option (free drainage) adopted by the NWM is used, where vertical surface runoff is calculated as excess water after precipitation supply infiltrates into the soil (Schaake et al. 1996). Within soil column (2 meters deep), Richards equation is deployed for infiltration of four layers, which have the thicknesses of 10, 30, 60, and 100 centimeters, respectively. Other hydrological processes are described in Niu et al. (2011), Yang et al. (2011), Cai et al. (2014), and Zheng and Yang (2016). A fully-unsteady, explicit diffusive wave formulation (Julien et al., 1995; Ogden, 1997) with steepest descent approach is deployed to solve overland flow routing. Subsurface lateral flow is calculated prior to overland flow, which allows exfiltration from fully saturated grid cells to be added to the infiltration excess calculated from the LSM (Senatore et al., 2015; Gochis et al., 2018). In order to represent overland and subsurface flow processes on higher spatial

resolution, the subgrid disaggregation-aggregation routines are used right after the main LSM loop and before the surface/subsurface routing loop; details are described in Gochis and Chen (2003). This study uses 1 km (in total 159×259 grid cells) and 100 m resolution for the LSM and hydrologic routing grids, respectively, with an aggregation factor of 10. Channel routing is solved using a variable-parameter Muskingum–Cunge (MC) method (see Gochis et al. 2018 for channel shape parameters used).

To allow for the flexibility to dismiss the re-infiltration process and simplify the use of related parameters, terrain routing can be turned off in WRF-Hydro as a namelist switching feature. Physically, the terrain-on and terrain-off scenarios in the model are illustrated in **Figure 2**. In terrain-on case (left), water available for infiltration includes both precipitation and overland surface runoff from upslope areas. While in terrain-off scenario (right), infiltration is caused by precipitation alone; hereafter, this process is referred as "local infiltration" (Corradini et al., 1998) to be differentiated from re-infiltration. With re-infiltration switched off, any infiltration excess is routed downstream without having chance to re-enter the soil columns, meaning local infiltration only; while the terrain-on scenario includes both local infiltration and re-infiltration. Switching on/off of this setting in WRF-Hydro allows us to perform a series of experiments to investigate and quantify re-infiltration.

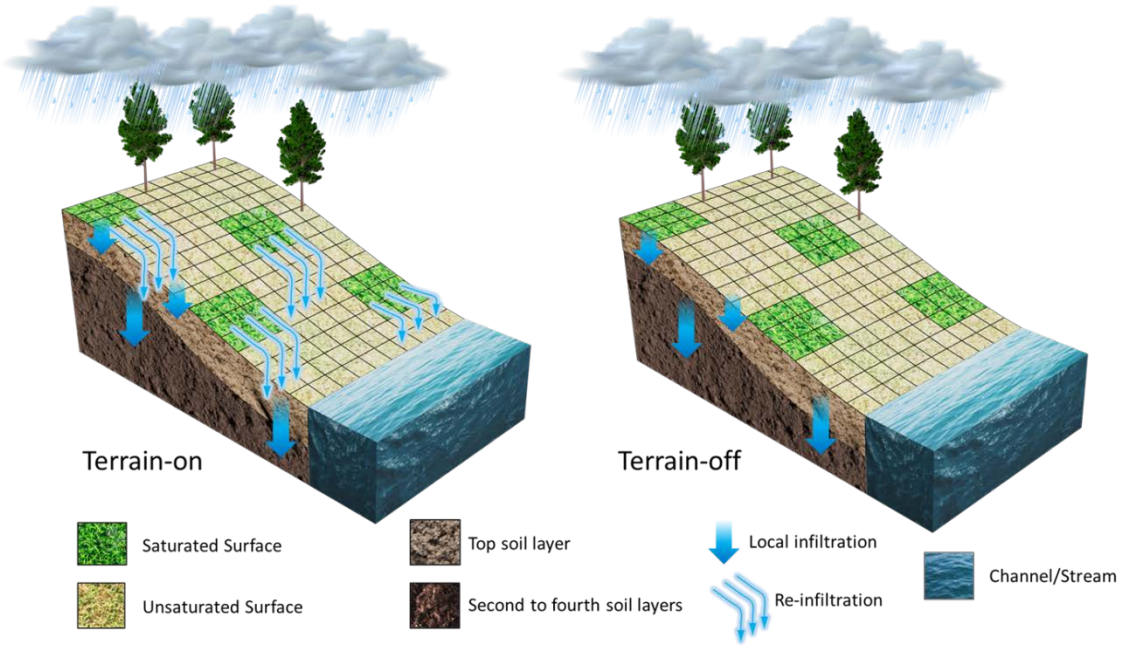

Figure 2: Illustration of mechanisms for terrain-on and terrain-off scenarios in WRF-Hydro.

2.2 MODEL EXPERIMENTS

We first conduct a series of idealized modeling experiments under different hydrometeorological, geographical conditions, and model parameters, as summarized below. Before each model run, a 1.5 months spin-up is conducted to achieve model equilibrium states which is considered appropriate for flood simulations with thin soils in Texas (Lin et al., 2018a; Lin et al., 2018b). Except for the experiments focusing on precipitation, other experiments all use 50.8 mm (2 inches) precipitation with 1-h duration. The amount of precipitation is chosen because it is approximately equivalent to a five-year storm as outlined in North Central Texas Council of Government integrated Stormwater Management Technical Hydrology Manual (NCTCOG iSWM, 2010). Other forcing variables (incoming shortwave and longwave radiation, specific humidity, air temperature, surface pressure and near surface u- and v-wind) are set to idealized conditions, which have either constant values in space and time or a fixed diurnal cycle (Gochis et al., 2018). The detailed forcing information can be found in **Table 1**. For each experiment, we conduct a 48-

h model run to ensure adequate time for water to flow from upstream to the outlet. In total, we conduct 9 sets of idealized modeling experiments with 150 runs.

Table 1. Description of idealized forcing input

Variable Name	***Range and Unit of Values***	***Timing***
Shortwave radiation	0 – 900 W/m^2	Diurnal cycle
Longwave radiation	375 – 425 W/m^2	Diurnal cycle
Specific humidity	0.01 kg/kg	Constant
Air temperature	287 – 293 K	Diurnal cycle
Surface pressure	100,000 Pa	Constant
Wind speed at u direction	1.0 m/s	Constant
Wind speed at v direction	1.0 m/s	Constant

2.2.1 Hydrometeorological Conditions

Table 2 shows the experimental design for varying input precipitation values and initial soil moisture. The precipitation is applied for a 1-h duration during the first hour of simulation with a total amount of 12.7 mm (0.5 inches) to 127 mm (5 inches), and the same precipitation is uniformly spread for the entire study area. Precipitation amount with 127 mm (5 inches) is approximately equivalent to a 500-year storm in the study region, which is set as the upper limit to cover all possible precipitation scenarios. For initial soil moisture, different saturation levels are applied to the top three soil layers (0-10 cm, 10-40 cm, and 40-100 cm) based on each grid cell's soil type at the start of each model simulation. Changing the saturation of the fourth layer (100-200 cm) is not included because saturating the fourth layer will lead to unrealistically high runoff amount (not shown here), due to the fact that Texas is dominated by thin soils with less than 1 meter (Furl et al., 2018; Lin et al., 2018). Therefore, it would be physically unreasonable to investigate the model sensitivity to the saturation level in the fourth soil layer.

Table 2. Experimental design for precipitation input and initial soil moisture condition

Setting		***Unit***	***Values***
Precipitation		mm	12.7, 25.4, 38.1, 50.8, 63.5, 76.2, 88.9, 101.6, 114.3, 127
Initial soil moisture	First layer	$m^3 m^{-3}$	Multiply maximum soil moisture by 0.2, 0.4, 0.6, 0.8, 1.0
	Second layer	$m^3 m^{-3}$	Multiply maximum soil moisture by 0.2, 0.4, 0.6, 0.8, 1.0
	Third layer	$m^3 m^{-3}$	Multiply maximum soil moisture by 0.2, 0.4, 0.6, 0.8, 1.0

2.2.2 Geographical Conditions

The experimental design for varying terrain slope and saturated hydraulic conductivity (K_{sat}) is shown in **Table 3**. Terrain slope is modified by changing the digital elevation model (DEM) underlying the model simulation. The terrain slope of study basins ranges from 0.31% to 1.12% with an average of 0.64%, and different multipliers were applied to change the terrain slope. Various multiplication factors are also uniformly applied for K_{sat} in each grid cell.

Table 3. Experimental design for terrain slope and saturated hydraulic conductivity

Setting	***Unit***	***Values***
Terrain slope	%	Multiply by 1, 2, 4, 6, 8, 10, 20
Saturated hydraulic conductivity	m/s	Multiply by 0.1, 0.5, 1.0, 1.5, 2.0, 2.5, 3, 4, 5

2.2.3 Model Parameters

Five empirical model parameters are selected for sensitivity analyses based on literature review (Senatore et al., 2015; Yucel et al., 2015; Silver et al., 2017; Kerandi et al., 2018), which includes REFKDT, RETDEPRTFAC, LKSATFAC, OVROUGHRTFAC, and SLOPE. These five parameters are unitless, often with no interpretable physical meaning, and are suggested to be adjusted through model calibration. Even in a physically-based model like WRF-Hydro, these physically-insignificant parameters are also unavoidable, which is resulted from our inability to

model all processes (Wagener and Montanari, 2011) hampering our understanding on other physically-based process components. Therefore, these parameters are carefully studied here.

REFKDT (K_{dtref}) is a constant parameter used with REFDK (K_{ref}), which corresponds to the saturation hydraulic conductivity for silty clay loam. Niu (2011) documented that REFKDT can significantly influence surface infiltration and partition of total runoff into surface and subsurface runoff, where increasing REFKDT leads to decrease in surface runoff (Schaake et al., 1996; Niu, 2011). The equation involving REFKDT (K_{dtref}) is

$$K_{dt} = K_{dtref} \times \frac{K_{sat}}{K_{ref}} \tag{1}$$

Where K_{sat} is saturated hydraulic conductivity, K_{ref} is saturated hydraulic conductivity for silty clay loam, and K_{dt} is a constant for calculating the maximum soil infiltration rate (I_{max}):

$$I_{max} = \frac{P \times \{\frac{d_{tot} \times \left[1 - e^{(-K_{dt} \times \Delta t)}\right]}{P + d_{tot} \times \left[1 - e^{(-K_{dt} \times \Delta t)}\right]}\}}{\Delta t} \tag{2}$$

where P is the effective precipitation intensity, d_{tot} is the total soil water depth (m) and Δt is the duration of time step.

RETDEPRTFAC, LKSATFAC, and OVROUGHRTFAC are multipliers for surface retention depth, lateral saturated hydraulic conductivity, and overland roughness, respectively. SLOPE is a coefficient for deep drainage. They have been documented in previous studies as sensitive parameters for runoff simulation, thus are chosen in this study. **Table 4** shows the experiment values for the model parameters; the default values of these parameters are globally uniform.

Table 4. Experimental design for model parameters

Parameters	*Unit*	*Min*	*Max*	*Default*	*Values*
REFKDT	–	0.5	5	3	0.5, 0.6, 0.7, 0.8, 0.9, 1, 1.5, 2, 3, 4, 5
RETDEPRTFAC	–	0	10	1	0, 1, 2, 4, 6, 8, 10
LKSATFAC	–	10	10000	1000	10, 100, 500, 1000, 5000, 10000
OVROUGHRTFAC	–	0.1	5	1	0.1, 0.5, 1, 2, 3, 4, 5
SLOPE	–	0.1	1	0.1	0.1, 0.5, 1

2.3 REAL CASE SIMULATION AND CALIBRATION

WRF-Hydro is configured in an "offline" mode (hydro components do not feedback to WRF) for two real case simulations: 2010 tropical storm Hermine (Sep 8th, 2010) and 2015 May storm (May 28th, 2015). To ensure adequate spin-up time, the model is initialized on July 1st, 2010 and April 1st, 2015, respectively, leaving about 1.5-2 months for model to spin-up. The North American Land Data Assimilation System (NLDAS-2) forcing variables and the National Centers for Environmental Prediction (NCEP) quality-controlled Stage IV precipitation estimates are utilized as the input meteorological forcings. **Figure 3** shows the spatial pattern of cumulative precipitation amounts for these two storm events by 4-km Stage IV product.

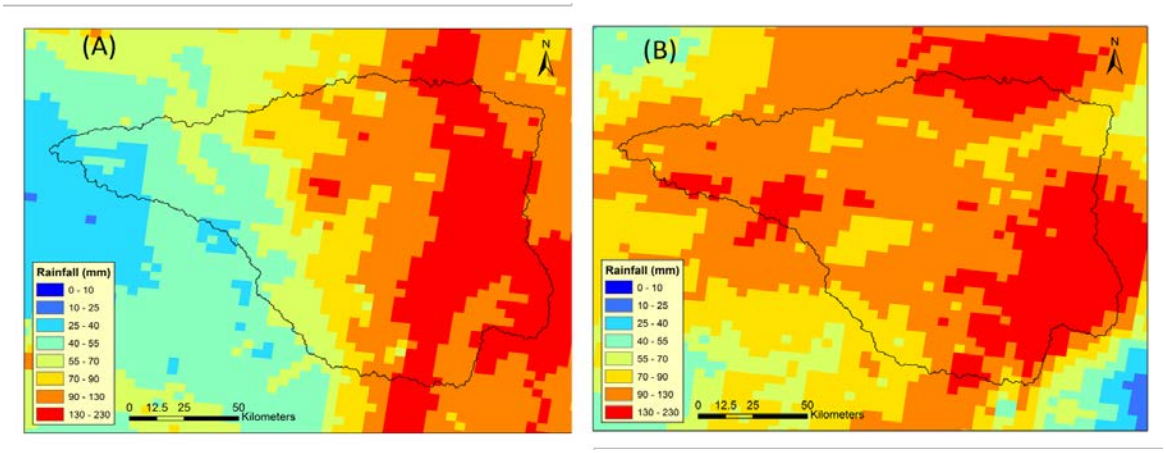

Figure 3: Cumulative precipitation amount from Stage IV estimates. (A) 2010 Tropical Storm Hermine (9/8/2010 00:00 UTC – 9/10/2010 23:00 UTC). (B) 2015 May Event (5/28/2015 00:00 UTC – 5/30/2015 23:00 UTC).

To obtain the best estimates of the local infiltration and re-infiltration amounts during the selected storm events, WRF-Hydro is calibrated with terrain-routing for 18 USGS stream gauges **(Figure 1B**). We utilize the dynamically dimensioned search (DDS) algorithm (Tolson and Shoemaker, 2007) for calibrations, because it was demonstrated to be suitable for computationally expensive and spatially-distributed models. Compared to other algorithms, DDS converges faster and can reach good global solutions within certain iterations (Tolson and Shoemaker, 2007). In a nutshell, DDS starts from a global search then switches to a more local search by dynamically adjusting the dimension of parameters; the adjustment from global to local search is achieved by dynamically and probabilistically reducing the number of dimensions in the neighborhood (Tolson and Shoemaker, 2007). To further expedite calibration, the simulation domain is reconfigured such that it is tailored to the 18 contributing basins towards all evaluation USGS gauges. The reduced simulation domain significantly shortens runtime per iteration, which allows us to assign a relatively large iteration number for improving calibration results. Lespinas at al. (2018) presents that the improvements in minimizing objective function using DDS are notable between 100 to 500 iterations and relatively moderate after 500 iterations. In terms of the objective function, Root-Mean-Square-Error (RMSE) indicates the magnitude of errors (streamflow difference) in time series between the simulated and observed hydrographs (Gupta et al., 2009). Based on the recommended information from previous studies, 500 iterations of DDS are used in the calibration with an objective function to minimize RMSE.

2.4 HYDROLOGIC METRICS

2.4.1 Re-infiltration Calculation

Re-infiltration amount is not a direct output from WRF-Hydro, but can be calculated by subtracting local infiltration value from total infiltration value (**Equation 3**).

Re-infiltration (mm) = Total infiltration (mm) – Local infiltration (mm) (3)

Based on the principle of water balance and considering negligible evapotranspiration during intense storm events, total infiltration can be calculated by subtracting runoff volume from precipitation amount in terrain-on simulation; local infiltration can be calculated by subtracting runoff volume from precipitation amount in terrain-off scenario. Re-infiltration ratio is defined as re-infiltration amount divided by total infiltration. In some occasions, re-infiltration ratio can be larger than 1, and this is interpreted as surface exfiltration occurring from saturated soil columns (Gochis et al., 2018).

2.4.2 Runoff Coefficient

Runoff coefficient has been widely used in hydrologic practices, ranging from flood frequency analyses (e.g. Gottschalk and Weingartner, 1998; Sivapalan et al., 2005) to flood forecasting (e.g. Borga et al., 2011). For a given storm event, runoff coefficient is defined as the portion of precipitation that becomes direct runoff. Higher (lower) runoff coefficient indicates more (less) flood proneness, and it is used to understand its relationship with re-infiltration ratio.

2.4.3 Calibration Statistics

Four statistics are used to evaluate the streamflow simulation results, including Pearson Correlation Coefficient (CC), Nash-Sutcliffe Efficiency (NSE), Root-Mean-Square-Error (RMSE), and Normalized Bias (NBIAS) (**Equations 4 – 7**).

$$CC = \frac{cov(Q_{obs}, Q_{mod})}{\sigma_{obs}\sigma_{mod}} \quad (4)$$

$$NSE = 1 - \frac{\sum_{i=1}^{n} (Q_{mod}^{i} - Q_{obs}^{i})^2}{\sum_{i=1}^{n} (Q_{obs}^{i} - \overline{Q_{obs}})^2} \quad (5)$$

$$RMSE = \sqrt{\sum_{i=1}^{n} (Q_{mod}^{i} - Q_{obs}^{i})^2 / n} \quad (6)$$

$$NBIAS = \frac{\sum_{i=1}^{n} (Q_{mod}^{i} - Q_{obs}^{i})}{\sum_{i=1}^{n} Q_{obs}^{i}} \quad (7)$$

where Q_{mod} and Q_{obs} denote the simulation and observation values, cov is the covariance, σ_{obs} and σ_{mod} represent standard deviation of the simulation and observation; $\sum_{i=1}^{n}$ means to sum up each time step from i =1 to n, and n is the number of time steps.

Each of these metrics is interpreted differently to facilitate a more comprehensive understanding of the model performance. CC (**Equation 4**) measures how strong a co-varying relationship is between the modeled results and the observation, which cannot be used to assess model biases. NSE (**Equation 5**) and RMSE (**Equation 6**) are two most commonly used criteria in hydrological evaluations, and they measure both the variability of time series and the magnitude of errors (Gupta et al., 2009). NSE normalizes the squared model error, using the variance of the observed data, and thus a value of zero suggests that the model is only as good as the mean observed data, while NSE = 1 suggests perfect model simulation and negative values indicate that the observation mean is a better predictor than the model (Gupta and Kling, 2011). NBIAS (**Equation 7**) is calculated to identify both the magnitude and the sign of errors as normalized by the mean of the observations.

3 RESULTS AND DISCUSSION

Idealized Numerical Experiments

Figure 4A shows the range, interquartile range, and median value of total infiltration at varying precipitation intensities; the range shows the variability among 18 gauges across the study domain. As the precipitation intensity becomes greater, the median total infiltration first increases rapidly, and then becomes steady. Because the precipitation input is only applied at the first hour of the simulation, so "precipitation intensity" is interchangeably used below as "precipitation amount". The one to one line in **Figure 4A** represents the situation where 100% of precipitation is infiltrated. For lower precipitation intensities (< 25.4 mm/hr), precipitation in all tested catchments

is completely infiltrated – indicated by the total infiltration values aligning with the reference line. For greater precipitation intensities, variation in the catchments' total infiltration starts to emerge as indicated by the increased range and interquartile range. This is related to the combination of antecedent soil moisture, soil properties, geographical factors in various catchments starts to exhibit differences within increasing precipitation intensity. Nonetheless, soils in some catchments still take in most of the precipitation even at high precipitation intensities as indicated by the upper limit of total infiltration values. Similar to **Figure 4A**, **Figures 4B** and **4C** show the same statistics (range, interquartile range, and median value) of local and re-infiltration for various precipitation intensities. In **Figure 4B**, it is counterintuitive for some local infiltration values to get below zero, which means that exfiltration occurred and runoff is thus greater than precipitation under the corresponding precipitation intensity and the "terrain-off" routing option. According to our approach of calculating re-infiltration (Section 2.4.1), the exfiltration condition causes the corresponding re-infiltration to be greater than total infiltration. Same as the case of total infiltration, greater precipitation intensities give rise to variations, or more precisely, heterogeneities among the catchments in local- and re-infiltration processes.

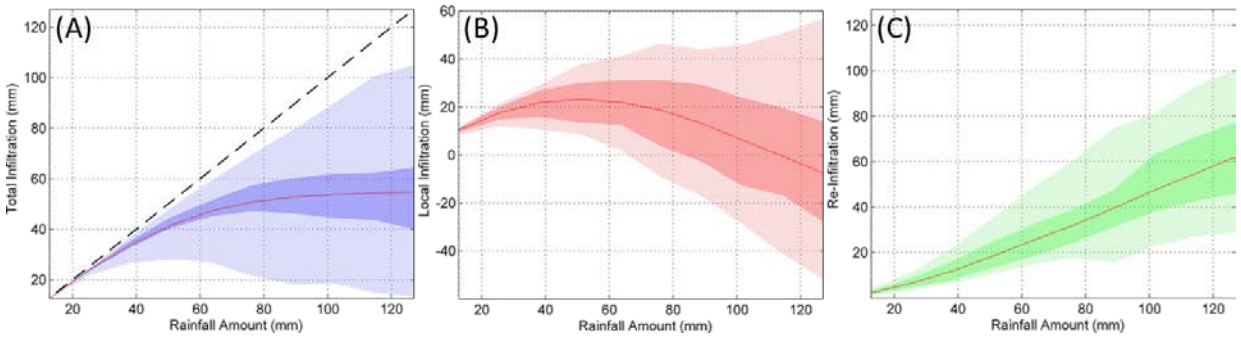

Figure 4: The range, interquartile range, and median value of (A) total infiltration, (B) local infiltration, and (C) re-infiltration amount for varying precipitation intensities.

Figures 5A to **5C** show total infiltration, local infiltration, and re-infiltration values at various saturation levels of initial soil moisture in the first soil layer (0−10 cm). Similarly, **Figures 5D** to **5F** and **5G** to **5I** show the trends of total, local and re-infiltration in the second (10−40 cm) and third (40−100 cm) soil layers, respectively. It can be found that in all three soil layers, as initial soil moisture gets closer to saturation, total infiltration and local infiltration both slowly decrease, while re-infiltration slightly increases. This behavior of re-infiltration seems counterintuitive because one may expect soil layers of higher saturation levels would result in smaller amount of re-infiltration due to decreased soil storage for water to go in. However, it has to be understood that local infiltration over the hillslopes happens prior to re-infiltration. Higher antecedent soil moisture means decreased local infiltration, which leaves more water available for going downstream over the hillslopes and re-infiltrating subsequently. Overall, local infiltration is still the dominant pathway for infiltration while re-infiltration is a secondary effect. It is also found that all three types of infiltration are most sensitive to change of soil moisture in the third layer of soil possibly because of its greater thickness/storage compared to the upper two soil layers.

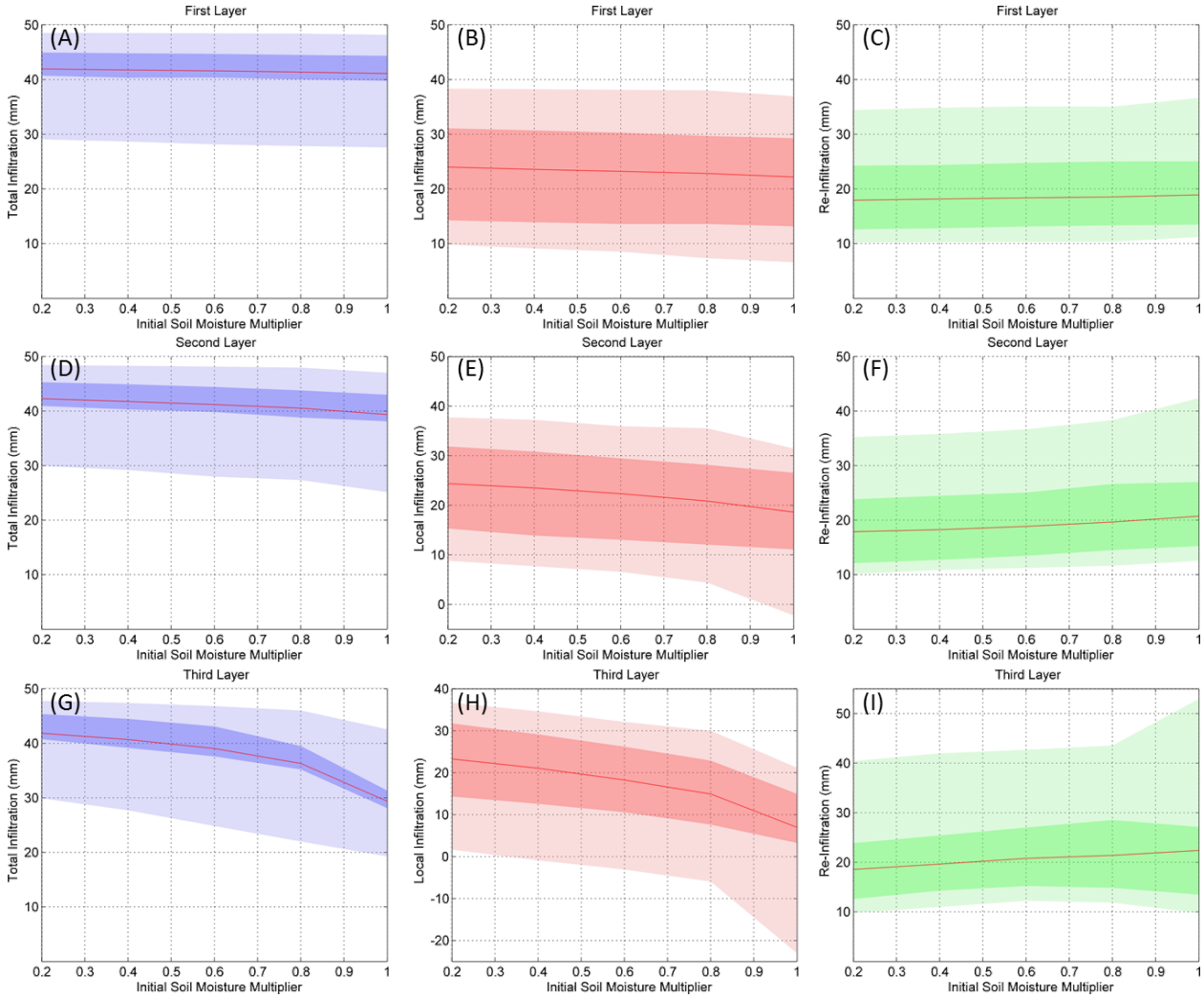

Figure 5: The range, interquartile range, and median value of different infiltration component for varying initial soil moisture conditions in different soil layers. (A)-(C) Total, local, and re-infiltration amount when changing initial soil moisture in first layer (0 - 10 cm); (D)-(F) Total, local, and re-infiltration amount when changing initial soil moisture in second layer (10 cm - 30 cm); (G)-(I) Total, local, and re-infiltration amount when changing initial soil moisture in third layer (30 cm - 100 cm).

Figures 6A to **6C** show the total infiltration, local infiltration, and re-infiltration values at various terrain slope levels, respectively. While local infiltration is generally unaffected by terrain slope, the total- and re-infiltration both first decrease and then become stable as terrain becomes

steeper. Note that local infiltration is calculated by only considering water transfer in the vertical columns of soil, plant, and atmosphere (in the Noah-MP LSM), thus it does not change as terrain slope changes. In comparison, re-infiltration is an augmented module by WRF-Hydro to describe the water loss during lateral water transfer pathways, therefore it can be influenced by terrain slope and thereby further influencing total infiltration amount. These results suggest that by neglecting re-infiltration, the effect of terrain slope on total infiltration may be underestimated. This is especially important for study domains of lower terrain slopes - the most obvious differences are seen for terrain slopes with smaller multipliers (less than 5). For steeper terrain slope ranges (multiplier smaller than 5), faster overland flow rate is expected and therefore it gives less chance for water to re-infiltrate, which explains why limited effect is seen in steeper terrain slope conditions. In addition to the above, we also found that the ranges and interquartile ranges of the three types of infiltration are almost constant with varying terrain slopes across gauges. This is in contrast with **Figure 4** and **Figure 5** where the ranges are generally larger, indicating little interaction between terrain slope and other factors in affecting infiltration processes.

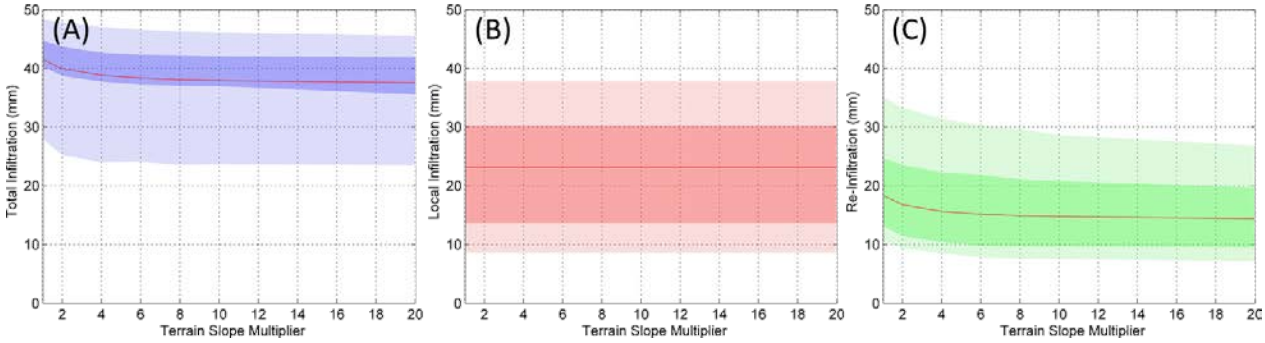

Figure 6: The range, interquartile range, and median value of (A) total infiltration, (B) local infiltration, and (C) re-infiltration amount for varying terrain slope.

Figures 7A, **7B**, and **7C** show the trends of total, local and re-infiltration as saturated hydraulic conductivity (K_{sat}) changes, respectively. First, local infiltration is found to increase with

greater K_{sat} because soil with higher K_{sat} is easier for water to pass through. Re-infiltration decreases with higher K_{sat} while total infiltration first increases rapidly and then becomes stable. The reason is that higher K_{sat} leads the majority of water to infiltrate locally, leaving less water to be re-distributed to downstream areas where re-infiltration occurs. In other words, water has a higher tendency or priority to infiltrate locally than re-infiltrate somewhere downstream. This finding is consistent with Niu et al. (2014) that larger K_{sat} facilitates surface water to infiltrate into deeper soils by gravity instead of flowing laterally. However, for soils with smaller K_{sat}, precipitation rate can readily exceed infiltration rate, which leaves more surface water for re-distribution and re-infiltration. In addition, for the three types of infiltration, the variation among tested catchments all decreases with greater K_{sat} values, as indicated by the decrease in the ranges. As K_{sat} increases, precipitation in any catchment is more likely to fully infiltrate via either local infiltration or re-infiltration or both. In essence, precipitation intensity, as the upper limit of infiltration rate, interacts with K_{sat} in affecting infiltration processes.

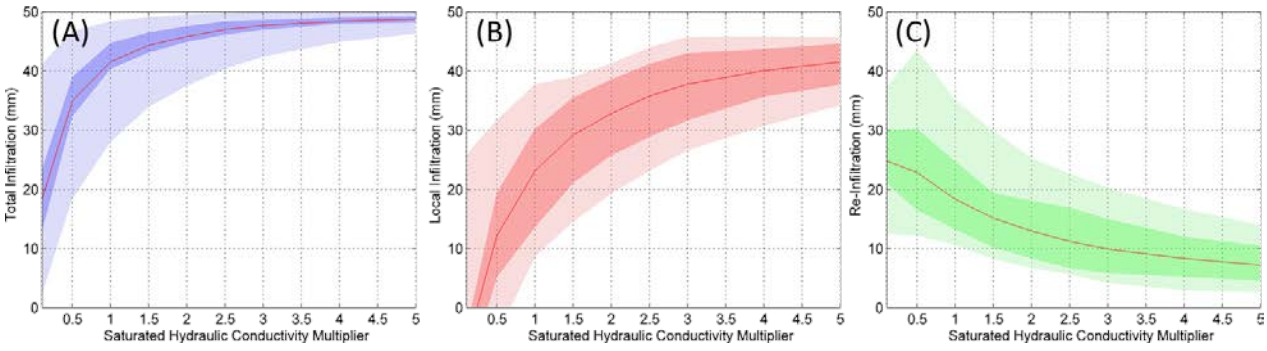

Figure 7: The range, interquartile range, and median value of (A) total infiltration, (B) local infiltration, and (C) re-infiltration amount for varying scale factor of saturated hydraulic conductivity.

After testing five model parameters (RETDEPRTFAC, LKSATFAC, SLOPE, REFKDT, and OVROUGHRTFAC), we found that infiltration processes are only sensitive to REFKDT and

OVROUGHRTFAC as shown in **Figures 8** and **9**. Note that the REFKDT essentially controls the partition between surface and subsurface runoff, and greater REFKDT means less (more) surface (subsurface) runoff. Such an effect is evident in **Figure 8B** where local infiltration increases with greater REFKDT, which is also consistent with findings from previous studies (Schaake et al., 1996; Niu, 2011). Contrary to local infiltration, re-filtration decreases with greater REFKDT. Re-infiltration reacts to the changing factor after the local influence. As seen previously in **Figures 5** and **7**, re-infiltration appears to be a secondary route for water to transfer into subsurface than local infiltration. The increasing trend of total infiltration flattens when REFKDT exceeds 3 (ranging from 0.5 to 5) due to the complete infiltration of precipitation. This is very similar to the case shown in **Figure 9A:** greater OVROUGHRTFAC slows down the water transfer over hillslopes and retains the runoff for infiltration to the point where 100% of precipitation seeps into soils. In **Figures 9B** and **9C**, it is found that local infiltration is not affected by the OVROUGHRTFAC values, while re-infiltration first increases rapidly and then slowly with greater OVROUGHRTFAC. The reason is that rougher surfaces cause slower overland flow rate further giving water more chance to re-infiltrate.

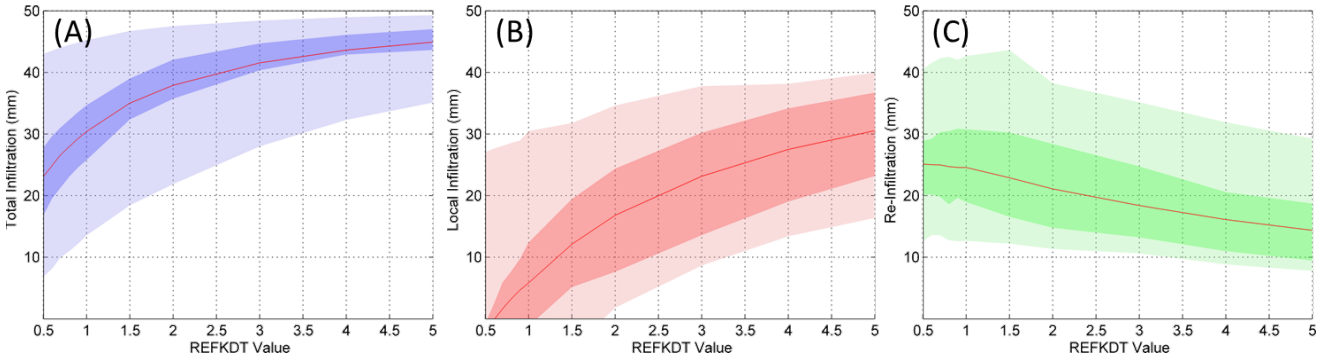

Figure 8: The range, interquartile range, and median value of (A) total infiltration, (B) local infiltration, and (C) re-infiltration amount for varying REFKDT value.

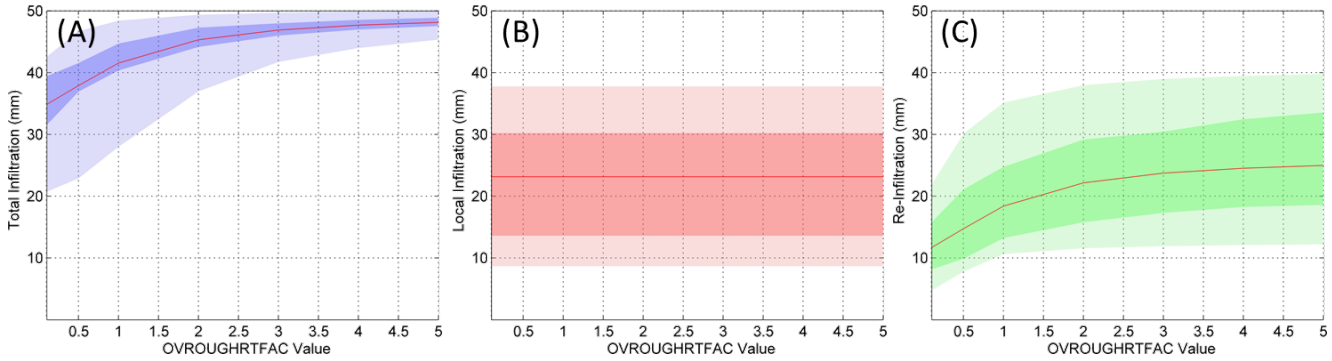

Figure 9: The range, interquartile range, and median value of (A) total infiltration, (B) local infiltration, and (C) re-infiltration amount for varying OVROUGHRTFAC value.

In summary, based on the experiments above, a common finding is reached as follows. Local infiltration is a more direct route than re-infiltration through which water transfers down into soils. Under the principle of mass conservation, the changes in local and re-infiltration due to a single factor can be opposite to each other as seen in the cases of precipitation intensity (**Figure 4**), K_{sat} (**Figure 7**), and REFKDT (**Figure 8**). More (less) water infiltrating locally means less (more) water to re-distribute to downstream cells and re-infiltrate. Such observation makes more sense when variations of the three types of infiltration are examined (**Figures 7** and **8)** among tested catchments: As the factor (K_{sat} or REFKDT) increases, total infiltration become less varied among the 18 catchments while variation of local- and re-infiltration remains steady. The common explanation is that the increasing factor causes precipitation to fully infiltrate in many catchments via both local- and re-infiltration, thus yielding the decreasing variation of total infiltration; and in these catchments where total infiltration is constrained, local- and re-infiltration yield the same sum though each bearing considerable variations among different catchments. When a factor only affects water transfer over the hillslopes instead of vertically, re-infiltration changes independently from local infiltration as seen in **Figure 6** and **Figure 9**.

The experiments also highlight the factors that can lead to increased re-infiltration while having no effect on or decreasing local infiltration. For instance, mild terrain slope and lower K_{sat} results in more re-infiltration while local infiltration is unaffected or even less (**Figures 6** and **7**). These results suggest that re-infiltration play an important role in hydrological processes for areas with flat terrain and clayey soils and thus needs to be sufficiently represented in hydrologic simulations. In order to better illustrate the portion of re-infiltration in total infiltration while assessing its relationship with flood potential, re-infiltration ratios and the corresponding runoff coefficients are shown in **Figures 10A** to **10F**. In **Figure 10**, results from one catchment are plotted as one dotted line. In scenarios of varying precipitation intensities (**Figure 10A**), initial soil moisture conditions (**Figure 10B**), K_{sat} values (**Figure 10C**), and REFKDT values **(Figure 10D**), we can consistently see that re-infiltration ratio increases with greater runoff coefficient. Although with varying terrain slopes (**Figure 10E**) and OVROUGHRTFAC values (**Figure 10F**) re-infiltration ratios show a decreasing trend with a magnitude much smaller than the other cases. We further use box-plots (**Figures 11A** and **11B**) to summarize the variance of re-infiltration ratios and variance of runoff coefficients as resulted from changes in different factors. It is found that precipitation, K_{sat}, and REFKDT have higher impact on both re-infiltration ratio and runoff coefficient compared to the other factors, which confirms our earlier conclusions.

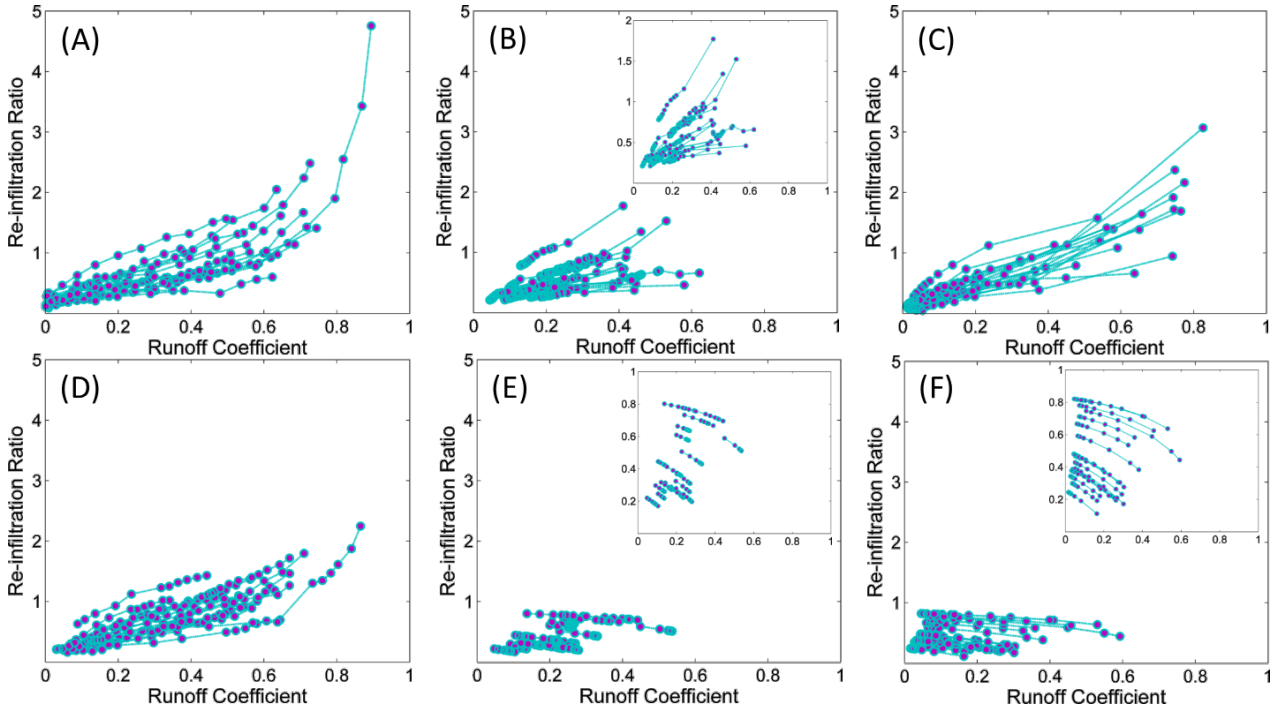

Figure 10: Trends of re-infiltration ratio for various runoff coefficients in different scenarios: (A) precipitation, (B) initial soil moisture, (C) saturated hydraulic conductivity, (D) REFKDT, (E) terrain slope, and (F) OVROUGHRTFAC. In each figure, one series of points is the result for one gauge and results of 18 gauges are plotted in total.

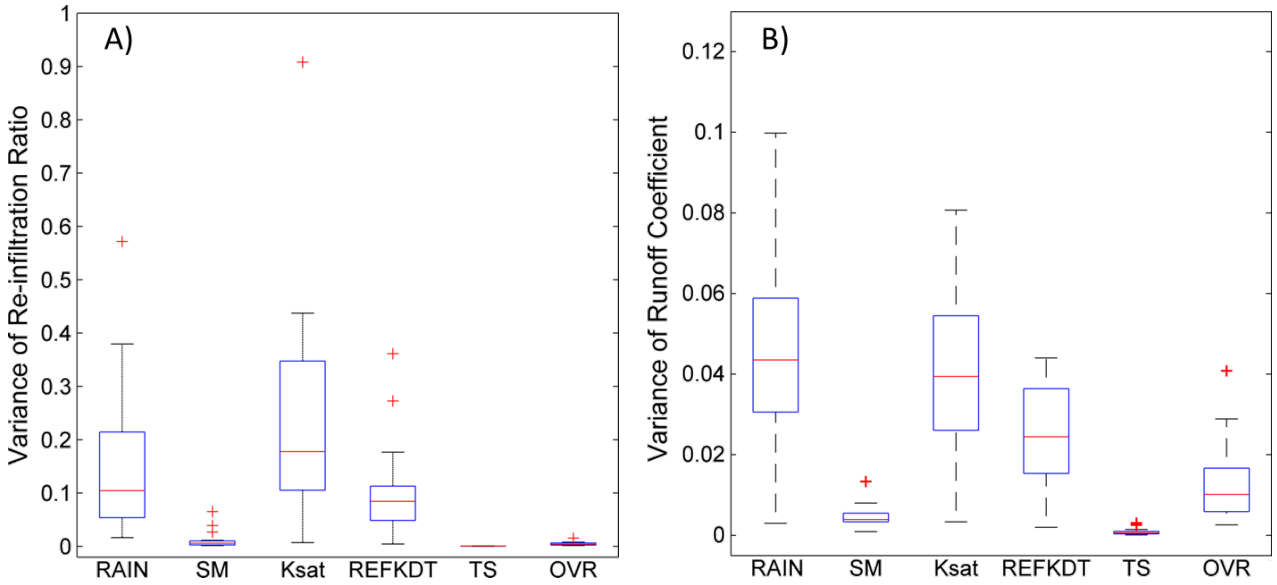

Figure 11: Box-plots of (A) variance of re-infiltration ratios (B) variance of runoff coefficient due to the change of different factors: precipitation (RAIN), soil moisture (SM), saturated hydraulic conductivity (Ksat), REFKDT, terrain slope (TS), and overland roughness (OVR).

Real Case Simulation and Calibration

Based on the above idealized modeling experiments, we choose 6 parameters for model calibration using DDS for the real-event simulation, which includes soil parameter K_{sat}, empirical runoff parameter REFKDT, scale factor of overland roughness OVROUGHRTFAC, and channel parameters (bottom width BtmWdth, side slope ChSlp, and Manning's roughness N). **Figures 12** and **13** show the comparisons of uncalibrated, calibrated and observed hydrographs at different gauge locations with for 2010 Hermine and 2015 May Storm, respectively. The default parameterization (uncalibrated) is used to benchmark the calibration results because it represents the current setting in the operational National Water Model. Note that there is no available discharge observations at two gauges (ID: 08048800, 08056500) during 2010 Hermine and thus results from only 16 gauges are plotted in **Figure 12**. After calibration, we can see great improvements at most gauges. **Figure 14** summarizes the CC, NSE, RMSE, and NBIAS statistics with boxplot. Our model calibration strategy brings CC and NSE much closer to 1, and RMSE and NBIAS much closer to 0. Improvement in RMSE and NBIAS indicates that calibration effectively corrected the underestimation of flow rates in the default simulation. The much narrower range of all four statistics also suggest that the calibration consistently improves the simulation performances at all tested gauges (**Figure 14**). The satisfactory calibration enables us to quantify the re-infiltration amount with better assurance during different types of storm events and covering a wide range of locations, which would be otherwise difficult to obtain due to a lack of existing observation techniques.

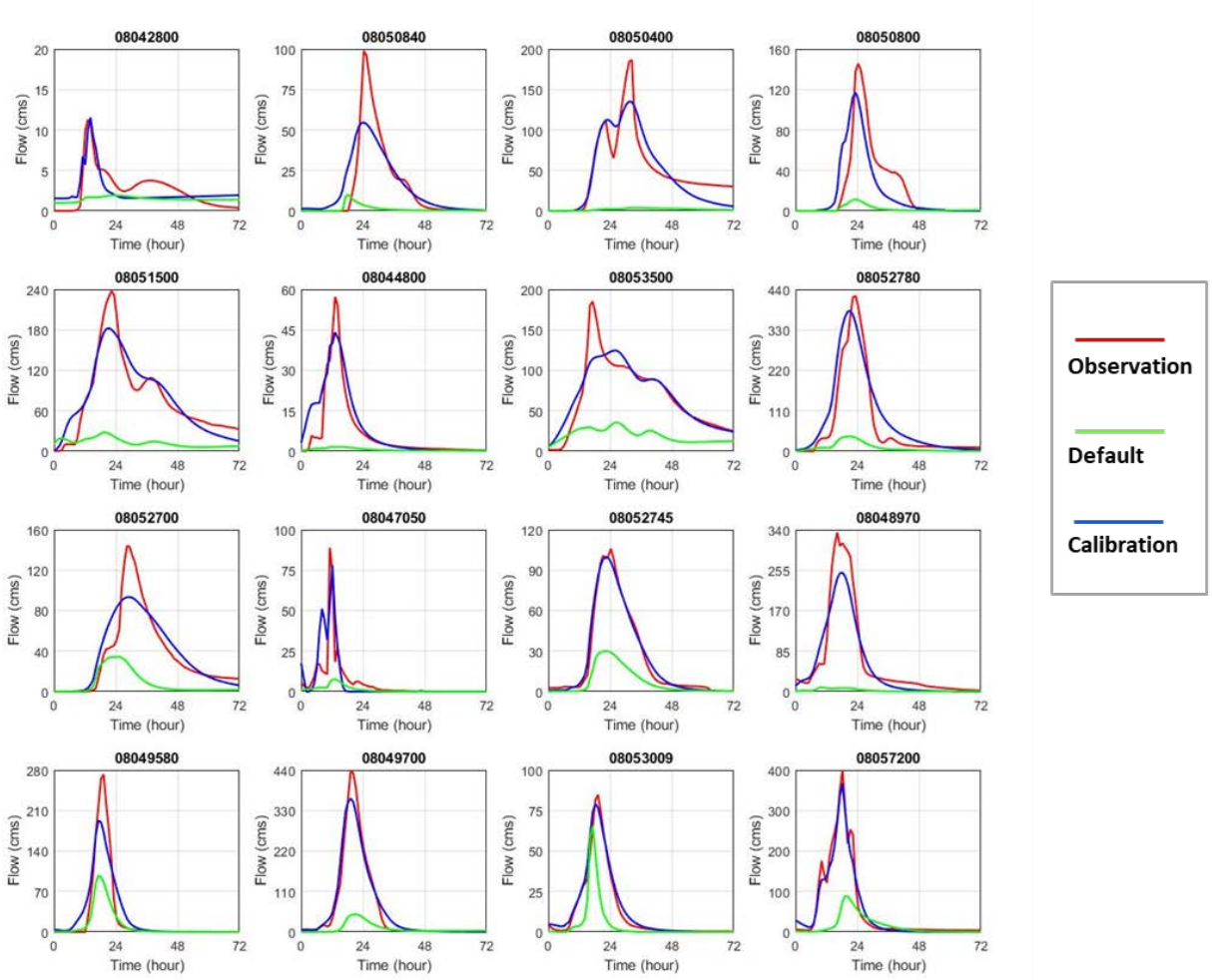

Figure 12: Calibration results of 2010 Tropical Storm Hermine for 16 gauges.

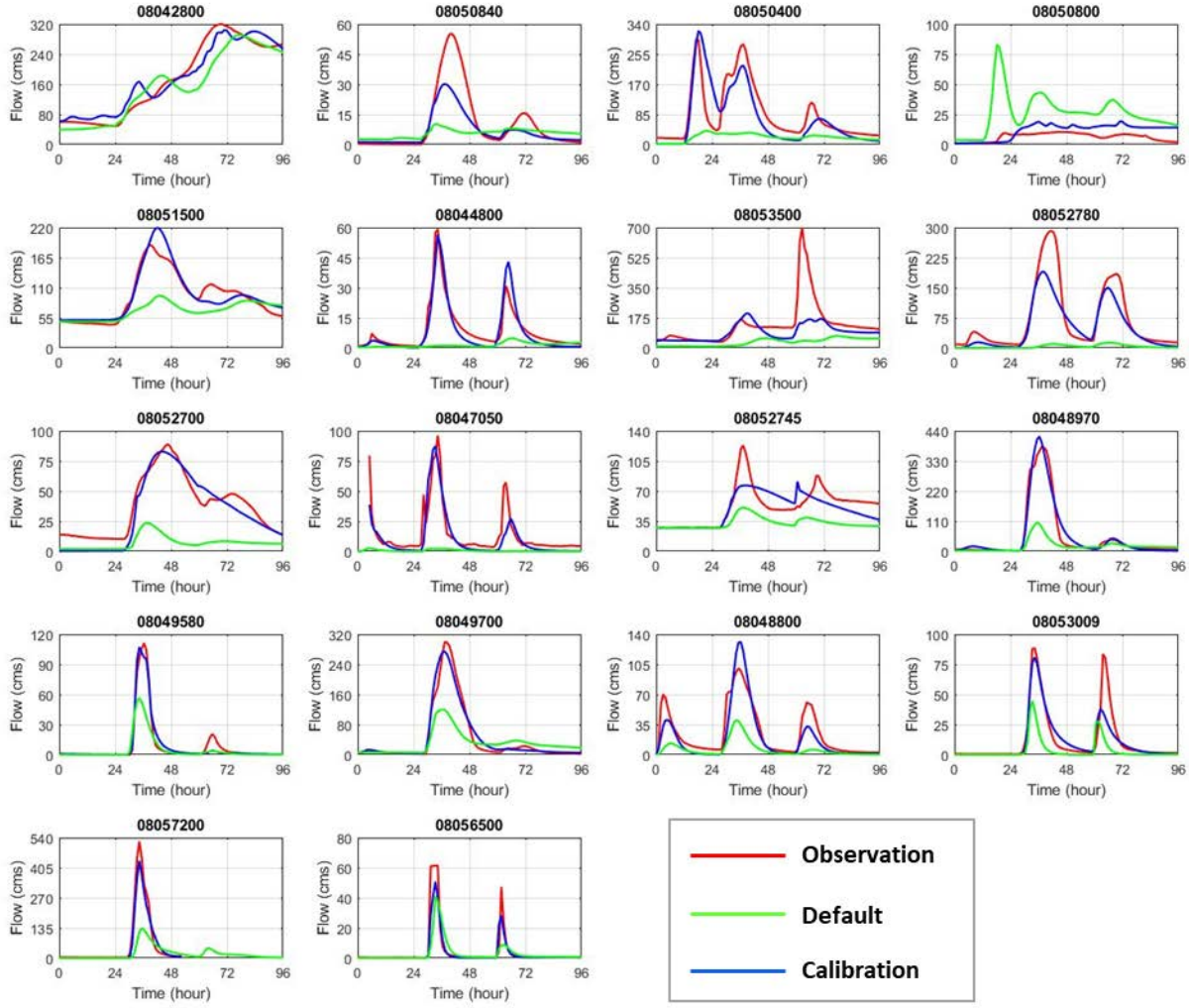

Figure 13: Calibration results of 2015 May Event for 18 gauges.

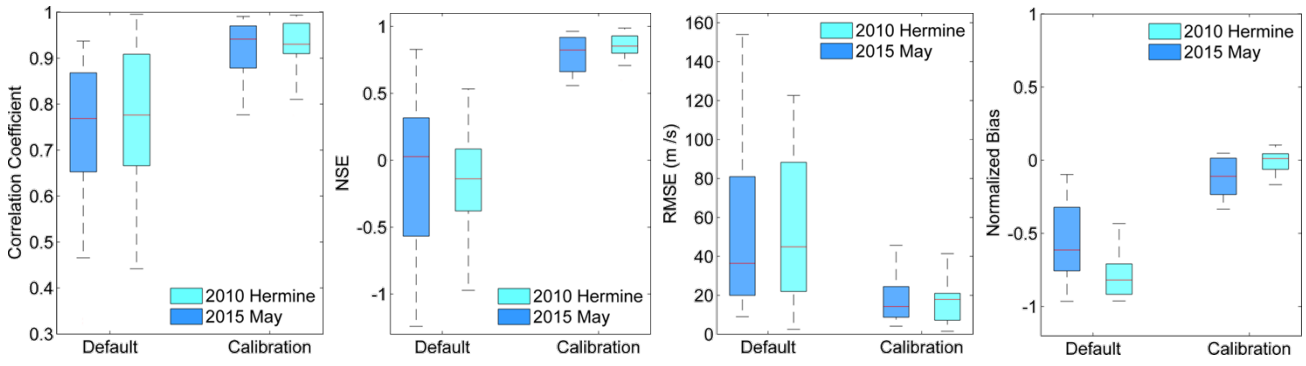

Figure 14: Before- and after-calibration statistics of 2010 Hermine (16 gauges) and 2015 May Event (18 gauges).

To calculate re-infiltration in the calibrated simulation, another set of "terrain-off" simulations are conducted using the calibrated parameters in order to get values required by **Equation 3**. **Figure 15** shows the relationship between runoff coefficient and re-infiltration ratio at all the testing catchments. It can be found that runoff coefficient and re-infiltration ratio are positively correlated, with the runoff coefficient ranging from 0 to 1. This is consistent with the idealized cases of varying precipitation, K_{sat}, initial soil moisture and REFKDT (see **Figures 10A** to **10D**). Scenarios with re-infiltration ratio being greater than one are noted, which possibly indicates that exfiltration would occur under terrain-off routing option. However, these six dots with seemingly unreasonable re-infiltration ratio are all from 2015 May event. To further investigate the possible reasons behind this, we examined the antecedent soil moisture and soil types (**Figure 16**), where we found these exfiltration processes are generally occurred in sub-basins with two common features, i.e., clayey soils and high antecedent soil moisture (>80% saturated in the top layer). Before our target event in May 2015, several storms occurred in North Central Texas, which have almost saturated the soil (Lin et al. 2018). These soil columns could very easily reach full saturation, and thus exfiltration may occur with much water contained in the soil storage. Without considering the re-infiltration process, the added amount of runoff from exfiltration would have no chance to enter the soils but to directly become streamflow in the channel. Should a calibration be conducted under such circumstance, parameters could be wrongfully adjusted to compensate the missing re-infiltration process.

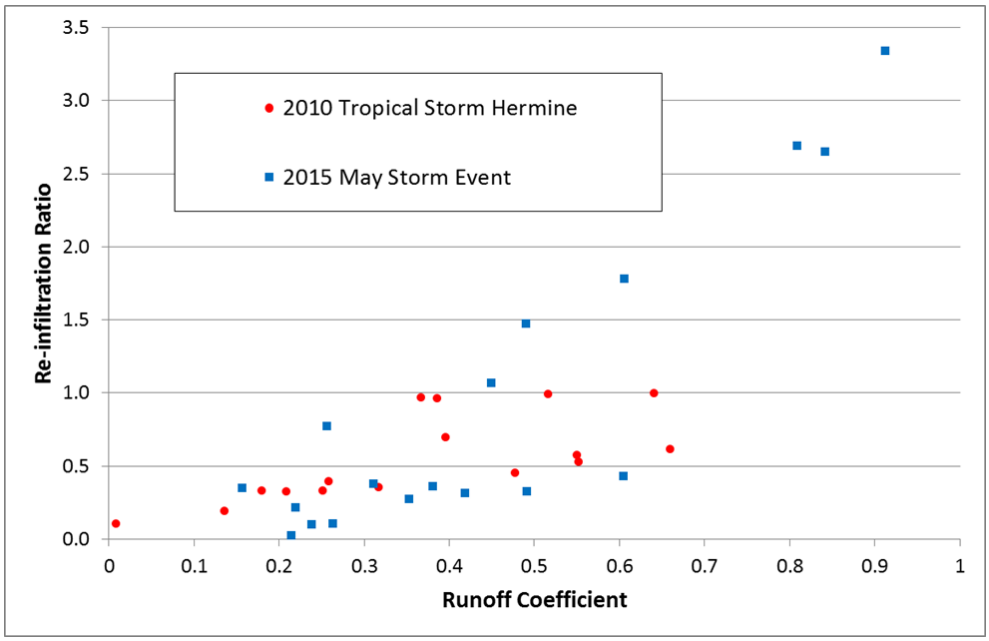

Figure 15: Trends of re-infiltration ratios for various runoff coefficients in two real events.

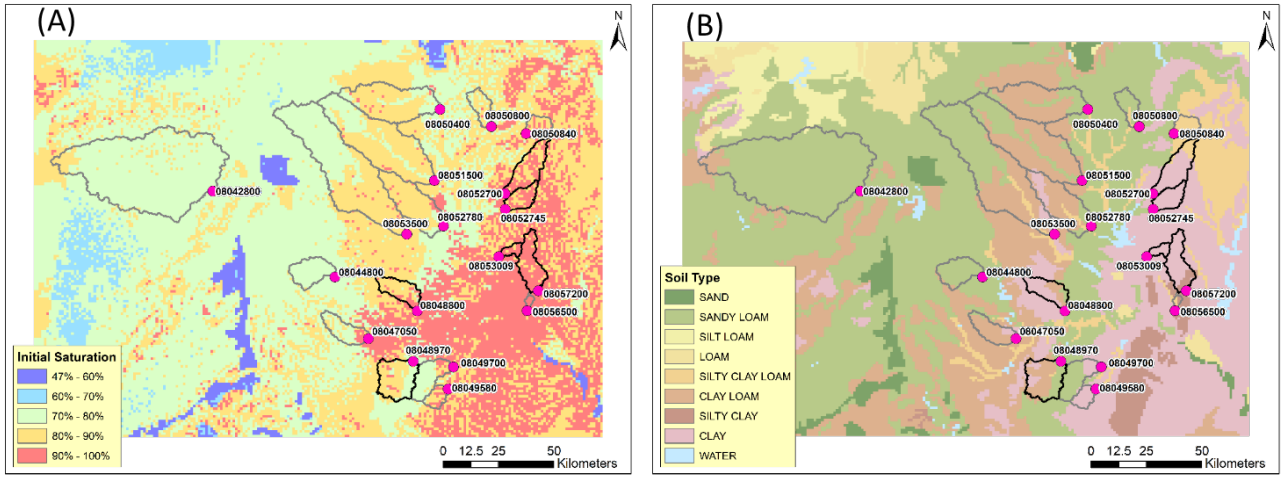

Figure 16: (A) Spatial pattern of the initial saturation level in the first layer soil (0-10 cm) at the beginning of 2015 May Event. (B) Soil type for 18 gauges in the study area. (Sub-basins with bold outlines are the ones with higher (>1) re-infiltration ratios).

4 CONCLUSIONS

In this study, the authors leverage the physically-based and distributed WRF-Hydro modeling framework to comprehensively assess the re-infiltration process (also referred to as the "run-on" process in literature), a process often missing in hydrologic models. In particular, we investigate the effects of hydrometeorological/geographical conditions and model parameters on re-infiltration simulations, aiming to provide a deeper understanding on re-infiltration than existing studies. Using UTRB as the test bed, a group of idealized numerical experiments are first conducted to focus on individual factors while holding the others constant. The results not only reveal the pattern and magnitude of individual effects, but also they inform the sensitivities of infiltration to each factor, providing guidance for the calibration effort in the subsequent analysis. In light of the idealized numerical experiments, two real storm events in UTRB are simulated and calibrated. Dominant factors to re-infiltration are identified from examining 18 sub-basins across the study area during these two events. In addition, the role of re-infiltration is investigated in relation with flood potential (indicated by runoff coefficient) to show the potential trade-offs in modeling re-infiltration for flood prediction purposes. The main conclusions from this study are summarized as follows:

1. Local infiltration is a more direct route for infiltration, a likely result of gravity, than re-infiltration through lateral water re-distribution. Under the principle of mass conservation, the changes in local and re-infiltration due to a single factor can be opposite to each other as seen in the cases of precipitation intensity, K_{sat} and REFKDT. More (less) water infiltrating locally means less (more) water to re-distribute to downstream cells and re-infiltrate.

2. The influence of re-infiltration on streamflow simulation can be substantial for areas with flat terrain and soil with high clay content (re-infiltration ratio is more than 50%).

3. Runoff coefficient and re-infiltration ratio are positively correlated, indicating that re-infiltration effects are more pronounced as flood potential increases and subsequently may be more important in urban than in rural regions.

For WRF-Hydro users, the insights from this study may also be helpful for strategically choosing overland routing options based on the study domain's hydro-meteorological and graphical conditions. Given the computational cost for the terrain-on option and the complexity in considering related parameters in WRF-Hydro, users could potentially save time and resources while achieving satisfactory simulation results if re-infiltration is expected to be less influential. For modelers studying hydrology and hydrology-atmosphere feedbacks, understanding how different factors synergize or counteract with each other to affect re-infiltration is rewarding, as re-infiltration can play an indispensable role in the hydrologic cycle and in feeding back to the atmosphere. For instance, Senatore et al. (2015) concluded that accurate representation of re-infiltration improves precipitation simulation when fully coupled with WRF, suggesting the need to represent this important physical realism in the model. For the community of flood emergency responders, increasingly detailed and realistic representations of physical processes marks a shift in the paradigm of operational flood forecast from a past that heavily relies on human judgment/adjustment towards a computationally expensive but more robust future. Although re-infiltration was found significant for flood prediction in UTRB, it may prove to be a lesser process elsewhere. However, it is our emphasis that similar studies are imperative to elucidate the cost for missing or simplifying re-infiltration.

DECLARATION OF COMPETING INTEREST

The authors declare that they have no known competing financial interests or personal relationships that could have appeared to influence the work reported in this paper.

ACKNOWLEDGMENT

The authors would like to thank the funding support from U.S. Army Corps of Engineers (Project number: W9126G-17-2-SOI-0977) and National Science Foundation (Project number: 1832065).

REFERENCES

Arnault, J., Wagner, S., Rummler, T., Fersch, B., Blieffernicht, J., Andresen, S., Kunstmann, H., 2015. Role of runoff-infiltration partitioning and additionally resolved overland flow on land-atmosphere feedbacks: a case study with the WRF-Hydro coupled modeling system for West Africa. J. Hydrometeorol. 17, 1489–1516. http://dx.doi.org/10.1175/JHM-D-15-0089.1.

Bergström, S., 1992. The HBV model: Its structure and applications. Swedish Meteorological and Hydrological Institute.

Borga, M., Anagnostou, E. N., Blöschl, G., & Creutin, J. D., 2011. Flash flood forecasting, warning and risk management: the HYDRATE project. Environmental Science & Policy, 14(7), 8

Burnash, R. J., Ferral, R. L., & McGuire, R. A., 1973. A generalized streamflow simulation system, conceptual modeling for digital computers.

Cai, X., Yang, Z. L., David, C. H., Niu, G. Y., & Rodell, M., 2014. Hydrological evaluation of the Noah-MP land surface model for the Mississippi River Basin. Journal of Geophysical Research: Atmospheres, 119(1), 23-38.34-844.

Corradini, C., Govindaraju, R. S., & Morbidelli, R., 2002. Simplified modelling of areal average infiltration at the hillslope scale. Hydrological processes, 16(9), 1757-1770.

Corradini, C., Morbidelli, R., & Melone, F., 1998. On the interaction between infiltration and Hortonian runoff. Journal of Hydrology, 204(1-4), 52-67.

Fang, Z., Bedient, P. B., Benavides, J., & Zimmer, A. L., 2008. Enhanced radar-based flood alert system and floodplain map library. Journal of Hydrologic Engineering, 13(10), 926-938.

FEMA, 2017. Historic Disaster Response to Hurricane Harvey in Texas. https://www.fema.gov/news-release/2017/09/22/historic-disaster-response-hurricane-harvey-texas

Furl, C., Sharif, H., Zeitler, J. W., El Hassan, A., & Joseph, J., 2018. Hydrometeorology of the catastrophic Blanco river flood in South Texas, May 2015. Journal of Hydrology: Regional Studies, 15, 90-104.

Gochis, D. J., W. Yu, and D. N. Yates, 2013. The WRF-Hydro Model Technical Description and User's Guide, Version 1.0, NCAR Technical Document, 120 pp., NCAR, Boulder, Colo. [Available at http://www.ral.ucar.edu/projects/wrf_hydro/.]

Gochis, D., Mc Creight, J., Yu, W., Dugger, A., Sampson, K., Yates, D., Wood, A., Clark, M., Rasmussen, R., 2015. Multi-Scale Water Cycle Predictions Using the Community WRF-Hydro Modeling System. NCAR, Boulder, Colo. Available at https://ral.ucar.edu/sites/default/files/public/projects/wrf-hydro-modeling-system/1-wrf-hydro-v40-intro.pdf

Gochis, D.J., M. Barlage, A. Dugger, K. FitzGerald, L. Karsten, M. McAllister, J. McCreight, J. Mills, A. RafieeiNasab, L. Read, K. Sampson, D. Yates, W. Yu, 2018. The WRF-Hydro modeling system technical description, (Version 5.0) . NCAR Technical Note. 107 pages. Available online at: https://ral.ucar.edu/sites/default/files/public/WRFHydroV5TechnicalDescription.pdf.

Gomi, T., et al., 2008. Dynamic runoff connectivity of overland flow on steep forested hillslopes: scale effects and runoff transfer. Water Resources Research, 44 (8), W08411, http://doi:10.1029/2007WR005894.

Gottschalk, L., & Weingartner, R., 1998. Distribution of peak flow derived from a distribution of rainfall volume and runoff coefficient, and a unit hydrograph. Journal of hydrology, 208(3-4), 148-162.

Güntner, A., & Bronstert, A., 2004. Representation of landscape variability and lateral redistribution processes for large-scale hydrological modelling in semi-arid areas. Journal of Hydrology, 297(1-4), 136-161.

Gupta, H.V., H. Kling, K.K. Yilmaz, and G.F. Martinez, 2009. Decomposition of the Mean Squared Error and NSE Performance Criteria: Implications for Improving Hydrological Modelling. Journal of Hydrology 377(1–2):80-91. https://doi.org/10.1016/j.jhydrol.2009.08.003.

Gupta, H. V., Kling, H., 2011. On typical range, sensitivity, and normalization of Mean Squared Error and Nash-Sutcliffe Efficiency type metrics. Water Resources Research, 47(10). https://doi.org/10.1029/2011WR010962.

Heras, M.M.L., et al., 2010. Plot-scale effects on runoff and erosion along a slope degradation gradient. Water Resources Research, 46 (4), W04503, http://doi:10.1029/2009WR007875.

IPCC, 2014. Climate change 2014: synthesis report. Contribution of Working Groups I. II and III to the Fifth Assessment Report of the intergovernmental panel on Climate Change. IPCC, Geneva, Switzerland, 151.

Julien, P., B. Saghafian, and F. Ogden, 1995. Raster-based hydrological modeling of spatially-varied surface runoff, Water Resour. Bull.,31(3), 523–536.

Kerandi, N., Arnault, J., Laux, P., Wagner, S., Kitheka, J., & Kunstmann, H., 2018. Joint atmospheric-terrestrial water balances for East Africa: a WRF-Hydro case study for the upper Tana River basin. Theoretical and applied climatology, 131(3-4), 1337-1355

Lespinas, F., A. Dastoor, and V. Fortin, 2017. Performance of the dynamically dimensioned search algorithm: influence of parameter initialization strategy when calibrating a physically based hydrological model. Hydrol. Res., 49 (4), 971–988.

Lin, P., Hopper Jr, L. J., Yang, Z. L., Lenz, M., & Zeitler, J. W., 2018. Insights into hydrometeorological factors constraining flood prediction skill during the May and October 2015 Texas Hill Country flood events. Journal of Hydrometeorology, 19(8), 1339-1361.

Lin, P., M.A.Rajib, Z.L.Yang, M. Somos-Valenzuela, V. Merwade, D.R.Maidment, et al., 2017. Spatiotemporal Evaluation of Simulated Evapotranspiration and Streamflow over Texas using the WRF-Hydro-RAPID Modeling Framework. Journal of the American Water Resources Association (JAWRA) 1-15. DOI: 10.1111/1752-1688.12585

Maidment, D.R., 2017. Conceptual Framework for the National Flood Interoperability Experiment. Journal of the American Water Resources Association 53(2): 245-257. DOI: 10.1111/1752-1688.12474

Morrs, R.E., 2010. Interactions among flood predictions, decisions, and outcomes: synthesis of three cases. Nat. Hazards Rev. 11 (3), 83–96.

Nahar, N., Govindaraju, R. S., Corradini, C., & Morbidelli, R., 2004. Role of run-on for describing field-scale infiltration and overland flow over spatially variable soils. Journal of Hydrology, 286(1-4), 36-51.

NCTCOG iSWM, 2010. North Central Texas Council of Government integrated Stormwater Management Technical Hydrology Manual. Available online at: http://iswm.nctcog.org/Documents/technical_manual/Hydrology_4-2010.pdf

Niu, G. Y., 2011. The community noah land-surface model (lsm) with multi-physics options. Tech. rep., National Centers for Environmental Prediction (NCEP), Oregon State University, Air Force, and Hydrology Lab–NWS, Available online at: https://www.jsg.utexas.edu/noah-mp/users-guide

Niu, G. Y., Troch, P. A., Paniconi, C., Scott, R. L., Durcik, M., Zeng, X., ... & Pelletier, J., 2014. An integrated modelling framework of catchment-scale ecohydrological processes: 2. The role of water subsidy by overland flow on vegetation dynamics in a semi-arid catchment. Ecohydrology, 7(2), 815-827.

Ogden, F.L., 1997. CASC2D Reference Manual. Storrs, CT, University of Connecticut

Poncea, V. M., & Shetty, A. V., 1995. A conceptual model of catchment water balance: 1. Formulation and calibration. Journal of Hydrology, 173(1-4), 27-40.

Saghafian, B., Julien, P.Y., Ogden, F.L., 1995. Similarity in catchment response, 1, Stationary rainstorms, Water Resour. Res., 31 (6), 1533-1541.

Senatore, A., G. Mendicino, D. J. Gochis, W. Yu, D. N. Yates, and H. Kunstmann, 2015. Fully coupled atmospherehydrology simulations for the central Mediterranean: Impact of enhanced hydrological parameterization for short and long time scales, J. Adv. Model. Earth Syst., 7, 1693–1715, doi:10.1002/2015MS000510.

Schaake, J. C., V. I. Koren, Q.-Y. Duan, K. Mitchell, and F. Chen, 1996: Simple water balance model for estimating runoff at different spatial and temporal scales. J. Geophys. Res., 101, 7461–7475, https://doi.org/10.1029/95JD02892.

Smith, R.E., Hebbert, R.H.B., 1979. A Monte Carlo analysis of the hydrologic effects of spatial variability of infiltration, Water Resour. Res., 15 (2), 419-429.

Silver, M., Karnieli, A., Ginat, H., Meiri, E., & Fredj, E., 2017. An innovative method for determining hydrological calibration parameters for the WRF-Hydro model in arid regions. Environmental modelling & software, 91, 47-69.

Sivapalan, M., Blöschl, G., Merz, R., & Gutknecht, D., 2005. Linking flood frequency to long-term water balance: Incorporating effects of seasonality. Water Resources Research, 41(6).

Tolson, B. A., and C. A. Shoemaker, 2007. Dynamically dimensioned search algorithm for computationally efficient watershed model calibration. Water Resour. Res., 43, W01413, https://doi.org/10.1029/2005WR004723.

U.S. Army Corps of Engineers (USACE), 2013. Corridor Development Certificate (CDC) – Upper Trinity River, Texas – Hydrologic and Hydraulic Model Update.

Wagener, T., & Montanari, A., 2011. Convergence of approaches toward reducing uncertainty in predictions in ungauged basins. Water Resources Research, 47(6).

Woolhiser, D.A., Smith, R.E., Giraldez, J.-V., 1996. Effects of spatial variability of saturated hydraulic conductivity on Hortonian overland flow, Water Resour. Res., 32 (3), 671-678.

Yair, A. and Kossovsky, A., 2002. Climate and surface properties: hydrological response of small arid and semi-arid watersheds. Geomorphology, 42 (1–2), 43–57.

Yair, A. and Raz-Yassif, N., 2004. Hydrological processes in a small arid catchment: scale effects of rainfall and slope length. Geomorphology, 61 (1–2), 155–169.

Yang, Z. L., Niu, G. Y., Mitchell, K. E., Chen, F., Ek, M. B., Barlage, M., ... & Xia, Y., 2011. The community Noah land surface model with multiparameterization options (Noah-MP): 2. Evaluation over global river basins. Journal of Geophysical Research: Atmospheres, 116(D12).

Yucel, I., Onen, A., Yilmaz, K. K., & Gochis, D. J., 2015. Calibration and evaluation of a flood forecasting system: Utility of numerical weather prediction model, data assimilation and satellite-based rainfall. Journal of Hydrology, 523, 49-66.

Zheng, H., and Z.-L. Yang, 2016: Effects of soil-type datasets on regional terrestrial water cycle simulations under different climatic regimes, J. Geophys. Res. Atmos., 121, 14 387–14 402, https://doi.org/10.1002/2016JD025187.

Chapter 4: Investigation of Loss Estimation to Facilitate Design Flood Practices in North Central Texas

Zhang. J., Gao, S., and Fang, Z.

ABSTRACT

As a fundamental component in hydrologic cycle, infiltration losses have drawn a lot of attention across the hydrology history. Accurate modeling of infiltration losses can provide better runoff estimation, which can further serve as flood design/protection criteria and water management schemes, etc. In design flood practices, the Initial Abstraction and Constant Loss (IACL) method has been widely applied due to its simplicity. However, due to a lack of physical equivalent properties, IACL method is often subject to issues in parameterization and has large dependency on calibration for every storm event. Despite the wide range/variability of IACL values, a single set of IA and CL values is adopted for specific flood frequency, which may introduce uncertainty and bias in the resulting peak streamflow. In this study, we first identified a total of 2,036 rainfall-runoff events for 18 watersheds in North Central Texas. Then the total losses with their IA and CL components from observed storm events are calculated based on time-series of mean areal precipitation (MAP) and streamflow data. Threshold behavior is found for all studied sub-basins, which is the relationship of the summation of gross rainfall and antecedent soil moisture versus runoff depth is largely linear above certain threshold. This finding provides a convenient way to estimate/predict total loss or runoff depth given MAP and antecedent soil moisture. It has also been found that the IA and CL values can be approximated by the Gamma and Weibull distributions, respectively. These stochastic IACL values can be applied in a Monte Carlo simulation framework to stochastically simulate numerous rainfall-runoff events for a flood frequency analysis. Due to a more realistic representation of the loss process, the Monte Carlo scheme promises to provide an alternative to the traditional deterministic approach.

KEY TERMS

Infiltration; Losses; Antecedent Soil Moisture (ASM); Rainfall; Runoff; Threshold Behavior; Initial Abstraction (IA), Constant Loss (CL); Distribution; Design Event; Flood Frequency

1 INTRODUCTION

As a fundamental component in hydrologic cycle, infiltration losses have drawn a lot of attention along the hydrology history. Accurate modeling of infiltration losses can provide better runoff estimation, which can further serve as flood design/protection criteria and water management schemes, etc. In general, infiltration models can be classified as three types (Mishra et al., 2003): physically based (or theoretical/mechanistic), semi-empirical and empirical/conceptual models. Physically based models refer to approach that is close to physical theory and has an analytical solution, including Green and Ampt (1911), Richards (1931), Phillip (1957, 1969), Mein and Larson (1971, 1973), and Smith (1972), etc. Semi-empirical models are based on simplified continuity equation and adopt certain hypotheses (e.g. Horton, 1938; Holtan, 1961; Overton, 1964; Burnash et al., 1973; Singh and Yu, 1990). Empirical/conceptual models are derived from experimental observations and represent the overall infiltration process (Singh and Yu, 1990). Examples of such models are SCS-Curve (Mockus, 1972), Collis-George (1977), Initial Abstraction and Constant Loss (IACL) models (USACE, 1992), and others.

Among numerous infiltration loss models, the Initial Abstraction and Constant Loss (IACL) method has been widely used due to its simplicity and relative accuracy. In flood frequency studies, IACL is adopted in Design Event Approach for ungauged area to estimate peak streamflow (USACE, 1992; USACE, 2013). The concept of IACL is that any watershed is assumed to store an absolute depth of rainfall at the beginning of the rainfall as initial abstraction (IA) and then reduce the rainfall rate at a constant loss (CL) rate. Therefore, the total loss of any storm events comprises of two components due to IA and CL, respectively.

At present, the design IACL values recommended by USACE (1992) are based on the percentage of sandy and clayey soils with respect to various storm return periods. This

recommendation was made under the assumption of equality between the rainfall, discharge, and IACL return periods. However, it has been questioned and argued that the assumption of equality of return period is generally not valid (Pilgrim and Cordery, 1975; Viglione et al., 2009). TxDOT and USGS have done a complex computational analysis of observed rainfall and runoff for applicable watersheds in Texas and developed regression equations and the regression trees to determine the optimal values of IACL (Asquith and Roussel, 2007; Thompson et al., 2008). The watershed characteristics like main-channel length, curve numbers (CN), etc. are all considered in regression methods as variables to estimate IA and CL values. Even though these regression methods utilize parameters with physical basis, no distinctly superior simulation is found than using the areal weighted method from sand percentage (Fang et al., 2017). The potential reason might be the regression methods were developed independent of various antecedent soil moisture conditions caused by different rainfall events (Asquith and Roussel, 2007; Thompson et al., 2008). And when the aforementioned IACL estimations are applied using the real rainfall events to validate, large discrepancies are found both in runoff volume and peak timing (Fang et al., 2017).

Therefore, due to the simplicity and the lack of physical equivalent properties, IACL is often subject to issues in parameterization and has large dependency on calibration for every storm event, which resulting in wide variation from events to events. Because of the non-linear behavior of the rainfall-runoff process, using a single set of IA and CL values for specific design frequency may introduce a large degree of uncertainty and bias in the resulting design flood estimation (Rahman et al., 2002; Loveridge et al., 2013). Thus, a substantial improvement in the accuracy and reliability of flood estimates could be expected from bringing in probability aspects of major input and parameters of the rainfall runoff process. This can be achieved through a Joint Probability Approach.

In contrast to the Design Event Approach, which is to generate frequency flood from a single combination (Eagleson, 1972; Beran, 1973), the Joint Probability Approach recognizes that any design flood characteristics (e.g. peak streamflow) could result from different combinations of rainfall input and other flood producing factors (e.g. loss-related variables). For example, the same peak streamflow can be generated by a small rainfall event with wet antecedent soil condition or a large rainfall with dry antecedent condition of the watershed. Thus, from the Joint Probability Approach, the distribution of the flood outputs can be directly estimated by simulating the likely combinations of model inputs and parameter values, leading to better estimation of frequency design flows. Meanwhile, subjective criteria in specifying model inputs can be eliminated, because the Joint Probability Approach treats model input and parameters values as random variable (Rahman et al., 2002). This can be done through a Monte Carlo simulation approach. The Monte Carlo simulation approach is essentially a compromise from the ideal continuous simulation approaches. Its main strength is that, as an event-based framework, it allows the processes that have a dominant influence on generating and modifying floods to be represented more realistically while simplifying other less influential processes. For each model run, a set of input and parameter values is randomly drawn from their respective distributions (for probability distributed variables), and by choosing a default representative value (for other variables). For example, rainfall duration, rainfall intensity, rainfall temporal pattern and losses can be treated as probability distributed variables.

To further assist frequency analyses using Joint Probability Approach (e.g. Monte Carlo simulation), it is therefore imperative for us to better determine these initial and constant losses that have been observed to occur. Finding loss values that is representative in a probability sense can overcome the potential weakness of specifying a single set of IA and CL values for design

purposes. This study is performed for 18 headwater catchments in the Upper Trinity River Basin located in North Central Texas focusing on three main objectives:

1. To identify the rainfall-runoff events from long-term observations of precipitation and streamflow.
2. To characterize the total loss for each identified event and examine the role of antecedent soil moisture in total loss estimation.
3. To separate the corresponding Initial Abstraction (IA) and Constant Loss (CL) components from the total loss and explore their statistical behavior from a large amount of identified storm events.

The paper is organized as follows: Section 2 describes the methodology including the study area, database, and event selection; Section 3 summarizes the results and conducts discussions; Section 4 provides the conclusions and suggestions for future work from this study.

2 METHODOLOGY

2.1 STUDY AREA

The study area is in the Upper Trinity River Basin (UTRB), where undeveloped areas are located at upstream while urban areas (the Greater Dallas -Fort Worth Metroplex) reside at mid- and downstream of the Basin (**Figure 1A**). Since a large percentage of the undeveloped areas within the Basin, accounting for infiltration loss as a vital component in the hydrologic processes is always challenging. Moreover, sitting in a region of temperate mean climatological conditions (USACE, 2013), UTRB experiences occasional extremes of temperature and rainfall with relatively short durations. The complexity of the infiltration process combining with the climate variability brings challenges to water resources engineering practices, especially in flood frequency analysis and flood forecasting. The study area has flat topography and the terrain slope

of 18 sub-basins ranges from 0.31% to 1.12% with an average of 0.64%. The area of 18 sub-basins varies from 16 km^2 to 1,734 km^2 with an average of 328 km^2.

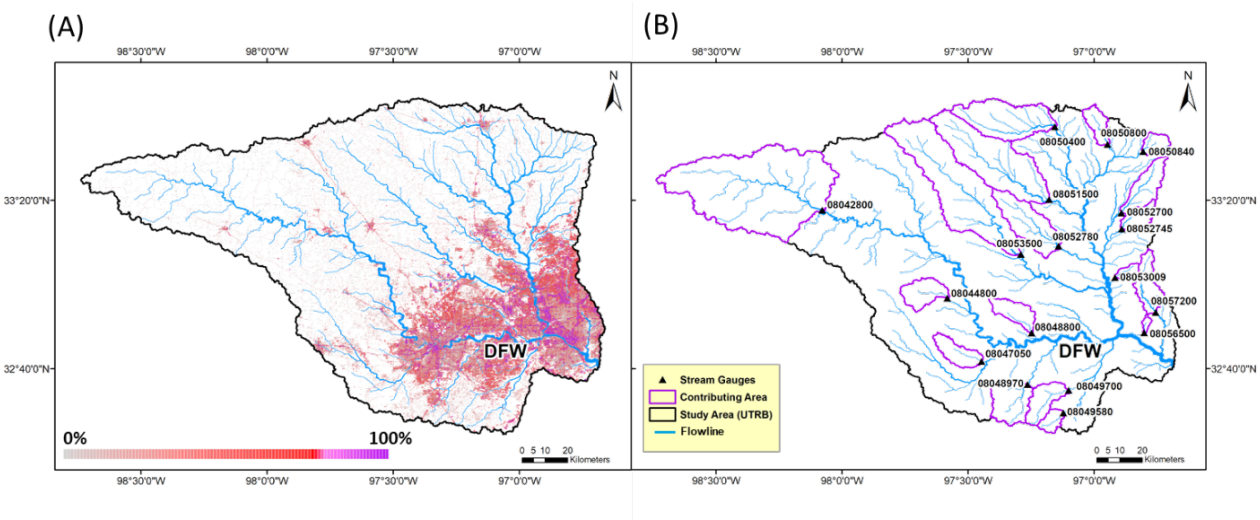

Figure 1. Study area in Upper Trinity River Basin (UTRB). (A) Imperviousness. (B) 18 USGS stream gauges and the corresponding contributing area.

2.2 DATABASE

Rainfall data is obtained from the National Centers for Environmental Prediction (NCEP) quality-controlled Stage IV Multi-sensor Precipitation Estimates (MPE) at 4 km/hourly spatiotemporal resolution. Fifteen years of data (2005-2019) are analyzed in this study and the mean annual precipitation for these sub-basins are 912 mm among the study period. The streamflow observations are downloaded from USGS gauges covering the same fifteen-year period as the precipitation data.

Since in situ soil moisture observations are limited in the study area, model-simulated soil moisture data are utilized to provide initial conditions. The initial soil moisture content (kg/m^2) data are obtained from the North American Land Data Assimilation System Version 2 (NLDAS-v2) Noah Land Surface Model (LSM) at 0-40 cm depth. The spatiotemporal resolution is 12.5 km

at hourly scale. Among four LSM outputs from NLDAS-v2, Noah LSM is selected since it is used as the land surface component in multiple weather forecast systems (e.g. Weather Research and Forecasting (WRF) regional atmospheric model; the NOAA NCEP coupled Climate Forecast System; and the Global Forecast System).

2.3 EVENTS SELECTION

Runoff events are selected throughout the entire study period (2005-2019) and we use the revised constant-k method (Mei and Anagnostou, 2015) to separate the baseflow. By assuming the baseflow storage is linear, streamflow at the recession curve can be defined as:

$$Q = Q_0 e^{-kt} \quad (1)$$

where Q is the streamflow at time t (m^3/s), Q_0 is the streamflow at the beginning of recession, and k is the recession coefficient and can be rearranged as:

$$k = -\frac{1}{Q}\frac{dQ}{dt} \quad (2)$$

Then the change rate of k (Δk) can be calculated:

$$\Delta k_t = \frac{k_t - k_{t-1}}{\Delta t} \quad (3)$$

As shown in **Figure 2A**, k is negative during the rising limb and positive during the falling limb. Because k is approximately constant going to the recession (Blume et al., 2007), we can identify the ending time of the runoff event when the change rate of k (Δk) is small enough and can be considered as "no change". **Figure 2B** illustrates the variation of Δk for a sample flow period of the watershed 08048800. Δk is stable during the recession while it shows large variation during the rising and the crest. From the variation of Δk, starting time of the event can also be identified. Then the straight-line method is applied by connecting the beginning and ending time to separate the baseflow.

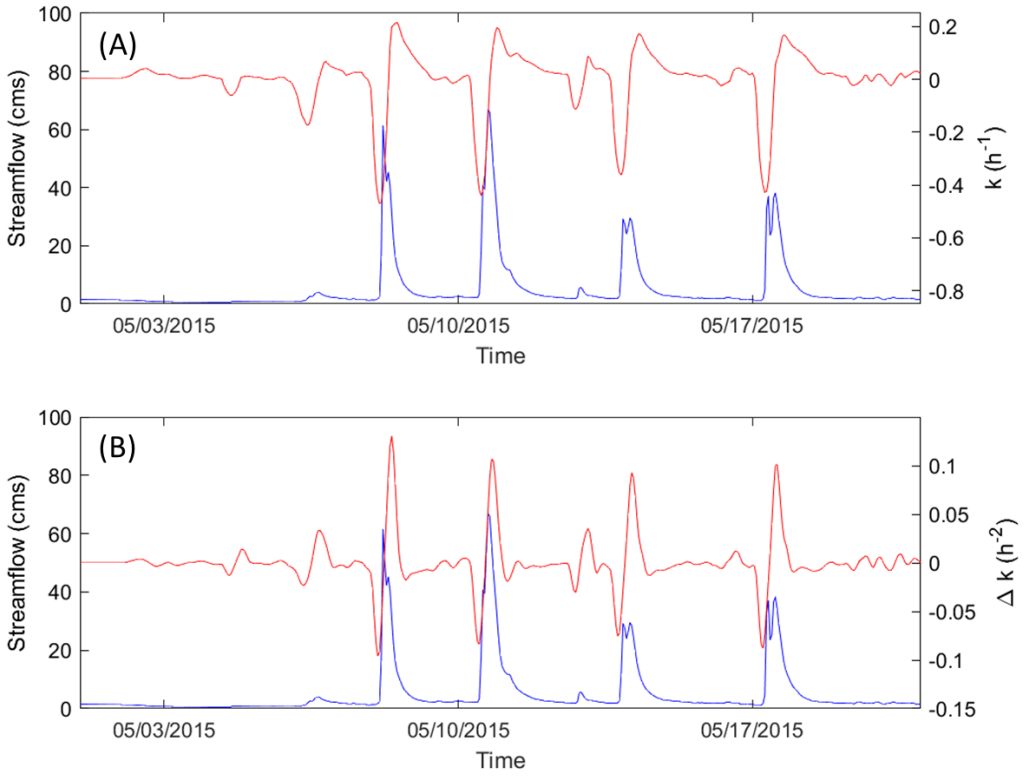

Figure 2. Variation of (A) recession coefficient (k) and (B) change rate of the recession coefficient (Δk) for a sample flow period of the Watershed 08048800 in Upper Trinity River Basin (UTRB).

Rainfall events are also identified based on time series of mean areal precipitation (MAP) for each gauge/sub-basin. This requires properly defining a threshold value for the minimum inter-arrival time (MIT) between any two storm events. Then we can determine whether any two positive rainfall values separated by zeros belong to the same storm event by checking whether the number of zeros is greater than MIT or not. To automate the optimization of MIT, we follow the following steps. First, MIT is initialized at a small inter-arrival value, say 1 hour. Second, a list of storm events can be identified from the MAP time series based on the initialized MIT value. Third, the inter-arrival times of the list of storm events can be calculated and fitted to an exponential distribution, which is done by assuming that storm occurrence follows Poisson process. Fourth,

the goodness-of-fit is evaluated to determine if the MIT is proper. If current MIT is not satisfactory, the new MIT value will be slightly increased, e.g. by 1 hour, and the procedure enters the next iteration starting from the first step until the updated MIT is proper. After identifying rainfall and runoff events identified independently, we match them by examining their overlay while minding that rainfall events should precede the runoff events.

2.4 LOSS ESTIMATION

With rainfall and runoff events identified, the total loss for each event can be calculated by subtracting surface runoff volume (i.e. the integral of hydrograph after removal of baseflow) from gross rainfall. Considering the non-linear nature of hydrological process, a family of previous studies have discovered that surface runoff is a threshold process controlled by the antecedent wetness of the catchment (van Meerveld and McDonnell, 2005; James and Roulet, 2007, 2009; Latron and Gallart, 2008; Penna et al., 2011). Furthermore, Detty and McGuire (2010a, 2010b) found a clear threshold relationship between the summation of antecedent wetness and gross rainfall and runoff volume: above certain threshold, runoff volume becomes linearly correlated with the sum of antecedent soil moisture and rainfall. One benefit of the quantifying the threshold behavior is that total loss can be easily calculated/predicted given antecedent soil moisture and gross rainfall. Therefore, we examine this threshold behavior of the studied catchments based on observations of streamflow, rainfall and antecedent soil moisture.

As the components of total loss, the corresponding initial loss and constant loss are then estimated. Based on the concept of the Initial Abstraction and Constant Loss (IACL), IA can be calculated as the amount of rainfall that occurs before the start of the runoff (Rahman et al., 2002):

$$IA = \sum_{i=1}^{t_0} I_i \quad (4)$$

where I_i is the hourly rainfall amount in mm and t_0 is the time duration (h) between rainfall starts and runoff starts as shown in **Figure 3**.

The total loss volume can be expressed as:

$$LOSS = Rainfall - Runoff = IA + CL \times (t - t_0) \quad (5)$$

where t is the rainfall duration.

Then the CL can be calculated as:

$$CL = \frac{LOSS - IA}{t - t_0} \quad (6)$$

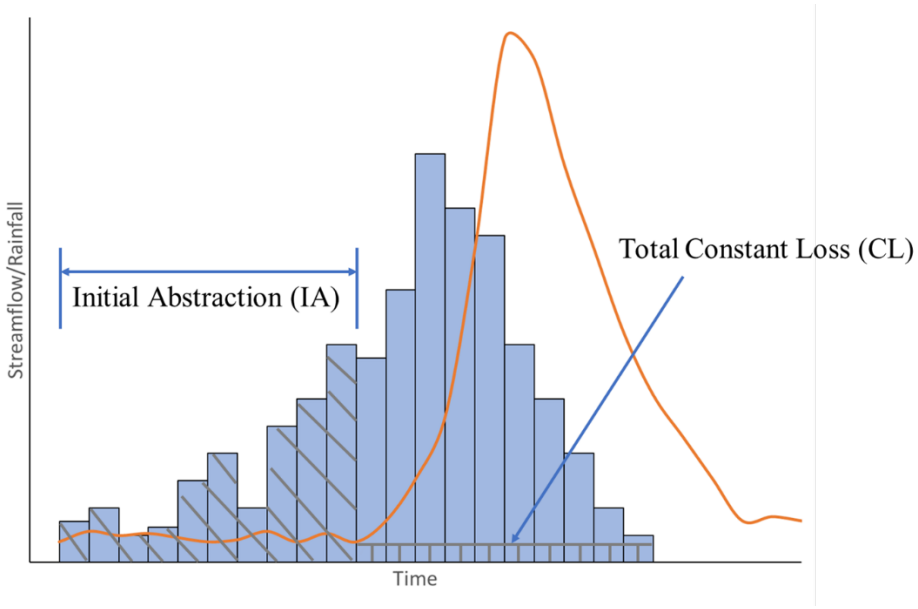

Figure 3. Initial Abstraction (IA) and Constant Loss (CL) for a given rainfall-runoff event.

2.5 DISTRIBUTION FITTING

The calculated IA and CL values are analyzed and fitted to both parametric and non-parametric probability distributions. Maximum likelihood estimates method is applied to fit the possible parametric distributions. Goodness-of-fit tests and plots, including the probability density function (PDF), probability-probability (P-P) and quantile-quantile (Q-Q) plots, are used to determine whether the fitted distribution is reasonable. For each fitted distribution, 10,000 random

values are generated to calculate the descriptive statistics (e.g. minimum and maximum values, mean, median, standard deviation, and skewness). These statistics from fitted distribution are compared to the descriptive statistics of the sample data set. Based on the results from the goodness of fit tests, P-P and Q-Q plots, and relative errors of the descriptive statistics, the best fitting distribution is selected. Three continuous probability distributions used in this study are defined in **Table 1**.

Table 1. Continuous probability distributions: Gamma, Weibull, and Lognormal distributions

Distribution	Probability density function	Parameters
Gamma	$f_X(x) = \frac{\lambda^\alpha x^{\alpha-1} e^{-\lambda x}}{\Gamma(\alpha)}$	α is the shape parameter ($\alpha > 0$) λ is the scale parameter ($\lambda > 0$) $\Gamma(\alpha)$ is the Gamma function: $\Gamma(\alpha) = \int_0^\infty x^{\alpha-1} e^{-x} dx \, (x > 0)$
Weibull	$f_X(x) = \frac{\alpha}{\lambda}(\frac{x}{\lambda})^{\alpha-1} e^{-(\frac{x}{\lambda})^\alpha}$	α is the shape parameter ($\alpha > 0$) λ is the scale parameter ($\lambda > 0$)
Lognormal	$f_X(x) = \frac{1}{x}\frac{1}{\sigma\sqrt{2\pi}} e^{[-\frac{(\ln x-\mu)^2}{2\sigma^2}]}$	σ is the shape parameter μ is the location parameter

3 RESULTS AND DISCUSSIONS

3.1 RAINFALL-RUNOFF EVENTS

Table 2 shows the number of identified rainfall-runoff events for 18 sub-basins over the 15-year observation period. From the rainfall and runoff statistics, we can see a large variety of events have been covered including both small and big events. In total 2,036 events are identified from 18 sub-basins in UTRB.

Table 2. Statistics of selected rainfall-runoff events for 18 sub-basins

Gauge ID	Area (Km^2)	Event Number	Rainfall Range (mm)			Runoff Range (mm)		
			Low	High	Mean	Low	High	Mean
08042800	1733.8	15	4.87	222.88	77.60	2.42	122.65	23.34
08044800	162.5	126	0.43	145.86	38.19	0.02	59.55	5.74
08047050	142.0	265	0.11	179.23	20.85	0.07	65.22	2.46
08048800	136.5	93	0.88	121.02	31.26	0.16	44.13	7.99
08048970	233.8	152	0.19	111.92	23.48	0.08	87.09	7.13
08049580	65.9	76	1.01	106.79	34.29	0.08	96.66	11.70
08049700	163.7	203	0.10	184.26	29.79	0.05	87.41	5.45
08050400	458.9	70	0.19	517.59	51.40	0.10	349.59	17.45
08050800	101.2	37	7.36	157.20	47.48	0.16	97.83	17.61
08050840	75.9	44	4.30	145.67	34.26	1.48	92.60	14.40
08051500	758.1	57	0.43	507.67	50.91	0.10	311.74	15.53
08052700	188.9	35	1.10	179.82	47.88	1.08	165.07	24.30
08052745	98.8	80	0.80	135.30	30.41	0.16	46.00	9.23
08052780	334.3	86	1.08	179.23	37.42	0.09	109.88	9.53
08053009	35.9	177	0.46	114.50	25.45	0.16	75.37	8.84
08053500	1033.0	29	1.73	502.06	61.52	0.35	223.32	18.39
08056500	16.3	212	0.27	116.02	23.63	0.17	73.05	7.31
08057200	172.2	279	0.71	132.38	23.20	0.14	70.87	5.87

3.2 THRESHOLD BEHAVIOR

From the identified rainfall-runoff events for 18 sub-basins in UTRB, we calculate the gross rainfall (MAP), runoff volume and total loss and extract the antecedent soil moisture content from the top 40 cm depth of soil layer for each event. A clear threshold behavior is found for all 18 sub-basins. Threshold is considered as the sum of antecedent soil moisture content (ASM) and total rainfall (MAP), which have been widely used from previous studies (Detty and McGuire, 2010; Fu et al., 2013; Saffarpour et al., 2016). The linear relationship between MAP + ASM and runoff gets stronger beyond the threshold, so we can identify the threshold based on the coefficient of determination R^2. **Figure 4** shows an example (gauge 08057200) of how the coefficient of determination R^2 changes when different threshold is selected. The coefficient of determination R^2

is calculated for a linear regression fit to 40 % of the sample points with MAP + ASM just above a moving threshold. With the moving threshold increasing, the R^2 value almost increases exponentially as illustrated in **Figure 4**. The optimal threshold is determined when R^2 increases above 0.8.

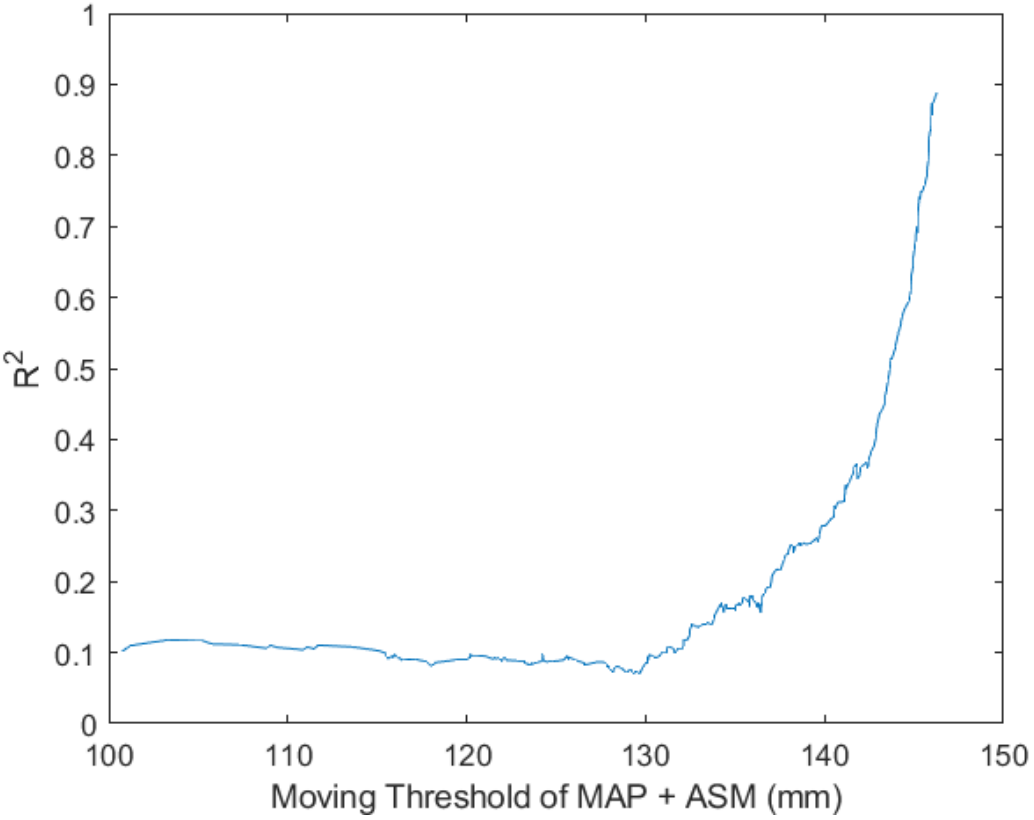

Figure 4. The coefficient of determination R^2 calculated for a linear regression between runoff volume and MAP + ASM above a moving threshold for a sample watershed 08057200.

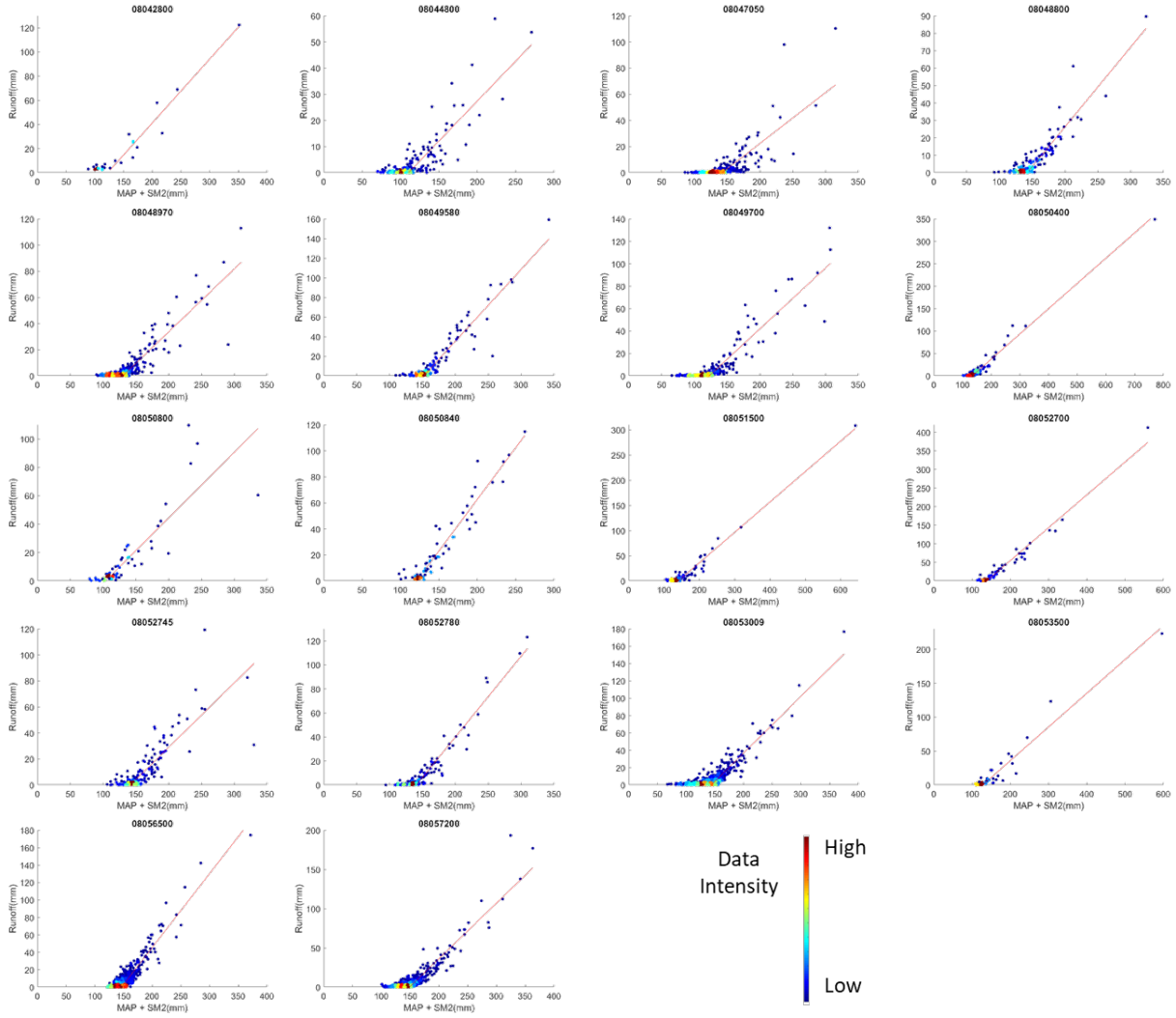

Figure 5. Threshold behavior of 18 sub-basins in UTRB.

As shown in **Figure 5,** below a certain threshold, the sum of ASM and gross rainfall is poorly correlated with runoff depth, and little runoff is generated. Above this threshold value, the relationship between MAP + ASM and runoff depth is highly correlated. The threshold behavior has long been discovered in previous studies using small headwater basins or experimental basins (Detty and McGuire, 2010a; Penna et al., 2011; Fu et al., 2013; Saffarpour et al., 2016). In this study, we confirm and expand the threshold behavior using more and larger-sized basins based on long-term rainfall, soil moisture, and streamflow observations. The threshold behavior can be used to estimate runoff and loss given total rainfall and antecedent soil moisture. For example, one can

predict the runoff volume in a basin using the real time soil moisture and quantitative precipitation forecast (QPF) ahead of a storm event based on the threshold behavior.

3.3 LOSS VALUES FROM SELECTED EVENTS

Initial and constant losses have been calculated for each event and **Table 3** summarizes the important statistics of the estimated IA and CL values for individual gauges. The mean IA and CL for the 18 sub-basins are 117 mm and 0.6 mm/hr respectively. The average skewness values for IA and CL are 1.67 and 2.08, indicating the IA and CL distributions are positively skewed. The reason is that the lower bounds of IA and CL are zero or close to zero while the upper bounds are varied and based on the data samples. For all sub-basins, the average ranges of IA and CL are 0 – 177 mm and 0 – 3.89 mm/hr respectively. Given such a wide range, the use of a single set of IACL values for specific design frequency, which is to convert specific rainfall (e.g. 100-yr design rainfall) to streamflow (e.g. 100-yr peak streamflow), seems unreliable.

Table 3. Statistics of IA and CL values for 18 sub-basins (SD meaning standard deviation)

Gauge ID	Event Number	IA (mm)					CL (mm/hr)				
		Range	Mean	Median	SD	Skew	Range	Mean	Median	SD	Skew
08042800	15	5 - 112	49	47	33.45	0.22	0.04 - 0.36	0.20	0.24	0.11	-0.09
08044800	126	0 - 116	28	20	25.12	1.61	0.03 - 2.51	0.39	0.27	0.45	2.45
08047050	265	0 - 99	15	9	17.67	1.93	0.00 - 8.50	0.69	0.37	1.08	4.43
08048800	93	1 - 118	25	17	24.24	1.75	0.01 - 1.30	0.51	0.40	0.44	0.53
08048970	152	0 -96	15	10	15.80	2.11	0.00 - 6.52	0.68	0.36	1.05	3.67
08049580	76	0 -104	27	19	24.11	1.50	0.01 - 2.49	0.64	0.28	0.83	1.37
08049700	203	0 - 121	24	16	25.80	2.07	0.00 - 3.05	0.48	0.22	0.67	2.36
08050400	70	0 - 178	35	31	29.01	2.24	0.00 - 9.19	0.80	0.21	2.11	3.78
08050800	37	0 - 110	33	28	26.83	1.33	0.03 - 1.76	0.47	0.31	0.60	1.67
08050840	44	0 - 92	28	23	19.39	1.10	0.06 - 3.92	1.06	0.56	1.62	1.40
08051500	57	0 - 130	31	27	29.45	1.52	0.01 - 6.30	0.75	0.43	1.38	3.65
08052700	35	0 - 102	30	27	22.25	1.05	0.05 - 0.85	0.41	0.39	0.32	0.18
08052745	80	0 - 135	24	18	24.63	2.30	0.01 - 4.71	0.80	0.23	1.32	2.32
08052780	86	0 - 112	29	21	25.94	1.53	0.00 - 0.99	0.26	0.11	0.32	1.37
08053009	177	0 - 114	20	13	20.46	1.96	0.03 - 6.70	0.94	0.37	1.43	2.46
08053500	29	0 - 123	38	33	28.96	1.08	0.00 - 0.45	0.18	0.14	0.15	0.62
08056500	212	0 - 116	19	13	21.47	2.23	0.01 - 5.82	0.83	0.51	1.11	2.77
08057200	279	0 - 132	18	12	21.60	2.55	0.00 - 4.61	0.71	0.33	1.00	2.46
Average	**113**	**0 - 117**	**27**	**21**	**24.23**	**1.67**	**0.00 - 3.89**	**0.60**	**0.32**	**0.89**	**2.08**

Figures 6A, 6B and 6C show the variability of IA (mm), total CL (mm) and CL (mm/hr) from all the 2,036 events of 18 sub-basins. The events are ranked in ascending order of the total rainfall amount. It can be found that the higher rainfall, the larger variations in IA and total CL (**Figures 6A** and **6B**). This finding is important for design applications, especially for extreme events with large rainfall amount. Because the greater variations/ranges of IA and total CL are expected for big events, it is questionable to assign a single set of IACL values for specific design scenario. The trend of variations in CL values is mixed as the rainfall increases (**Figure 6C**). This can be explained by the fact that CL is the loss rate, so it also depends on the rainfall duration other than rainfall amount.

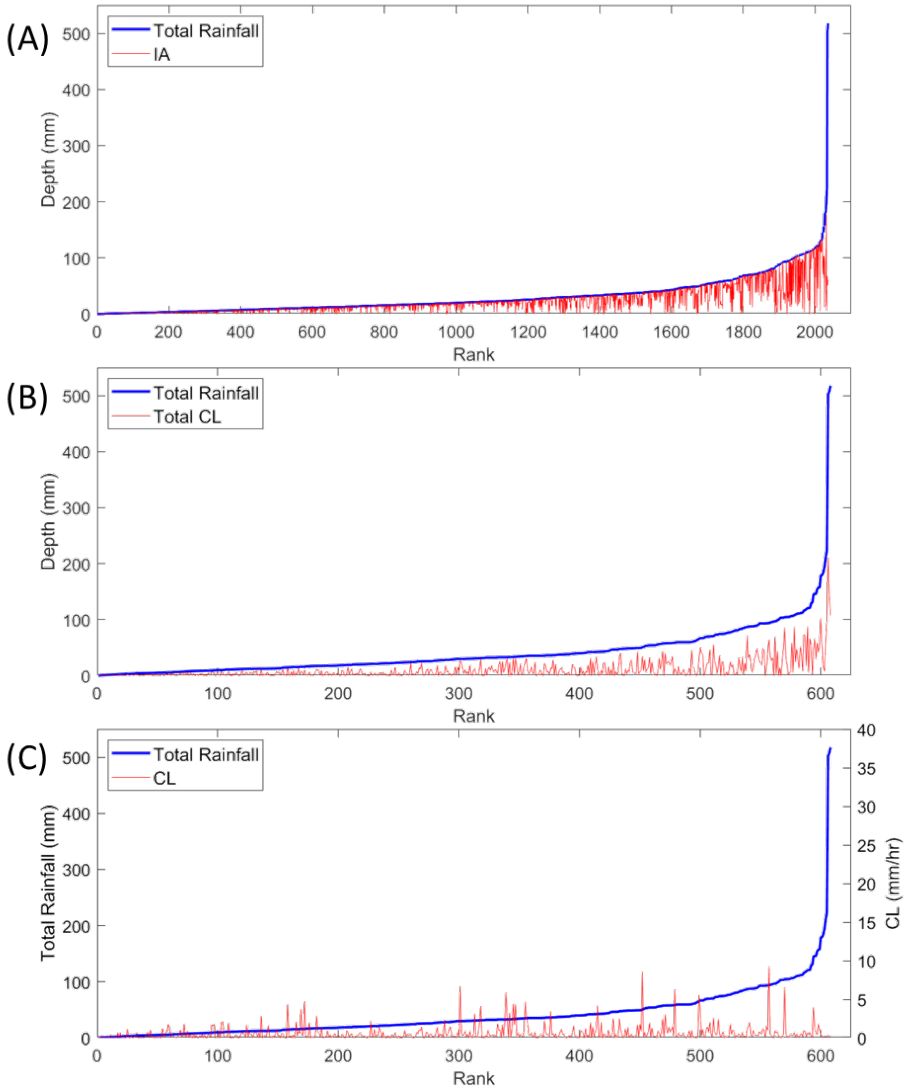

Figure 6. The variability of (A) IA, (B) Total CL, (C) CL with the ascending order of total rainfall.

3.4 DISTRIBUTION FITTINGS

Gamma, Weibull, and Lognormal distributions are fitted to the calculated IA and CL values for 18 sub-basins. As shown in **Table 3**, the events identified for some sub-basins are not statistically significant, because sample size of the calculated IA and CL values is not big enough to generate a reasonable distribution. Therefore, we only show the results of distribution fittings for six sub-basins which have more than 150 events identified.

Figure 7 shows the histogram of IA values and the fitted probability density function (pdf) of Gamma, Weibull, and Lognormal distributions. From the goodness of fit statistics (**Table 4**), Lognormal distribution is found to have the lowest p-values and less than 0.05 for most gauges, indicating poor evidence for the null hypothesis, which means Lognormal is not suitable for fitting the distribution of IA. Gamma and Weibull distributions show the similar Anderson-Darling statistics. **Table 5** shows the comparison of the descriptive statistics between the calculated and generated (sample size: 10,000 values) IA values from Gamma and Weibull distributions. Compared with the calculated mean of IA, the Gamma-generated and Weibull-generated mean both show 1% average differences from six sub-basins. For the standard deviation, the average difference between calculated and Gamma/Weibull-generated IA is 8%/10%. The upper limit of Gamma-generated IA is closer to the calculated upper limit than Weibull. Overall, the generated IA values from Gamma fitted distribution preserve the statistics of the calculated IA data well.

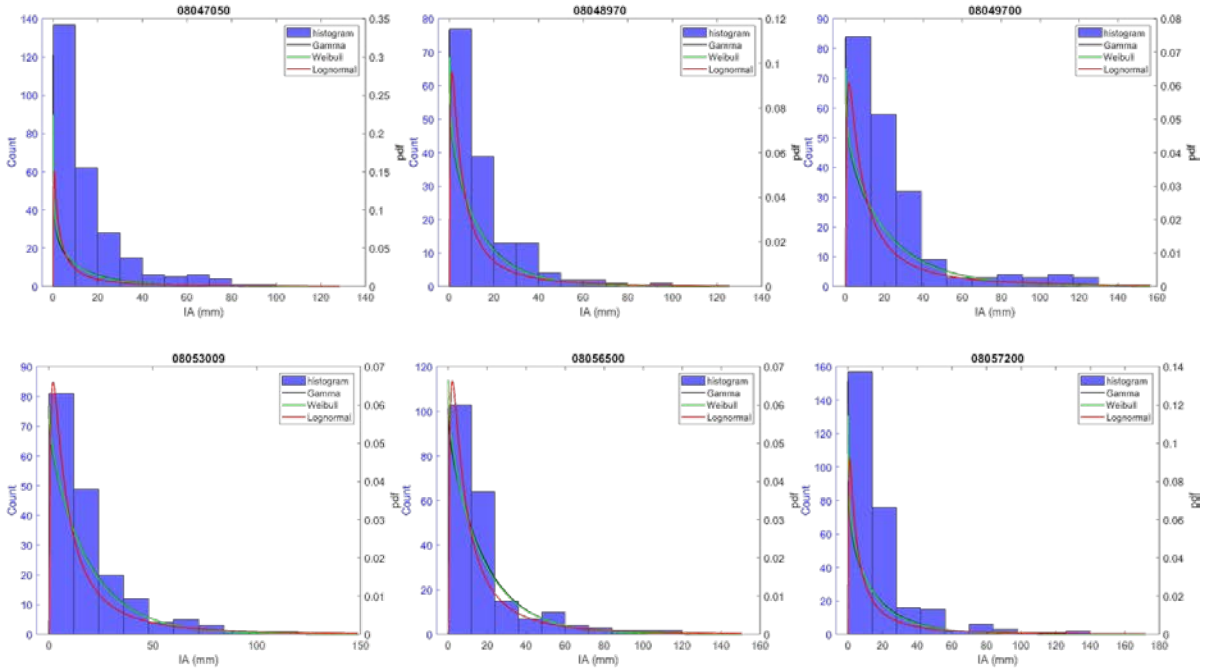

Figure 7. Histogram and fitted probability density function (pdf) of three distributions of the Initial Abstraction (IA) values for sub-basins with identified events more than 150.

Table 4. Goodness of fit test statistics of the fitted Gamma, Weibull, and Lognormal distributions of the IA data

Gauge ID	Distribution	Anderson-Darling	
		P-value	Statistics
08047050	Gamma	0.813	0.435
	Weibull	0.812	0.436
	Lognormal	0.007	4.198
08048970	Gamma	0.997	0.165
	Weibull	0.997	0.164
	Lognormal	0.093	1.991
08049700	Gamma	0.442	0.857
	Weibull	0.448	0.848
	Lognormal	0.005	4.419
08053009	Gamma	0.983	0.222
	Weibull	0.986	0.213
	Lognormal	0.068	2.236
08056500	Gamma	0.212	1.367
	Weibull	0.224	1.325
	Lognormal	0.045	2.581
08057200	Gamma	0.223	1.329
	Weibull	0.269	1.196
	Lognormal	0.001	5.650

Table 5. Comparison of the statistics of the calculated and generated IA values (SD meaning standard deviation)

Gauge ID	IA Number	Initial Abstraction (IA) (mm)					
			Range	Mean	Median	SD	Skew
08047050	265	Calculated	0 - 99	15.20	9.18	17.67	1.93
		Gamma	0 - 160	14.87	8.92	17.37	2.21
		Weibull	0 - 279	15.42	8.62	19.30	2.79
08048970	152	Calculated	0 -96	14.76	9.74	15.80	2.11
		Gamma	0 - 153	14.71	9.51	15.85	2.18
		Weibull	0 - 151	14.59	9.53	15.61	2.24
08049700	203	Calculated	0 - 121	23.76	16.17	25.80	2.07
		Gamma	0 - 235	23.72	15.95	24.69	2.06
		Weibull	0 - 248	23.52	15.06	25.54	2.17
08053009	177	Calculated	0 - 114	19.59	13.35	20.46	1.96
		Gamma	0 - 197	19.36	13.21	19.65	2.14
		Weibull	0 - 206	19.38	13.08	19.70	2.01
08056500	212	Calculated	0 - 116	19.17	12.61	21.47	2.23
		Gamma	0 - 187	19.34	13.27	19.52	2.00
		Weibull	0 - 226	19.05	12.94	19.62	2.12
08057200	279	Calculated	0 - 132	18.06	11.95	21.60	2.55
		Gamma	0 - 151	17.76	11.30	19.26	2.08
		Weibull	0 - 223	18.05	11.40	20.37	2.40

Figure 8 shows the histogram of CL values and the fitted probability density function (pdf) of Gamma, Weibull, and Lognormal distributions. From the goodness of fit statistics (**Table 6**), we can see p-values of three distributions for six gauges are all larger than 0.05, indicating the null hypothesis is not rejected. However, Anderson-Darling statistics of Lognormal are always larger than Gamma and Weibull distributions, indicating Lognormal is less suitable for fitting CL compared with Gamma and Weibull. Weibull has smaller Anderson-Darling statistics than Gamma, meaning Weibull distribution fits CL better. **Table 7** shows the comparison of the descriptive statistics between the calculated and generated (sample size: 10,000 values) CL values from Gamma, Weibull, and Lognormal distributions. From the statistics, we can see the fitted

Lognormal has much higher values for the upper limit of CL than Gamma and Weibull. The average difference in calculated and Gamma/Weibull-generated means is only 1%/2%; for the standard deviation (SD) the average difference is 18%/11%. The Weibull distribution is therefore found to be of best fit and well preserves the statistics of the calculated CL values.

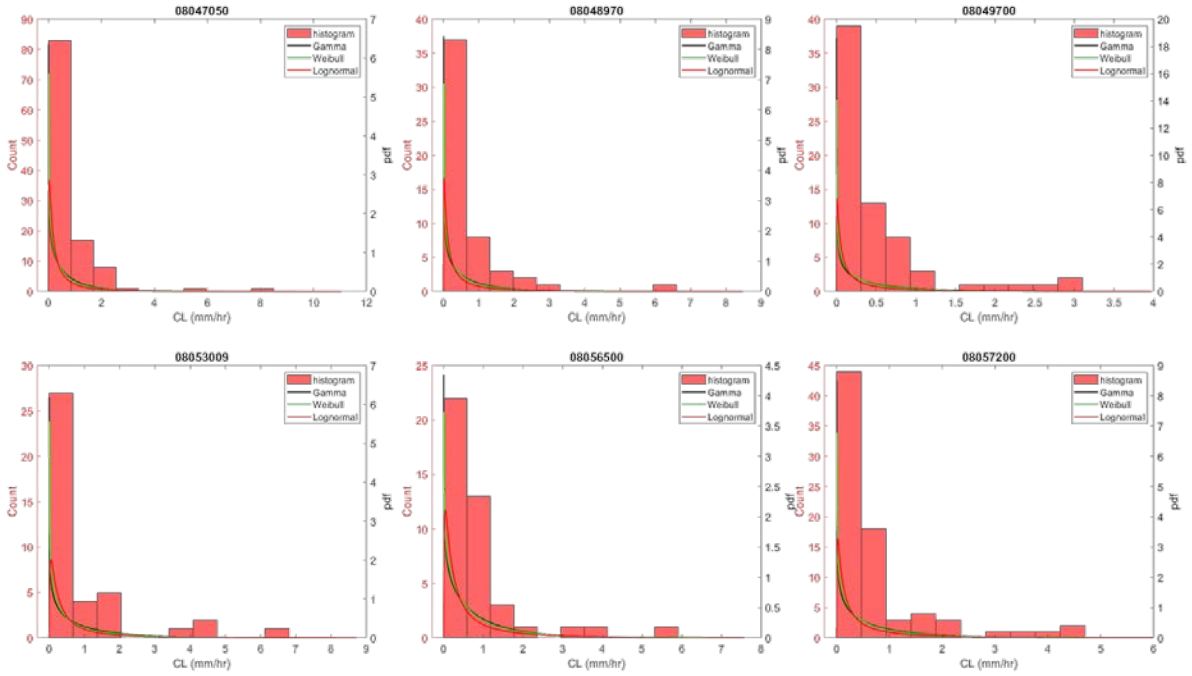

Figure 8. Histogram and fitted probability density function (pdf) of three distributions of the Constant Loss (CL) values for sub-basins with identified events more than 150.

Table 6. Goodness of fit test statistics of the fitted Gamma, Weibull, and Lognormal distributions of the CL data.

Gauge ID	Distribution	Anderson-Darling	
		P-value	Statistics
08047050	Gamma	0.666	0.581
	Weibull	0.959	0.269
	Lognormal	0.528	0.737
08048970	Gamma	0.759	0.487
	Weibull	0.896	0.351
	Lognormal	0.355	1.004
08049700	Gamma	0.895	0.351

	Weibull	0.974	0.243
	Lognormal	0.275	1.179
08053009	Gamma	0.331	1.050
	Weibull	0.592	0.660
	Lognormal	0.277	1.236
08056500	Gamma	0.955	0.276
	Weibull	0.987	0.210
	Lognormal	0.693	0.552
08057200	Gamma	0.548	0.713
	Weibull	0.806	0.442
	Lognormal	0.340	1.034

Table 7. Comparison of the statistics of the calculated and generated CL values (SD meaning standard deviation)

Gauge ID	CL Number	Constant Loss (CL) (mm/hr)					
			Range	Mean	Median	SD	Skew
08047050	111	Calculated	0.00 - 8.50	0.69	0.37	1.08	4.43
		Gamma	0.00 - 9.38	0.68	0.40	0.81	2.42
		Weibull	0.00 - 12.76	0.68	0.37	0.89	2.92
		Lognormal	0.00 - 94.70	0.91	0.29	2.76	15.31
08048970	52	Calculated	0.00 - 6.52	0.68	0.36	1.05	3.67
		Gamma	0.00 - 11.29	0.68	0.37	0.85	2.53
		Weibull	0.00 - 11.59	0.67	0.34	0.91	3.18
		Lognormal	0.00 - 208.72	1.10	0.27	4.11	22.17
08049700	69	Calculated	0.00 - 3.05	0.48	0.22	0.67	2.36
		Gamma	0.00 - 6.03	0.47	0.25	0.61	2.53
		Weibull	0.00 - 12.01	0.49	0.23	0.73	3.90
		Lognormal	0.00 - 558.81	0.94	0.17	6.88	60.90
08053009	40	Calculated	0.03 - 6.70	0.94	0.37	1.43	2.46
		Gamma	0.00 - 13.07	0.94	0.53	1.14	2.47
		Weibull	0.00 - 19.99	0.90	0.46	1.25	3.32
		Lognormal	0.00 - 97.48	1.00	0.37	2.44	13.96
08056500	42	Calculated	0.00 - 5.82	0.83	0.51	1.11	2.77
		Gamma	0.00 - 9.34	0.83	0.50	0.94	2.27
		Weibull	0.00 - 11.87	0.82	0.47	1.02	2.79
		Lognormal	0.00 - 86.59	1.11	0.38	2.67	10.05
08057200	77	Calculated	0.00 - 4.61	0.71	0.33	1.00	2.46
		Gamma	0.00 - 7.54	0.70	0.39	0.85	2.37
		Weibull	0.00 - 15.48	0.72	0.38	0.98	3.29
		Lognormal	0.00 - 171.24	1.06	0.29	3.66	22.53

All IA and CL values from 18-subbasins are used to extract exceedance probabilities. **Figures 9** and **10** show the resulting non-parametric distribution with 90% confidence interval for the sample IA and CL data. The resulting distributions are compared with the design IA and CL values generated based on sand percentage data (USACE, 1992). The two ends of horizonal lines mark the range of design IA (CL) values, with the mean represented by the intersection points with the non-parametric distribution of IA (CL). First, The IAs (CLs) derived from runoff events well encompass those based on design criteria with the maximum IA (CL) being 130 mm (8.5 mm/hr). Second, both the mean and variation of design IA(CL) decreases with greater return period.

As implied by the return periods, the more frequently an IA (CL) value is observed in real events, the rarer (more intense) a design storm event this value corresponds to. This points to a tendency of the current design criteria in which a small loss percentage is intentionally assigned to intense design storms for conservative purpose, but unfortunately contradicts the observations. Alternatively, a probabilistic approach of flow frequency analysis can potentially provide a more robust and realistic representation of loss using a Monte Carlo framework. Random IA(CL) values can be drawn from the statistical distributions as derived here and then drive the hydrologic simulation. A large number of simulations closely preserve the statistical moments of event-based IA (CL) as also demonstrated here. The drawing of random IA(CL) values can be independent by assuming no significant correlation with other inputs (e.g. rainfall) or parameters. If correlation is instead found statistically significant between two parameters/inputs, their random values can then be generated simultaneously from their joint distribution. For example, IA is dependent on the total rainfall depth because the former must be smaller than the latter. Therefore, the conditional pdf of IA given a total rainfall depth is truncated, which should be reflected by the fitted joint distribution. Due to the limited data samples, the fitting of a joint distribution is determined beyond

the scope of this study. However, we are currently investigating regionalization approaches to aggregate data at multiple sub-basins and form regional independent or joint distributions of rainfall and loss variables.

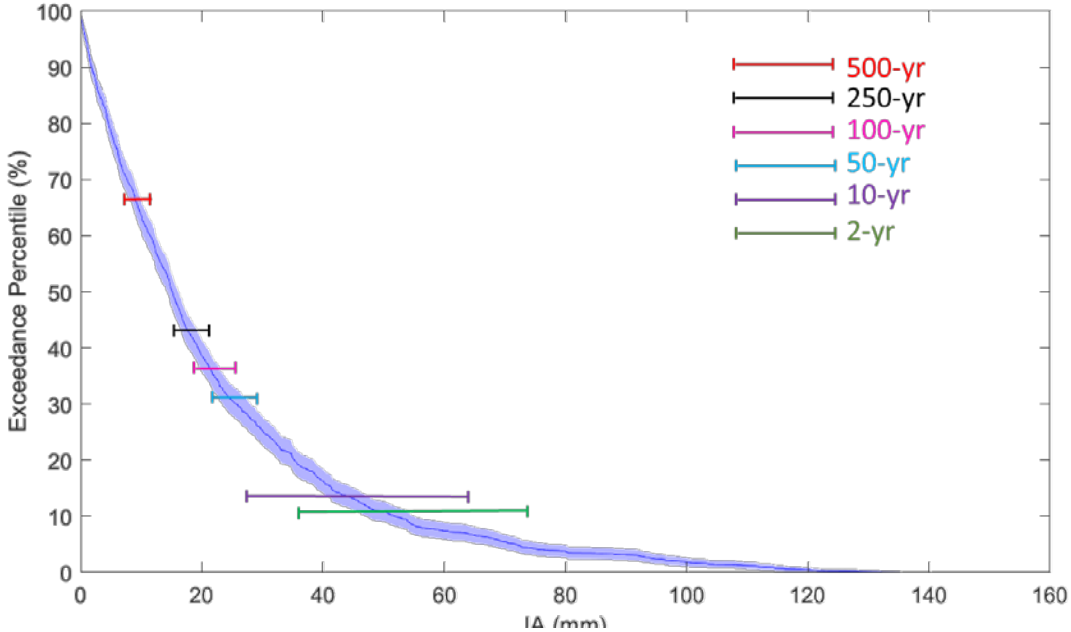

Figure 9. Comparison between non-parametric distribution of all Initial Abstraction (IA) values and design IA values.

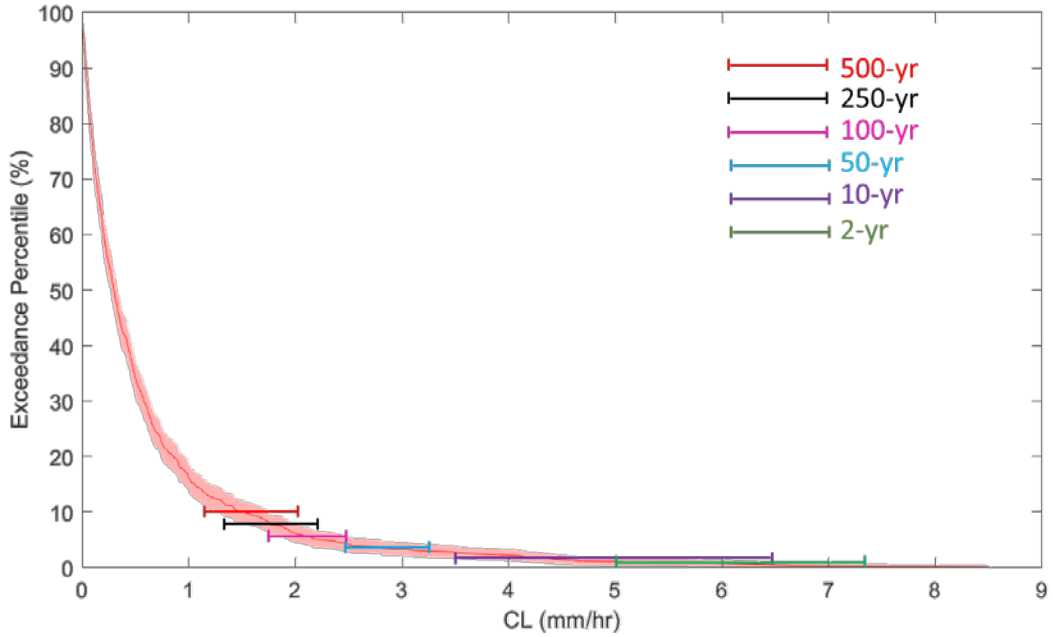

Figure 10. Comparison between non-parametric distribution of all Initial Abstraction (IA) values and design CL values.

4 CONCLUSIONS AND FUTURE WORK

This study focuses on loss estimation for 18 headwater catchments in North Central Texas using 15-year (2005-2019) Stage IV rainfall and USGS streamflow. By developing automatic algorithms, we identify a total of 2,036 rainfall-runoff events, from which a series of statistical analyses are made on total loss with its initial abstraction (IA) and constant loss (CL) components. It has demonstrated a wide variability in IA values, reflecting inherent uncertainties/bias in losses for flood modeling. The statistical behavior of the IACL is explored and the distribution tested in this study show promising results in preserving the statistical moments. The statistics from this exhaustive list of events establish a solid foundation for future Monte-Carlo rainfall-runoff simulation, which can provide a better estimation in derived flood frequency curves. The major findings are summarized as follows:

1. Unique from previous schemes, the automatic identification of rainfall-runoff events ensures that the occurrence of events follow a Poisson process. The larger number of events suffice the requirement in deriving statistical distribution of loss-related variables.
2. Threshold behavior is found for all studied sub-basins. In UTRB, the relationship between MAP + ASM and runoff is largely linear above certain threshold, which indicates a convenient way to estimate/predict total loss or runoff given gross rainfall and antecedent soil moisture.
3. Using a simplistic framework, IA and CL can be roughly estimated based on hyetograph and hydrograph. Estimated IA and CL can be fit to positively skewed distributions. Out of

the tested distributions, Gamma distribution has the best goodness of fit for IA and Weibull distribution has the best goodness of fit for CL.

For future directions, we will implement the distributions of IA and CL derived in this study in a Monte Carlo framework to simulate numerous rainfall-runoff events for a flood frequency analysis. Joint distribution of loss parameters with rainfall or other influential inputs/parameters will be considered as possible ways to capture the probabilistic nature of loss-related variables even more accurately. Due to the more realistic representation of the loss process, we expect the simulations will have good chance in matching the streamflow observations in terms of extreme value distribution. Furthermore, the results will enable us to resolve the discrepancies between the rainfall and flood frequencies.

DECLARATION OF COMPETING INTEREST

The authors declare that they have no known competing financial interests or personal relationships that could have appeared to influence the work reported in this paper.

ACKNOWLEDGMENT

The authors would like to thank the funding support from U.S. Army Corps of Engineers (Project number: W9126G-17-2-SOI-0977).

REFERENCES

Asquith, W. H., & Roussel, M. C. (2007). An initial-abstraction, constant-loss model for unit hydrograph modeling for applicable watersheds in Texas (No. 2007-5243). US Geological Survey.

Beran, M. A. (1973, June). Estimation of design floods and the problem of equating the probability of rainfall and runoff. In Madrid Symposium (pp. 4-9).

Blume, T., Zehe, E., & Bronstert, A. (2007). Rainfall—runoff response, event-based runoff coefficients and hydrograph separation. Hydrological Sciences Journal, 52(5), 843-862.

Burnash, R. J. C. (1995). The NWS river forecast system-catchment modeling. In: Singh, V.J., (Ed.), Computer Models of Watershed Hydrology, Water Resources Publication, Highlands Ranch, Colorado, pp. 311–366.

Burnash, R. J. C., Ferral, R. L., McGuire, R. A. (1973). A Generalized Streamflow Simulation System: Conceptual Modeling for Digital Computers, Joint Federal-State River Forecast Center, Sacramento, CA.

Collis-George, N. (1977). Infiltration equations for simple soil systems. Water resources research, 13(2), 395-403.

Detty, J. M., & McGuire, K. J. (2010a). Threshold changes in storm runoff generation at a till-mantled headwater catchment. Water Resources Research, 46(7).

Detty, J. M., & McGuire, K. J. (2010b). Topographic controls on shallow groundwater dynamics: implications of hydrologic connectivity between hillslopes and riparian zones in a till mantled catchment. Hydrological Processes, 24(16), 2222-2236.

Eagleson, P. S. (1972). Dynamics of flood frequency. Water Resources Research, 8(4), 878-898.

Fang, Z. (2017). Hydrologic Analysis of Urbanization and Infiltration for the Fort Worth Floodway. Technical Report.

Fu, C., Chen, J., Jiang, H., & Dong, L. (2013). Threshold behavior in a fissured granitic catchment in southern China: 1. Analysis of field monitoring results. Water Resources Research, 49(5), 2519-2535.

Green, W. H., & Ampt, G. A. (1911). Studies on Soil Physics. The Journal of Agricultural Science, 4(1), 1-24.

Holtan, H. N. (1961). A concept of infiltration estimates in watershed engineering. ARS41-51, U.S. Department of Agricultural Service, Washington, DC.

Horton, R. I. (1938). The interpretation and application of runoff plot experiments with reference to soil erosion problems. Soil Science Society of America Proceedings, 3: 340–349.

James, A. L., & Roulet, N. T. (2007). Investigating hydrologic connectivity and its association with threshold change in runoff response in a temperate forested watershed. Hydrological Processes: An International Journal, 21(25), 3391-3408.

James, A. L., & Roulet, N. T. (2009). Antecedent moisture conditions and catchment morphology as controls on spatial patterns of runoff generation in small forest catchments. Journal of Hydrology, 377(3-4), 351-366.

Latron, J., & Gallart, F. (2008). Runoff generation processes in a small Mediterranean research catchment (Vallcebre, Eastern Pyrenees). Journal of Hydrology, 358(3-4), 206-220.

Loveridge, M., Rahman, A., Hill, P., & Babister, M. (2013). Investigation into probabilistic losses for design flood estimation: a case study for the Orara River catchment, NSW. Australasian Journal of Water Resources, 17(1), 13-24.

Mei, Y., & Anagnostou, E. N. (2015). A hydrograph separation method based on information from rainfall and runoff records. Journal of Hydrology, 523, 636-649.

Mein, R. G., & Larson, C. L. (1971). Modeling the infiltration component of the rainfall-runoff process. WRRC Bull. 43, Water Resources Research Center, University of Minnesota, Minneapolis.

Mein, R. G., & Larson, C. L. (1973). Modeling infiltration during a steady rain. Water Resources Research, 9(2): 384–394.

Mishra, S. K., Tyagi, J. V., & Singh, V. P. (2003). Comparison of infiltration models. Hydrological processes, 17(13), 2629-2652.

Mockus, V. (1972). Estimation of direct runoff from storm rainfall. SCS national engineering handbook. Section, 4, 10-1.

Overton, D. E. (1964). Mathematical refinement of an infiltration equation for watershed engineering. ARS 41–99, U.S. Department of Agricultural Service, Washington, DC.

Penna, D., Tromp-van Meerveld, H. J., Gobbi, A., Borga, M., & Dalla Fontana, G. (2011). The influence of soil moisture on threshold runoff generation processes in an alpine headwater catchment. Hydrology and Earth System Sciences, 15(3), 689-702.

Philip J. R. (1969). Theory of infiltration. In Advances in Hydroscience, Chow VT (ed.). Academic Press: New York; 215–296.

Philip, J. R. (1957). The theory of infiltration. Soil science, 84(3), 257-264.

Pilgrim, D.H., Cordery, I. (1975). Rainfall temporal patterns for design floods. J. Hydraul. Div. 101 (1), 81–95.

Rahman, A., Weinmann, E., & Mein, R. G. (2002). The use of probability-distributed initial losses in design flood estimation. Australasian Journal of Water Resources, 6(1), 17-29.

Richards, L. A. (1931). Capillary conduction of liquids through porous mediums. Physics, 1(5), 318-333.

Saffarpour, S., Western, A. W., Adams, R., & McDonnell, J. J. (2016). Multiple runoff processes and multiple thresholds control agricultural runoff generation.

Singh, V. P., & Yu, F. X. (1990). Derivation of infiltration equation using systems approach. Journal of Irrigation and Drainage Engineering, 116(6), 837-858.

Smith, R. E. (1972). The infiltration envelope: results from a theoretical infiltrometer. Journal of Hydrology, 17: 1–21.

Thompson D. B., Cleveland, T.G., Copula, D.B., and Fang, X. (2008). Lost-Rate Functions for Selected Texas Watershed. Texas Department of Transportation Research Report 0-4193-6, http://www.techmrt.ttu.edu/reports.php

U.S. Army Corps of Engineers (USACE) (1992). Upper Trinity River Reconnaissance Study.

U.S. Army Corps of Engineers (USACE) (2013). Corridor Development Certificate (CDC) – Upper Trinity River, Texas – Hydrologic and Hydraulic Model Update.

van Meerveld, I. T., & McDonnell, J. J. (2005). Comment to "Spatial correlation of soil moisture in small catchments and its relationship to dominant spatial hydrological processes, Journal of Hydrology 286: 113–134". Journal of Hydrology, 303(1-4), 307-312.

Viglione, A., Merz, R., Blöschl, G., 2009. On the role of the runoff coefficient in the mapping of rainfall to flood return periods. Hydrol. Earth Syst. Sci. 13 (5), 577–593.

Chapter 5: Conclusion and Future Research

This section summarizes the conclusions from previous chapters and provides suggestions for future research.

CONCLUSIONS

With recent advances in remote sensing, high-performance computing, and in-situ measurements, hydrologic/hydraulic (H/H) simulation has been reaching higher levels of spatiotemporal granularity and scale. However, enormous gaps exist between the scientific exploration and engineering practices. What's more, one might argue the such gap is becoming increasingly wider with the exponentially faster pace in data/computer science. In addition, the past two decades has witnessed real challenges from climate change and extreme weather to the infrastructure and engineering designs. Therefore, it is imperative for the engineering community to demonstrate the necessity and benefits of adopting more data and better science as well as to innovate engineering methods/practices. This doctoral research explores the hydrologic and hydraulic practices in the following two aspects: 1) comparing different inundation modeling approaches based on the observation derived using remote sensing techniques, and 2) investigating the representation of infiltration loss using realistic and abstract infiltration schemes in various hydrologic models.

To this end, Chapter 2 presents the comparative analyses between terrain-based model (HAND) and hydraulic-based model (iRIC) for a large flooding event occurring in May of 2016 in the Brazos River. Using the inundation extent derived from Landsat-8 Satellite imagery as the benchmark/observation, the performances of HAND and iRIC are evaluated based on the goodness of overlapping between the simulation and observation. The quantitative results show that iRIC

performs better (~70% of AFI) than HAND (~56%) during this extreme flood event. The study demonstrates that the catchment-based calculation of HAND does not explicitly account for inter-catchment flows between the main stem and its tributaries. However, the modified HAND method, which re-defines the channel network by stream orders, can provide a remedy to this issue when strategically applied the areas overlooked by HAND. Also, several lessons are learned from this work. First, simplification on the intricacy of flow dynamics has relatively minor influence on predictions for extreme events, which can positively justify the utility of HAND for large-scale inundation mapping. Second, terrain-based and hydraulic-based models have their own strength and weakness, hence can be used jointly to achieve the best accuracy and efficiency. Third, the low computational cost and ease to couple with the National Water Model (NWM) of HAND method, which provides great potential to support real-time continental inundation forecast in the future.

Chapter 3 explores the representation of infiltration loss in WRF-Hydro by comprehensively assessing the re-infiltration process, which is often ignored in conceptual/simplified hydrologic models. The effects of hydrometeorological, geographical conditions and model parameters on re-infiltration are evaluated by conducting a group of idealized numerical experiments in Upper Trinity River Basin (UTRB). The results not only reveal the pattern and magnitude of individual effects, but also inform the sensitivities of infiltration to each factor, providing guidance for the calibration efforts. Meanwhile, two real storm events in UTRB are simulated and calibrated to investigate the role of re-infiltration in real events. The study highlights that the local infiltration is a more direct route for infiltration than re-infiltration through lateral water re-distribution. Under the principle of mass conservation, the changes in local and re-infiltration due to a single factor can be opposite to each other. In addition, it is found that the

influence of re-infiltration on streamflow simulation can be substantial for areas with flat terrain and soil with high clay content (re-infiltration ratio is more than 50%). From both idealized and real events simulations, the runoff coefficient and re-infiltration ratio are positively correlated. Insights gained from this exploratory work are: (1) Re-infiltration effects are more pronounced as flood potential increases and subsequently may be more important in urban than in rural regions; (2) For WRF-Hydro users, one can strategically choose overland routing options based on the study domain's hydro-meteorological and graphical conditions.

Chapter 4 investigates the loss estimation of the Initial Abstraction and Constant Loss (IACL) method in HEC-HMS, which is widely used in the engineering practices due to its simplicity and relative accuracy. The exhaustive list of rainfall-runoff events has been identified and the corresponding total losses with their IA and CL components are calculated based on time-series of mean areal precipitation (MAP) and streamflow data. Threshold behavior is found for all studied watersheds, which is the linear relationship of the gross rainfall plus antecedent soil moisture versus runoff depth above certain threshold. This finding provides a convenient way to estimate/predict total loss or runoff depth given MAP and antecedent soil moisture. It has also been found that the IA and CL values can be approximated by the Gamma and Weibull distributions, respectively. These stochastic IACL values can be applied in a Monte Carlo simulation framework to stochastically simulate numerous rainfall-runoff events for a flood frequency analysis. Since the probabilistic nature of loss process is better represented, the Monte Carlo scheme promises to provide an alternative to the traditional deterministic approach.

FUTURE RESEARCH

This doctoral research includes three studies to investigate the Hydrologic and Hydraulic (H/H) modeling as introduced in Chapters 2, 3, and 4, respectively. For the study in Chapter 2,

there is room for future investigation in uncertainty analysis of observations using multiple sources of raw imagery along with various classification techniques. Potential sources of raw imagery can be used including synthetic aperture radar (SAR), unmanned aerial vehicle (UAV) and so on; while classification methods like Delta-cue change detection on pre/during flooding scenarios, normalized difference water index and image fusion techniques can be also used to generate inundation extents.

Chapter 3 introduces the study about headwater catchments in the North Central Texas. However, the findings need to be expanded to cover other places featuring a wider variety of hydrometeorological and graphical conditions. Since re-infiltration can play an indispensable role in the hydrologic cycle and in feeding back to the atmosphere, how different factors synergize and counteract with each other under hydrology-atmosphere interacting condition (coupling with WRF) would be an interesting topic to investigate.

The research effort in Chapter 4 sets a solid foundation for future implementation in Monte Carlo framework. Numerous rainfall-runoff events can be simulated to generate flood peaks, which in turn feed a flood frequency analysis (FFA). Moreover, the joint distribution of loss parameters with rainfall or other influential inputs/parameters can be considered as possible ways to capture the probabilistic nature of loss-related variables even more accurately. To further validate this probabilistic approach, a comparison with the existing FFA results at gauged locations is necessary. As the ultimate targets, ungauged areas will benefit the most from this simulation scheme which essentially generates streamflow time series as realistic as observed in neighboring gauged basins.